

“smartPearls” – novel dermal delivery system for amorphous actives

Inaugural-Dissertation

to obtain the academic degree

Doctor rerum naturalium (Dr. rer. nat.)

submitted to the Department of Biology, Chemistry and Pharmacy

at Freie Universität Berlin

by

David Hespeler

2019



The present work was performed under supervision of Prof. Dr. Rainer H. Müller at the Institute of Pharmacy at Freie Universität Berlin from October 2016 until September 2019.

1st Reviewer: Prof. Dr. Rainer H. Müller

2nd Reviewer: Prof. Dr. Cornelia M. Keck

Date of defense: 9. September 2019

In Gedenken an meine Großmutter

Index of Content

INTRODUCTION	1
1. THE NEED OF A NOVEL DERMAL DELIVERY SYSTEM	1
1.1. Obstacles in dermal delivery -----	1
1.2. Relevant delivery systems for dermal application-----	2
1.3. Properties and opportunities of amorphous actives -----	4
1.4. Dermal formulation solution for amorphous actives – smartPearls-----	5
1.4.1. Silica structures as stabilizing matrix	5
1.4.2. Loading methods	7
1.5. Pre-requisite for market introduction -----	9
1.5.1. Formulation requirements	9
1.5.2. Demands of an efficient delivery system	9
1.5.3. Production requirements	9
1.6. Aims of the thesis -----	11
References -----	12
GENERAL CONSIDERATIONS	21
2. SMARTPEARLS – NOVEL PHYSICALLY STABLE AMORPHOUS DELIVERY SYSTEM FOR POORLY SOLUBLE DERMAL ACTIVES	21
RESULTS AND DISCUSSION	45
3. SMARTPEARLS FOR DERMAL BIOAVAILABILITY ENHANCEMENT – LONG-TERM STABILIZATION OF SUSPENSIONS BY VISCOELASTICITY	45
4. DERMAL SMARTPEARLS – OPTIMIZED SILICA PARTICLES FOR COMMERCIAL PRODUCTS & MECHANISTIC CONSIDERATIONS	73
5. NANOPOROUS DERMAL SMARTPEARLS – IDENTIFICATION OF OPTIMAL SILICA TYPES & SCALE-ABLE PRODUCTION PROCESS AS PRE-REQUISITES FOR MARKETED PRODUCTS	101
6. GLABRIDIN SMARTPEARLS – SILICA SELECTION, PRODUCTION, AMORPHOUS STABILITY AND ENHANCED SOLUBILITY	127
SUMMARY	151
ZUSAMMENFASSUNG	153
PUBLICATIONS	157
STATEMENT OF CONTRIBUTIONS	161
ACKNOWLEDGEMENTS	163
CURRICULUM VITAE	165

Introduction

1. The need of a novel dermal delivery system

1.1. Obstacles in dermal delivery

The skin with its outer surface of 1.8 m² is one of the largest human organs and protects the body against exogenous substances, damages by radiation, and other exposures [1]. In addition, it is easily accessible for drug delivery. Dermal delivery can be divided in transdermal and topical dermal delivery. Either applications have a systemic (transdermal) or local and regional restricted (dermal) effects. Advantage of transdermal delivery is the partially avoidance of the first-pass effect [2]. Dermal delivery has advantages such as targeted delivery and reduction of systemic side effects. Thus, topical dermal delivery is perfectly suited for treating of skin diseases like psoriasis or dermatosis but also for prevention of skin aging and pollution induced damages. This led to an estimated revenue of about 19 billion USD only for skin applications in the OTC pharmaceutical market 2018 [3].

Actives are supposed to show certain physicochemical properties enabling penetration and efficacy in dermal delivery. According to the “Rule of 5” [4] low molecular weights (<500 kDa) and a log P below 5 are physicochemical pre-requisites since most penetration depends on passive diffusion regardless the route (intercellular, transcellular, and through hair follicles) [5-7]. This physicochemical properties are mostly applicable for actives with a certain water solubility – leading to high penetration rates and good dermal performance [8].

Many drugs and actives – especially from natural origin – are poorly soluble in water and sometimes simultaneously poorly soluble in lipophilic media. In case of new chemical entities in the pharmaceutical industry 40% of them are practically insoluble in water [9], leading to an insufficient penetration and bioavailability [10; 11].

Therefore, novel approaches are needed to address bioavailability issues. This results in increasing research regarding suitable dermal delivery systems.

1.2. Relevant delivery systems for dermal application

Liposomes are considered as one of the major inventions in dermal delivery. They were invented in 1961 [12], entered the cosmetic market in 1986 and shortly after the pharmaceutical market [13]. Liposomes are vesicles consisting of a phospholipid bilayer in an aqueous phase. Lipophilic actives can be dissolved in the phospholipid layer and thus their solubility in the formulation is increased [14].

Another system are microemulsions, a thermodynamically stable system with lipophilic and hydrophilic domains in the nanometer range. They are able to increase the saturation solubility of actives in their composition of lipophilic and hydrophilic domains stabilized with a high surfactant concentration. Advantage of the microemulsions is their thermodynamic stability. After application, the formulation spontaneously disperses into an emulsion due to contact with water (e.g. due to the skin or the gastrointestinal tract). Thereby the active is solubilized [15]. In case of dermal application, the reached supersaturation state leads to an increased diffusion pressure into the skin [13]. However, the high surfactant concentration and potential active instability limits dermal application.

At the beginning of the 1990s invention of the next major delivery system followed with the solid lipid nanoparticles (SLN) [16]. They avoided the disadvantages of previous delivery systems such as possible active degradation and high surfactant concentrations. Meanwhile these solid lipid nanoparticles are developed in the 3rd generation called “smartLipids®” after solid lipid nanoparticles (1st generation) and nanostructured lipid carriers (NLC, 2nd generation) [17]. Principle behind these systems is the incorporation of actives into a lipid matrix staying solid at skin temperature. For SLN one lipid is melted, mixed with an aqueous stabilizer solution and high pressure homogenized. Solid lipid particles in the nanometer range are obtained after cooling. They are dispersed and stabilized in the aqueous phase. In case of NLC and smartLipids® a more complex lipid matrix is used resulting in higher loading capacities and increased physical stability [18]. Moreover, release can be easily modified by the lipid composition [18]. Depending on the stabilizer and used excipients these suspensions can be applied by various administration routes, even intravenous [19]. Identically to polymeric nanoparticles, controlled release is inherent in these systems because of the solid particle structure which releases the active [19]. Further the actives are protected against degradation. In dermal application they form an occlusive film on the skin which enhance

penetration and repair the “brick and mortar” structure of the stratum corneum [20]. The NLC entered the cosmetic market in 2005. Examples of products are Nanorepair (Dr. Rimpler, Germany), products in the line IOPE (AmorePacific, Korea), and swiss cellular white (la prairie, Switzerland) [21].

Nanocrystals were reported as delivery system by Liversidge et al. [22]. They show high potential to reduce solubility problems of BCS (biopharmaceutical classification system) II (low solubility, high permeability) and BCS IV (low solubility, low permeability) classified actives [23]. They consist of crystals in the nanometer range (<1000 nm), stabilized by a surfactant in an aqueous or non-aqueous dispersion medium. Dissolution pressure of a solid crystal increases at the solid/liquid interface with decreasing particle size. This process is similar to the increasing vapor pressure of a decreasing liquid droplet on the liquid/gas interface. It can be described by the Kelvin equation [24]. Outstanding advantage of nanocrystals/submicron particles is the increased saturation solubility. Additionally, the dissolution velocity is enhanced according to the Noyes-Whitney equation [25]. Decreasing particle size leads to an increase of the total surface area which is responsible for this increase. Both effects result in a subsequently improved penetration and hence better bioavailability [25]. Furthermore, the increased surface of nanocrystals enhances the adhesiveness compared to microcrystals. This is responsible for further increase in efficacy [26]. Application is possible by several administration routes including intravenous, pulmonary, oral and dermal [25; 27]. Production of nanocrystals can be performed by top down or bottom up methods, whereby the top-down methods are more efficient and result in higher concentrated suspensions [28]. If 50% of particles (number distribution) are below 100 nm “nano” declaration is mandatory due to the European Union regulation EC No 1223/2009. Thus particle size, especially in cosmetics, is mostly above 100 nm to avoid the “nano” declaration because of consumer reluctance. However, apart from that definition of “nano” all particles between 1 and 1000 nm are physically in the nanometer-range and take advantage of their properties. For better differentiation, particles between 100 and 1000 nm can be described as submicron particles. They possess the properties of nanoparticles but are no nanoparticles according the legal definition.

Since the last two decades a newer approach attracts more attention. Solid dispersions are able to prevent re-crystallization of amorphous actives [29]. Actives in the amorphous state

show many advantages compared to their crystalline counterpart such as higher solubility and better dissolution behavior (cf. Chapter 1.3) [30; 31]. To prepare solid dispersions several technologies are available. Widely known is the distribution of the active in a polymer matrix [32]. Re-crystallization can be inhibited. However, use of polymer matrices is limited by regulatory aspects (e.g. toxicology of monomers, excipients used for polymerization) and the lack of predictable miscibility and stability of the solid dispersions [29]. Further, the saturation solubility potential of amorphous actives decreases in a mixture with a polymer [33]. Increasing concerns towards polymers appeared in recent years, especially towards the use in cosmetic products due to the microplastic discussion.

Besides polymer matrices, mesoporous silica attracted increasing attention as matrix since about 2005. Amorphous stability is ensured by the defined properties of the used silica (cf. Chapter 1.4.1). However, up to now most of the research focus on oral dosage forms. Similar to nanostructured lipid carrier and nanocrystals the following step is to transfer this technology to other administration routes such as dermal [34].

1.3. Properties and opportunities of amorphous actives

A crystal has per definition a crystal lattice which is, caused by its low internal energy, responsible for a high stability of the molecules in the crystal lattice. Disadvantage is the energy needed for dissolution. In contrast, the amorphous state is similar to the liquid state of an active. Differently to the liquid state the molecules are immobile to each other. Thus, amorphous substances are also called “solidified melts”. Special feature of the amorphous state is the high internal energy due to the absence of the crystal lattice. The molecules are in a non-ordered orientation. This results in an easier access to the molecules in media and requires less energy to dissolve the molecules.

The most obvious benefit of using the amorphous state in drug delivery systems is the high internal energy. The saturation solubility and dissolution velocity increase manifolds compared to the crystalline low energy form. Dissolution is facilitated by the high internal energy (absence of a crystalline lattice) and easier solvation of the non-ordered molecule structure. Thus, there is a high potential to increase the bioavailability of poorly soluble actives by using the solubility and dissolution advantages of the amorphous state.

Problem is the tendency of the molecules to reach a more stable state – the crystal lattice – which can lead to spontaneous re-crystallization. Occurring re-crystallization reduces the highly soluble amount of amorphous active. Dissolution velocity and saturation solubility decrease after solution of the amorphous part, limit the solubility advantage and changes dosing. Moreover, crystallization nuclei might introduce complete crystallization and terminate thereby the solubility advantage of the amorphous state. This limits the general use of amorphous actives and leads to the need of suitable delivery systems, to stabilize this state.

1.4. Dermal formulation solution for amorphous actives – smartPearls

The advantage of amorphous actives (cf. Chapter 1.3) making them also interesting to overcome problems in dermal delivery (cf. Chapter 1.1). The increased saturation solubility of the amorphous active leads to a higher concentration gradient between the formulation and the skin. Penetration of poorly soluble actives and hence their bioavailability are improved. Mesoporous silica as stabilizing matrix are preferred compared to polymer matrices (cf. Chapter 1.2). Amorphous solid dispersions using mesoporous silica are a promising approach to improve the dermal bioavailability of poorly soluble actives.

Since most of the research is focusing on oral application more research towards dermal application is needed. To differentiate between oral and dermal application, the dermal delivery system is called smartPearls. This delivery system was submitted as patent application in 2014 [34]. Data of superiority in dermal delivery of amorphous actives stabilized in mesoporous silica were published shortly after [35]. Amorphous stability of several actives (e.g. hesperidin, rutin, cyclosporine A) were proven for several years and published from Jin N. et al. [36]. Increased active penetration due to the smartPearls system compared to previous dermal delivery systems were demonstrated by tape stripping studies [36]. Maximum application concentrations were defined (cf. Chapter 1.5.2). However, several issues are still unresolved relating silica selection, appropriate loading methods, industrial feasibility, and implementation.

1.4.1. Silica structures as stabilizing matrix

Mesoporous silica are defined as porous particles with pores between 2 and 50 nm. Mostly they are highly porous having pore volumes of 0.1 up to 2.0 mL and surface areas of 100 up

to 1000 m²/g. In pharmaceutical applications mesoporous silica are widely used as functional and non-functional excipients.

Beside their use as filler for tableting, they are used as carrier for liquid substances because of their good adsorption properties both for aqueous and lipophilic media. Due to their use as functional excipients, interactions between used actives and silica were discovered. Based on this, a new application area appeared for the silica as amorphous active delivery carrier [37].

Stabilization of amorphous actives with mesoporous silica particles were already reported in the 1970s [38; 39]. A major concern was the stability of the amorphous state [37]. After invention of ordered mesoporous silica structures in the 1990s [40] the researchers showed more interest in them as amorphous stabilizing matrix. Ordered mesoporous silica show defined pore size with narrow distribution and pore structure [41-43]. With the advantage of defined properties, the stability concerns declined. Thus, ordered mesoporous silica particles are widely used in pharmaceutical research for stabilization of amorphous actives. This helped to understand which impact pore parameters have on amorphous stabilization [44].

On the contrary, up to now ordered mesoporous silica are not regulatory accepted which is a hurdle for fast realization of products. Additionally, ordered mesoporous silica are about 10 times more expensive than non-ordered mesoporous silica as they show a narrower pore size distribution. However, since non-ordered mesoporous silica are used for decades in pharmaceutical applications, they are available in a huge variety with different properties depending on the respective need [37]. The industry has lots of practical experience because of the present use. This and the price make them reasonable for development of novel delivery systems. In consequence, several researchers are working with non-ordered mesoporous silica showing similar potential of amorphous active stabilization [44-48]. In addition, non-ordered silica are generally GRAS proven, dermally applicable, and most important being accepted in cosmetic formulations.

Re-crystallization of the amorphous state is prevented by incorporation into the mesopores of silica. Surface interactions and/or size restrictions are discussed as main reasons for stabilization of the amorphous active [37]. Hempel et al. recognize surface interaction between active and silica as the main stabilizing effect [46; 49]. The high impact of the surface is underlined by research regarding surface modification to improve the stabilization effects [50]. However, too high active carrier binding affinity can lead adversely to an

unintended retarded and/or incomplete release. In addition, modification of the surface leads to excipients which are regulatorily not accepted and need a separate approval. Industrially desired is of course one fitting solution for as much actives as possible. Therefore, chemical modification of the silica would rather diminish the field of application than increasing it. Since pore size and surface area are connected to each other they are both supposed as essential for stabilization of the amorphous active [33; 45].

Pore size is frequently discussed to hinder re-crystallization due to space restriction [51-53]. Investigated pore sizes reach mostly from 2 to 25 nm. Smallest useable pore size for effective stabilization of the amorphous state is mostly defined by the molecule size [49]. The maximum possible pore size is depending on the smallest possible crystal, which can be formed if the pore size is larger than 12 times the molecule size [54]. Thus, a pore size molecule ratio of 12 should not be exceeded. By use of non-ordered silica, the polydisperse pore size distribution must be considered. Re-crystallization can theoretically already occur if few pores are above the maximum molecule pore size ratio.

The nano-dispersion of the active in the silica and the eased wettability, due to the hydrophilic silica structure, are discussed to enhance the solubility [51]. This assumption is supported by the exceeding saturation solubility of cyclosporine A incorporated in mesoporous silica compared to respective amorphous nanoparticles [36]. Better understanding of the mechanism is desired to increase the predictability of increase in saturation solubility.

Besides that, several other issues need further investigation. The optimum pore parameters in dependency of the active are one of it. Also, more research towards the impact of the loading method on the active deposition in the mesoporous structure is needed. Furthermore, it must be investigated, how the deposition influences the stability and release of the active.

1.4.2. Loading methods

Loading of the silica particles can be performed by several approaches, divided into solvent and solvent free methods. Obviously, solvent free methods are preferable since solvents are a cost factor and the proof of absence of potential solvent residues can be omitted. The solvent free methods are melting methods (e.g. hot melt extrusion) [42; 47; 55], co-grinding [56; 57], and sublimation mass transfer [33; 58]. Hot melt extrusion is the most applicable despite the limitation to low melting actives whereby degradation can be

excluded [29]. Since higher temperatures are applied during the process, this process is not suitable for thermolabile actives. Co-grinding is mostly insufficient to convert the complete active into the amorphous state. Loading via sublimation mass transfer takes long time and leads to low loading levels [59].

Between solvent free and solvent using methods stands the loading with supercritical carbon dioxide [60-62]. Thereby active is transferred into the pores in a high-pressure chamber [60]. After depressurization, the active optimally remains in the loaded silica. Due to the use of carbon dioxide, solvent residues can be excluded. However, the cost intensity is above other methods.

For screening of potential silica structures, solvent methods are helpful because of the easy change of loading parameters and used active. Especially for thermal labile actives this is the preferred option for loading. Problems with possible solvent residues can be prevented by using easily vaporizing and dermally compatible solvents.

Solvent methods are all based on the same principal – the active is dissolved in a suitable solvent and mixed with the silica particles. After a certain contact time solvent or remaining active solution is removed. Methods can be classified into impregnation [53] and immersion methods [63]. The impregnation exploits the pore volume which is filled partly or completely by active solution. Solution is added by spraying it onto the silica or by adding it dropwise. Spraying is preferred to achieve an even distribution. Afterwards, the solvent is removed by use of heat and/or vacuum, whereby the active precipitates in the pores. Crystallization by precipitation outside the pores can easily be excluded since the whole added solution is soaked into the pores (capillary forces). Adverse are the multiple steps needed to reach a certain loading. Number of loading steps depends on pore volume and active concentration in the solution.

For the immersion method, silica is dispersed in the active solution. Removal of the excessive active solution or removal of the solvent after a certain time lead to – at least partly – loaded silica. Solvent can be removed either by filtration or by evaporation [64]. Filtration leads to low loading efficacies, depending on the partitioning of the active between the liquid phase and the silica surface/pores. However, they are highly stable [63]. Evaporation increases the concentration of the active in the liquid phase and forces the system repeatedly to reach the partition equilibrium by precipitation of the active at the silica surface. This can lead to

crystallization if the solvent is evaporated too fast. However, high loadings can be reached – even if the active is just slightly soluble. The reachable loadings make this method highly industrially feasible. Applicable processes for solvent removal are spray drying [65], drying in a compartment dryer [51] or solvent evaporation in a rotary evaporator [64].

1.5. Pre-requisite for market introduction

1.5.1. Formulation requirements

The size of smartPearls can be up to 50 μm . For oral application and tableting this is no challenge. It even fulfils the requirement for dermal application of the Ph.Eur. and fits the limitation of fine powders (180 μm) [66]. However, in dermal formulations a risk of sedimentation exists due to the size and the high density around 2.2 g/mL of silica particles, sedimentation must be excluded by selecting an appropriate formulation. Therefore, dermal formulations have to fulfil certain viscoelastic requirements prior incorporation of smartPearls.

1.5.2. Demands of an efficient delivery system

According Jin et al. the amount of smartPearls in dermal formulation is limited by the occurrence of sandy feeling [36]. The limitation varies depending on the silica used but is mainly at 5%. Depending on the used active and aimed application concentrations of up to 1% active, an active loading of smartPearls of about 20% is required. Therefore, silica must have a sufficient pore volume and surface area to stabilize an adequate amount of active. Additionally, the pore diameter should be well above 2 nm to allow not only access of small molecules (up to 500 kDa, molecule diameters around 1 nm) but also larger active molecules. Even though there is current research about ordered mesoporous silica (cf. Chapter 1.4.1), use of non-ordered silica is more feasible because of the price and the regulatory status. Thus, development should be based on non-ordered commercially available silica.

1.5.3. Production requirements

Several different loading methods (cf. Chapter 1.4.2) are available and certain requirements are needed for an industrial feasible production. Thereby, processes are favored which are already in use in the pharmaceutical industry since experience and the equipment are already

available. The selected process should be as easy and inexpensive as possible without compromises in scalability and versatile use.

For industrial realization predominate the ease of use and more versatile applicability of a solvent evaporation process the advantages of solvent free methods. Experience with solvent based methods is already available due to previous research in the group of Prof. R.H. Müller [36; 67]. Impregnation evaporation (cf. Chapter 1.4.2) is used up to now in small scale studies because of the easy change of loading parameters. This process is time consuming and highly vulnerable for mistakes. In addition, scaling is difficult. Reproducibility is problematic and the process is not industrially feasible. Transfer of the technology to a scalable, easy one step process is required for industrial implementation. The immersion evaporation (cf. Chapter 1.4.2) process shows all the required advantages. It can be performed with a commercial rotary evaporator. Scalability up to several kilograms batch size can be achieved.

1.6. Aims of the thesis

Stabilization of amorphous actives by use of porous silica for oral administration is under investigation over a number of years. Transferring the technology to dermal administration (smartPearls) took place at the end of 2014 as a joint development of the research groups R. H. Müller (Freie Universität Berlin) and C. M. Keck (Philipps-Universität Marburg) in co-operation with the US silica company GRACE. Thus, there is still a need of basic investigations to make this technology applicable. The **general aim of this thesis** was to contribute with basic investigations to a better understanding of the system and its industrial implementation.

The **first aim** was to summarize the existing knowledge in an overview, that means writing a so called “white paper” reviewing the state of the art of the smartPearls technology. The performance of smartPearls should be critically discussed and compared to other existing dermal delivery technologies, especially the gold standard nanocrystals.

Application of the silica in fluid/semi-solid dermal formulations instead as a dry powder in a tablet or capsule creates a new formulation challenge. The 2-50 µm sized particles undergo sedimentation in traditional gels which is not acceptable for a dermal formulation. The **second aim** was therefore to develop physically stable, non-sedimenting formulations based on viscoelasticity.

A variety of silica particles is available, differing in their particle size, pore size, and pore volume. Subsequently the **third aim** was to identify silica particles optimal for loading with dermal actives. Ideal silica types should allow a high loading and at the same time preserving the amorphous state in the formulation efficiently. To specify ideal silica properties avobenzonone und rutin were chosen as model actives. At the same time, rutin is an interesting antioxidant for anti-pollution strategies being a hot topic in dermopharmacy.

The **fourth aim** was to develop a loading process, which is scale-able to industrial scales. To enable up-scaling the immersion-evaporation method should be optimized. This method should be designed to allow medium sized cosmetic companies to produce products based on smartPearls.

As **final aim** the acquired knowledge should be used to formulate a challenging cosmetic active. Glabridin an highly effective whitening agent with poor solubility was selected for investigation. Use of excess amounts to compensate solubility and penetration problems is

not possible due to the high costs of glabridin (10,000 USD/kg). SmartPearls might be the formulation solution to obtain whitening effects already with small amounts of active.

Attention should also be given to explore underlying mechanisms, e.g. for factors affecting stability of the amorphous state and the technical process of loading on large scale. Understanding the mechanisms allows more efficient development of the smartPearls technology.

References

- [1] Farage, M.A.; Miller, K.W.; Maibach, H.I.; 2017. Degenerative Changes in Aging Skin, in: Farage, M.A.; Miller, K.W.; Maibach, H.I. (Eds.), Textbook of Aging Skin. Springer, Berlin Heidelberg, 15-30. https://doi.org/10.1007/978-3-662-47398-6_4
- [2] Prausnitz, M.R.; Langer, R.; 2008. Transdermal drug delivery. *Nature Biotechnology* 26(11), 1261. <https://doi.org/10.1038/nbt.1504>
- [3] Brinckmann, M.; Statista, 2019. OTC Pharmaceuticals Report 2019 – Skin Treatment. document no. 48741, May. <https://de.statista.com/statistik/studie/id/48741/dokument/otc-pharmaceuticals-report-skin-treatment/> [accessed: 2019 May 16]
- [4] Lipinski, C.A.; Lombardo, F.; Dominy, B.W.; Feeney, P.J.; 1997. Experimental and computational approaches to estimate solubility and permeability in drug discovery and development settings. *Advanced Drug Delivery Reviews* 23(1-3), 3-25. [https://doi.org/10.1016/S0169-409X\(96\)00423-1](https://doi.org/10.1016/S0169-409X(96)00423-1)
- [5] Pelikh, O.; Stahr, P.-L.; Huang, J.; Gerst, M.; Scholz, P.; Dietrich, H.; Geisel, N.; Keck, C.M.; 2018. Nanocrystals for improved dermal drug delivery. *European Journal of Pharmaceutics and Biopharmaceutics* 128, 170-178. <https://doi.org/10.1016/j.ejpb.2018.04.020>
- [6] Scheuplein, R.J.; Blank, I.H.; 1971. Permeability of the Skin. *Physiological Reviews* 51(4), 702-747. <https://doi.org/10.1152/physrev.1971.51.4.702>
- [7] Lademann, J.; Richter, H.; Teichmann, A.; Otberg, N.; Blume-Peytavi, U.; Luengo, J.; Weiß, B.; Schaefer, U.F.; Lehr, C.-M.; Wepf, R.; 2007. Nanoparticles—an efficient carrier for drug delivery into the hair follicles. *European Journal of Pharmaceutics and Biopharmaceutics* 66(2), 159-164. <https://doi.org/10.1016/j.ejpb.2006.10.019>

- [8] Abla, M.J.; Singh, N.D.; Banga, A.K.; 2016. Role of Nanotechnology in Skin Delivery of Drugs, in: Dragicevic, N.; Maibach, H.I. (Eds.), *Percutaneous Penetration Enhancers Chemical Methods in Penetration Enhancement: Nanocarriers*. Springer, Berlin Heidelberg, 1-13. https://doi.org/10.1007/978-3-662-47862-2_1
- [9] Savjani, K.T.; Gajjar, A.K.; Savjani, J.K.; 2012. Drug solubility: importance and enhancement techniques. *ISRN pharmaceuticals 2012*, Article ID 195727. <https://doi.org/10.5402/2012/195727>
- [10] Müller, R.H.; Peters, K.; 1998. Nanosuspensions for the formulation of poorly soluble drugs: I. Preparation by a size-reduction technique. *International Journal of Pharmaceutics* 160(2), 229-237. [https://doi.org/10.1016/S0378-5173\(97\)00311-6](https://doi.org/10.1016/S0378-5173(97)00311-6)
- [11] Douroumis, D.; Fahr, A.; 2013. *Drug Delivery Strategies for Poorly Water-Soluble Drugs*. Advances in Pharmaceutical Technology. John Wiley & Sons Ltd. ISBN: 978-0-470-71197-2
- [12] Bangham, A.D.; Horne, R.W.; 1964. Negative staining of phospholipids and their structural modification by surface-active agents as observed in the electron microscope. *Journal of Molecular Biology* 8(5), 660-668. [https://doi.org/10.1016/S0022-2836\(64\)80115-7](https://doi.org/10.1016/S0022-2836(64)80115-7)
- [13] Müller, R.H.; Radtke, M.; Wissing, S.A.; 2002. Solid lipid nanoparticles (SLN) and nanostructured lipid carriers (NLC) in cosmetic and dermatological preparations. *Advanced Drug Delivery Reviews* 54, 131-155.
- [14] Fahr, A.; Liu, X.; 2007. Drug delivery strategies for poorly water-soluble drugs. *Expert Opinion on Drug Delivery* 4(4), 403-416. <https://doi.org/10.1517/17425247.4.4.403>
- [15] Chaudhary, A.; Nagaich, U.; Gulati, N.; Sharma, V.K.; Khosa, R.L.; Partapur, M.U.; 2012. Enhancement of solubilization and bioavailability of poorly soluble drugs by physical and chemical modifications: A recent review. *Journal of Advanced Pharmacy Education & Research* 2(1), 32-67.
- [16] Müller, R.H.; Mehnert, W.; Lucks, J.S.; Schwarz, C.; Zur Mühlen, A.; Meyhers, H.; Freitas, C.; Rühl, D.; 1995. Solid lipid nanoparticles (SLN): an alternative colloidal carrier system for controlled drug delivery. *European Journal of Pharmaceutics and Biopharmaceutics* 41(1), 62-69.

- [17] Ding, Y.; Pyo, S.M.; Müller, R.H.; 2017. smartLipids® as third solid lipid nanoparticle generation–stabilization of retinol for dermal application. *Die Pharmazie – An International Journal of Pharmaceutical Sciences* 72(12), 728-735.
<https://doi.org/10.1691/ph.2017.7016>
- [18] Radtke, M.; Müller, R.H.; 2001. Nanostructured lipid drug carriers. *New Drugs* 2, 48-52.
- [19] Müller, R.H.; Shegokar, R.; Keck, C.M.; 2011. 20 years of lipid nanoparticles (SLN & NLC): present state of development & industrial applications. *Current Drug Discovery Technologies* 8(3), 207-227. <https://doi.org/10.2174/157016311796799062>
- [20] Wissing, S.A.; Müller, R.H.; 2002. The influence of the crystallinity of lipid nanoparticles on their occlusive properties. *International Journal of Pharmaceutics* 242(1), 377-379. [https://doi.org/10.1016/S0378-5173\(02\)00220-X](https://doi.org/10.1016/S0378-5173(02)00220-X)
- [21] Pardeike, J.; Hommoss, A.; Müller, R.H.; 2009. Lipid nanoparticles (SLN, NLC) in cosmetic and pharmaceutical dermal products. *International Journal of Pharmaceutics* 366(1), 170-184. <https://doi.org/10.1016/j.ijpharm.2008.10.003>
- [22] Liversidge, G.G.; Conzentino, P.; 1995. Drug particle size reduction for decreasing gastric irritancy and enhancing absorption of naproxen in rats. *International Journal of Pharmaceutics* 125(2), 309-313. [https://doi.org/10.1016/0378-5173\(95\)00148-C](https://doi.org/10.1016/0378-5173(95)00148-C)
- [23] Kesisoglou, F.; Mitra, A.; 2012. Crystalline Nanosuspensions as Potential Toxicology and Clinical Oral Formulations for BCS II/IV Compounds. *The AAPS Journal* 14(4), 677-687. <https://doi.org/10.1208/s12248-012-9383-0>
- [24] Romero, G.B.; Chen, R.; Keck, C.M.; Müller, R.H.; 2015. Industrial concentrates of dermal hesperidin smartCrystals® – production, characterization & long-term stability. *International Journal of Pharmaceutics* 482(1), 54-60.
<https://doi.org/10.1016/j.ijpharm.2014.11.039>
- [25] Pardeike, J.; 2009. Nanosuspensions and nanostructured lipid carriers for dermal application [doctoral thesis]. [Germany]: Freie Universität Berlin.
urn:nbn:de:kobv:188-fudissthesis000000008241-5
- [26] Pyo, S.M.; 2016. Nanocrystals & Lipid Nanoparticles for Optimized Delivery of Actives [doctoral thesis]. [Germany]: Freie Universität Berlin.

- [27] Müller, R.H.; Keck, C.M.; 2012. Twenty years of drug nanocrystals: where are we, and where do we go? *European Journal of Pharmaceutics and Biopharmaceutics* 80(1), 1-3. <https://doi.org/10.1016/j.ejpb.2011.09.012>
- [28] Keck, C.M.; Kobierski, S.; Mauludin, R.; Müller, R.H.; 2013. Novel Top-Down Technologies: Effective Production of Ultra-Fine Drug Nanocrystals, *Drug Delivery Strategies for Poorly Water-Soluble Drugs*. John Wiley & Sons Ltd, 247-263. <https://doi.org/10.1002/9781118444726.ch8>
- [29] Li, S.; Jones, D.S.; Andrews, G.P.; 2013. Hot Melt Extrusion: A Process Overview and Use in Manufacturing Solid Dispersions of Poorly Water-Soluble Drugs, *Drug Delivery Strategies for Poorly Water-Soluble Drugs*. John Wiley & Sons Ltd, 325-358. <https://doi.org/10.1002/9781118444726.ch11>
- [30] Hancock, B.C.; Parks, M.; 2000. What is the True Solubility Advantage for Amorphous Pharmaceuticals? *Pharmaceutical Research* 17(4), 397-404. <https://doi.org/10.1023/A:1007516718048>
- [31] Hancock, B.C.; Carlson, G.T.; Ladipo, D.D.; Langdon, B.A.; Mullarney, M.P.; 2002. Comparison of the mechanical properties of the crystalline and amorphous forms of a drug substance. *International Journal of Pharmaceutics* 241(1), 73-85. [https://doi.org/10.1016/S0378-5173\(02\)00133-3](https://doi.org/10.1016/S0378-5173(02)00133-3)
- [32] Ahmed, N.; Mora-Huertas, C.E.; Jaafar-Maalej, C.; Fessi, H.; Elaissari, A.; 2013. Polymeric Drug Delivery Systems for Encapsulating Hydrophobic Drugs, *Drug Delivery Strategies for Poorly Water-Soluble Drugs*. John Wiley & Sons Ltd, 151-197. <https://www.doi.org/10.1002/9781118444726.ch5>
- [33] Qian, K.K.; Bogner, R.H.; 2012. Application of Mesoporous Silicon Dioxide and Silicate in Oral Amorphous Drug Delivery Systems. *Journal of Pharmaceutical Sciences* 101(2), 444-463. <https://doi.org/10.1002/jps.22779>
- [34] Monsuur, F.H.; Hofer, H.H.; Keck, C.M., inventors; Grace GmbH & Co. KG, Pharmasol GmbH, assignee; 2014. Active-loaded particulate materials for topical administration. International Publication Number WO 2016/041992 A1, patent application PCT/EP2015/071138, Sep 15.
- [35] Müller, R.H.; Monsuur, F.; Höfer, H.H.; Jin, N.; Staufenbiel, S.; Keck, C.M.; 2014. smartPearls - novel amorphous delivery system based on porous materials to increase skin penetration of anti-oxidants, Workshop NutriOX, Metz, 1-3 October.

- [36] Jin, N.; 2017. Nanocrystals & loaded porous silica for increased dermal bioavailability [doctoral thesis]. [Germany]: Freie Universität Berlin. urn:nbn:de:kobv:188-fudissthesis000000105191-3
- [37] Choudhari, Y.; Hoefler, H.; Libanati, C.; Monsuur, F.; McCarthy, W.; 2014. Mesoporous silica drug delivery systems, in: Shah, N.; Sandhu, H.; Choi, D.; Chokshi, H.; Malick, A. (Eds.), *Amorphous Solid Dispersions*. Springer, New York, 665-693.
https://doi.org/10.1007/978-1-4939-1598-9_23
- [38] Monkhouse, D.C.; Lach, J.L.; 1972. Use of Adsorbents in Enhancement of Drug Dissolution II. *Journal of Pharmaceutical Sciences* 61(9), 1435-1441.
<https://doi.org/10.1002/jps.2600610918>
- [39] Monkhouse, D.C.; Lach, J.L.; 1972. Use of Adsorbents in Enhancement of Drug Dissolution I. *Journal of Pharmaceutical Sciences* 61(9), 1430-1435.
<https://doi.org/10.1002/jps.2600610917>
- [40] Kresge, C.T.; Leonowicz, M.E.; Roth, W.J.; Vartuli, J.C.; Beck, J.S.; 1992. Ordered mesoporous molecular sieves synthesized by a liquid-crystal template mechanism. *Nature* 359(6397), 710-712. <https://doi.org/10.1038/359710a0>
- [41] Vialpando, M.; Backhuijs, F.; Martens, J.A.; Van den Mooter, G.; 2012. Risk assessment of premature drug release during wet granulation of ordered mesoporous silica loaded with poorly soluble compounds itraconazole, fenofibrate, naproxen, and ibuprofen. *European Journal of Pharmaceutics and Biopharmaceutics* 81(1), 190-198. <https://doi.org/10.1016/j.ejpb.2012.01.012>
- [42] Mellaerts, R.; Jammaer, J.A.G.; Van Speybroeck, M.; Chen, H.; Humbeeck, J.V.; Augustijns, P.; Van den Mooter, G.; Martens, J.A.; 2008. Physical state of poorly water soluble therapeutic molecules loaded into SBA-15 ordered mesoporous silica carriers: a case study with itraconazole and ibuprofen. *Langmuir* 24(16), 8651-8659.
<https://doi.org/10.1021/la801161g>
- [43] Garcia-Bennett, A.E.; Lau, M.; Bedford, N.; 2018. Probing the Amorphous State of Pharmaceutical Compounds Within Mesoporous Material Using Pair Distribution Function Analysis. *Journal of Pharmaceutical Sciences* 107(8), 2216-2224.
<https://doi.org/10.1016/j.xphs.2018.03.029>

- [44] Delle Piane, M.; Corno, M.; Ugliengo, P.; 2013. Does Dispersion Dominate over H-Bonds in Drug–Surface Interactions? The Case of Silica-Based Materials As Excipients and Drug-Delivery Agents. *Journal of Chemical Theory and Computation* 9(5), 2404-2415. <https://doi.org/10.1021/ct400073s>
- [45] Wei, Q.; Keck, C.M.; Müller, R.H.; 2015. CapsMorph® technology for oral delivery–theory, preparation and characterization. *International Journal of Pharmaceutics* 482(1), 11-20. <https://doi.org/10.1016/j.ijpharm.2014.10.068>
- [46] Hempel, N.-J.; Brede, K.; Olesen, N.E.; Genina, N.; Knopp, M.M.; Löbmann, K.; 2018. A fast and reliable DSC-based method to determine the monomolecular loading capacity of drugs with good glass-forming ability in mesoporous silica. *International Journal of Pharmaceutics* 544(1), 153-157. <https://doi.org/10.1016/j.ijpharm.2018.04.035>
- [47] Aerts, C.A.; Verraedt, E.; Depla, A.; Follens, L.; Froyen, L.; Van Humbeeck, J.; Augustijns, P.; Van den Mooter, G.; Mellaerts, R.; Martens, J.A.; 2010. Potential of amorphous microporous silica for ibuprofen controlled release. *International Journal of Pharmaceutics* 397(1), 84-91. <https://doi.org/10.1016/j.ijpharm.2010.06.053>
- [48] Aerts, C.A.; Verraedt, E.; Mellaerts, R.; Depla, A.; Augustijns, P.; Van Humbeeck, J.; Van den Mooter, G.; Martens, J.A.; 2007. Tunability of pore diameter and particle size of amorphous microporous silica for diffusive controlled release of drug compounds. *The Journal of Physical Chemistry C* 111(36), 13404-13409. <https://doi.org/10.1021/jp0735076>
- [49] Bavnhøj, C.G.; Knopp, M.M.; Madsen, C.M.; Löbmann, K.; 2019. The role interplay between mesoporous silica pore volume and surface area and their effect on drug loading capacity. *International Journal of Pharmaceutics: X* 1, 100008. <https://doi.org/10.1016/j.ijpx.2019.100008>
- [50] Li, J.; Xu, L.; Wang, H.; Yang, B.; Liu, H.; Pan, W.; Li, S.; 2016. Comparison of bare and amino modified mesoporous silica@poly(ethyleneimine)s xerogel as indomethacin carrier: Superiority of amino modification. *Materials Science and Engineering: C* 59, 710-716. <https://doi.org/10.1016/j.msec.2015.10.072>

- [51] Wei, Q.; Keck, C.M.; Müller, R.H.; 2017. Preparation and tableting of long-term stable amorphous rutin using porous silica. *European Journal of Pharmaceutics and Biopharmaceutics* 113(Supplement C), 97-107.
<https://doi.org/10.1016/j.ejpb.2016.11.009>
- [52] Thomas, M.J.K.; Slipper, I.; Walunj, A.; Jain, A.; Favretto, M.E.; Kallinteri, P.; Douroumis, D.; 2010. Inclusion of poorly soluble drugs in highly ordered mesoporous silica nanoparticles. *International Journal of Pharmaceutics* 387(1), 272-277.
<https://doi.org/10.1016/j.ijpharm.2009.12.023>
- [53] Wei, Q.; Keck, C.M.; Müller, R.H.; 2017. Oral hesperidin—Amorphization and improved dissolution properties by controlled loading onto porous silica. *International Journal of Pharmaceutics* 518(1–2), 253-263.
<http://dx.doi.org/10.1016/j.ijpharm.2016.11.005>
- [54] Sliwinska-Bartkowiak, M.; Dudziak, G.; Gras, R.; Sikorski, R.; Radhakrishnan, R.; Gubbins, K.E.; 2001. Freezing behavior in porous glasses and MCM-41. *Colloids and Surfaces A: Physicochemical and Engineering Aspects* 187–188, 523-529.
[http://dx.doi.org/10.1016/S0927-7757\(01\)00637-9](http://dx.doi.org/10.1016/S0927-7757(01)00637-9)
- [55] Gupta, M.K.; Goldman, D.; Bogner, R.H.; Tseng, Y.-C.; 2001. Enhanced Drug Dissolution and Bulk Properties of Solid Dispersions Granulated with a Surface Adsorbent. *Pharmaceutical Development and Technology* 6(4), 563-572.
<https://doi.org/10.1081/PDT-120000294>
- [56] Watanabe, T.; Hasegawa, S.; Wakiyama, N.; Kusai, A.; Senna, M.; 2002. Prediction of apparent equilibrium solubility of indomethacin compounded with silica by ¹³C solid state NMR. *International Journal of Pharmaceutics* 248(1–2), 123-129.
[http://dx.doi.org/10.1016/S0378-5173\(02\)00428-3](http://dx.doi.org/10.1016/S0378-5173(02)00428-3)
- [57] Vadher, A.H.; Parikh, J.R.; Parikh, R.H.; Solanki, A.B.; 2009. Preparation and Characterization of Co-Grinded Mixtures of Aceclofenac and Neusilin US2 for Dissolution Enhancement of Aceclofenac. *AAPS PharmSciTech* 10(2), 606-614.
<https://doi.org/10.1208/s12249-009-9221-6>

- [58] Qian, K.K.; Suib, S.L.; Bogner, R.H.; 2011. Spontaneous crystalline-to-amorphous phase transformation of organic or medicinal compounds in the presence of porous media, part 2: Amorphization capacity and mechanisms of interaction. *Journal of Pharmaceutical Sciences* 100(11), 4674-4686. <https://doi.org/10.1007/s11095-012-0734-4>
- [59] Konno, T.; Kinuno, K.; Kataoka, K.; 1986. Physical and Chemical Changes of Medicinals in Mixtures with Adsorbents in the Solid State. I. : Effect of Vapor Pressure of the Medicinals on Changes in Crystalline Properties. *Chemical & Pharmaceutical Bulletin* 34(1), 301-307. <https://doi.org/10.1248/cpb.34.301>
- [60] Bouledjoudja, A.; Masmoudi, Y.; Van Speybroeck, M.; Schueller, L.; Badens, E.; 2016. Impregnation of Fenofibrate on mesoporous silica using supercritical carbon dioxide. *International Journal of Pharmaceutics* 499(1), 1-9. <https://doi.org/10.1016/j.ijpharm.2015.12.049>
- [61] Cha, K.-H.; Cho, K.-J.; Kim, M.-S.; Kim, J.-S.; Park, H.J.; Park, J.; Cho, W.; Park, J.-S.; Hwang, S.-J.; 2012. Enhancement of the dissolution rate and bioavailability of fenofibrate by a melt-adsorption method using supercritical carbon dioxide. *International Journal of Nanomedicine* 7, 5565-5575. <https://doi.org/10.2147/IJN.S36939>
- [62] Miura, H.; Kanebako, M.; Shirai, H.; Nakao, H.; Inagi, T.; Terada, K.; 2011. Influence of particle design on oral absorption of poorly water-soluble drug in a silica particle–supercritical fluid system. *Chemical and Pharmaceutical Bulletin* 59(6), 686-691. <https://doi.org/10.1248/cpb.59.686>
- [63] Vogt, F.G.; Roberts-Skilton, K.; Kennedy-Gabb, S.A.; 2013. A Solid-State NMR Study of Amorphous Ezetimibe Dispersions in Mesoporous Silica. *Pharmaceutical Research* 30(9), 2315-2331. <https://doi.org/10.1007/s11095-013-1075-7>
- [64] Limnell, T.; Santos, H.A.; Mäkilä, E.; Heikkilä, T.; Salonen, J.; Murzin, D.Y.; Kumar, N.; Laaksonen, T.; Peltonen, L.; Hirvonen, J.; 2011. Drug delivery formulations of ordered and nonordered mesoporous silica: comparison of three drug loading methods. *Journal of Pharmaceutical Sciences* 100(8), 3294-3306. <https://doi.org/10.1002/jps.22577>

- [65] Safari, M.; Ebrahimi, A.; Langrish, T.; 2016. A novel formulation for solubility and content uniformity enhancement of poorly water-soluble drugs using highly-porous mannitol. *European Journal of Pharmaceutical Sciences* 83, 52-61.
<https://doi.org/10.1016/j.ejps.2015.12.016>
- [66] Jacobsen, S.; 2013. *Arzneiformlehre: ein Wegweiser in Bildern*, 2nd ed. Wissenschaftliche Verlagsgesellschaft, Stuttgart. ISBN: 978-3804731615
- [67] Wei, Q.; 2016. *Nanocrystals & loaded porous silica for increased oral bioavailability* [doctoral thesis]. [Germany]: Freie Universität Berlin. urn:nbn:de:kobv:188-fudissthesis000000104838-8

General Considerations

2. smartPearls – Novel physically stable amorphous delivery system for poorly soluble dermal actives¹

Abstract

Dermally applied poorly soluble actives whether in cosmetics or pharmaceuticals show insufficient skin penetration. Especially actives being insoluble in both phases of dermal vehicles, i.e. water and oil have no or less real effect. An approach to overcome this obstacle is the use of amorphous actives instead of the crystalline ones. The higher saturation solubility creates an increased concentration gradient between the formulation and skin. Thus, the diffusive flux into the skin is improved. However, the amorphous state of actives is highly labile, and the durability of such formulations would be too short for a marketable product. smartPearls is a novel technology efficiently long-term stabilize the amorphous state. They consist of μm sized particles with mesopores (e.g. silica: SYLOID[®], AEROPERL[®], Neusilin[®]), in which the active can be loaded and preserved in amorphous state. Due to the tightness of the pores, not enough space is given for re-crystallization. In this work, the skin penetration of poorly soluble actives loaded in smartPearls is compared to the present “gold standards” in dermal delivery, e.g. amorphous microparticles, amorphous nanoparticles and nanocrystals. The performance was at least similar or even better than the gold standards, explainable by the increased saturation solubility of active due to a) amorphous state and b) nanostructure inside the μm -sized particles. Sedimentation investigations showed, that the physical stabilization of very dense smartPearls in semi-solid vehicles is possible by viscoelastic repulsion. Also, the technical, regulatory, and marketing aspects for the use of smartPearls technology in products are discussed, e.g. status of excipients used, and advantages of not being a nanoparticle, but being as efficient as them. Overall, smartPearls proved to be a promising dermal delivery technology for poorly soluble actives with a high market potential.

¹ This chapter has been published as:

Müller, R.H.; Hespeler, D.; Jin, N.; Pyo, S.M.; 2019. smartPearls – Novel physically stable amorphous delivery system for poorly soluble dermal actives. *International Journal of Pharmaceutics* 555, 314-321.
<https://doi.org/10.1016/j.ijpharm.2018.11.018>

2.1. Introduction

Many poorly soluble actives in cosmetics and pharmaceuticals show insufficient skin penetration, not reaching the minimum required concentration for real effect. The low passive diffusion of active into the skin can be explained by the active's low solubility, not creating an adequate concentration gradient between formulation and skin ($C_s - C_{skin}$). Especially actives being poorly soluble in water and at the same time in organic solvents, e.g. oils in creams and ointments, are highly problematic. Saturation solubilities of so-called poorly soluble actives are below 1 mg/mL, including many cosmetically highly interesting antioxidants, e.g. rutin in water (75 $\mu\text{g/mL}$) and resveratrol in water (30 $\mu\text{g/mL}$) [1; 2]. Also pharmaceutical drugs have low solubilities and therewith related penetration problems, e.g. cyclosporine A, 6.6 $\mu\text{g/mL}$ in water [3]. Even if those actives are better soluble in the oil phase of dermal vehicles, penetration can still be extremely limited since a lipophilic molecule prefers the lipophilic surrounding in the oil instead of the lipophilic-hydrophilic skin structure (question of partitioning coefficient K). As an old "pharmaceutical rule" for dermal formulations for such molecules, the application as aqueous suspension is preferable.

One strategy to increase the penetration of those actives is the generation of higher concentration gradient between formulation and skin by increasing their solubility. A meanwhile very old approach is complexation for example with macromolecules, e.g. polyethylene glycol or cyclodextrin. The pitfall for such complexes is their potentially high binding constant, which even hinders the diffusion of the complexed actives into the skin. In case of molecules soluble in organic solvents, water solvent mixtures might be used in the dermal formulation. However, after skin application, the organic co-solvent (very often ethanol) typically evaporates fast, leading to precipitation of large active crystals on the skin. These solid actives are unable to penetrate anymore. Even when using slow evaporating co-solvents, e.g. glycerol with a boiling point 290 °C, the active can precipitate in case the co-solvent penetrates faster into the skin than the active molecule [4]. This particularly happens, when the diffusion coefficient D is considerably higher for the low molecular weight co-solvent compared to the high molecular weight active molecule, e.g. glycerol 91 g/mol vs. rutin 611 g/mol.

A highly efficient and well-known strategy to increase the saturation solubility C_s of actives is the simple change of their physical state, like creating amorphous particles in the dermal

formulation. The amorphous state has generally a higher saturation solubility C_s , precisely a so called “supersaturated concentration C_{ss} ”, compared to the crystalline state. For example, solubility of crystalline rutin is 75 $\mu\text{g}/\text{mL}$ in water, but 4,000 $\mu\text{g}/\text{mL}$ in the amorphous state [2]. However, the limitation for the use of amorphous actives is their lack of physical long-term stability. Re-crystallization is a statistical event. Thus, physical stability cannot be calculated as the chemical stability by using the Arrhenius equation. Due to the non or difficult predictable shelf life, amorphous dermal formulations play practically no industrial role.

An industrially feasible change of particles physical property is the reduction of their size to below 1 μm , the so-called nanocrystals. The saturation solubility C_s in a suspension is the equilibrium between dissolving molecules (dissolution pressure) and molecules re-crystallizing on the surface of crystals (re-crystallization pressure). Below the crystal size of about 1 μm , the dissolution pressure increases, and the equilibrium is shifted in favor of dissolved molecules, C_s increases. For example, rutin microcrystals have the C_s of 75 $\mu\text{g}/\text{mL}$ (= thermodynamic equilibrium solubility), but rutin nanocrystals with a size of 727 nm possess a C_s of 133 $\mu\text{g}/\text{mL}$ [5]. This technology was originally developed from Liversidge and co-workers to increase the bioavailability of poorly soluble drugs for oral administration (company Nanosystem/élan) [6] under the name NanoCrystals. Later on, the nanocrystal technology was transferred to the dermal application route by PharmaSol, Germany, under the name smartCrystals [7]. Products containing this technology are already on the cosmetic market. The first one was introduced in 2007 by Juvena Switzerland and shortly after La Prairie followed with the product line Platinum Rare. Besides, various cosmetic actives are commercially available as smartCrystal concentrates ready to be admixed into cosmetic products (e.g. rutin, hesperidin). The strategy of changing the physical state of actives proved to be highly effective for nanocrystals.

Thus, as next logical development step, both changes (nano-size and amorphous state) were combined, to superimpose the solubility enhancing effects of both technologies. According to these thoughts, the company BASF generated particles being at the same time in the nanodimension and amorphous state. This combination technology developed by Auweter and co-workers is called NanoMorph [8] and used in the food sector (e.g. carotenoids for soft drinks, LycoVit® [9]), where physical stability criteria is not as strict as in the pharma. In the

pharmaceutical sector, this technology was marketed by the company Abbott, but with little success, because of the fear of re-crystallization during the shelf life of the final product.

In summary, the smartest approach for solubility enhancement is the combination of nano-dimension and amorphous state. However, pre-requisite for industrial use is an effective stabilization of the amorphous state in nano-dimension. This was realized by the novel smartPearls technology. smartPearls are mesoporous particles made from, e.g. silica or polymers and the cosmetic or pharmaceutical active is loaded into the mesopores in the amorphous state. The location of active in the pores stabilizes its amorphous state for more than 5 years [2]. This article briefly describes the historical development of smartPearls and the physics behind the technology, quantifies the penetration enhancement compared to already existing technologies, i.e. microsuspensions, nanosuspensions, and outlines the production of marketable dermal formulations using viscoelastic gel systems.

2.2. Historical development

Identical to nanocrystals, the technology was originally developed for the oral administration route with the aim of optimally deliver poorly soluble drugs for an increased bioavailability. In 1979, Yang et al. improved the dissolution of the drugs prednisolone, digoxin and griseofulvin in GI fluids by incorporating them in mesoporous silica particles and many other researchers followed working on this principal. A list of the most commonly processed drugs is given in table 1.

Table 1: Overview of the three most frequently incorporated drugs in mesoporous silica.

drug	examples for publications
Ibuprofen	2004 Charnay et al. [10]
NSAID	2009 Fernandez-Nunez et al. [11]
	2011 Shen et al. [12]
	2012 Vialpando et al. [13]
	2013 Delle Piane et al. [14]
Naproxen	2004 Cavallero et al.[15]
NSAID	2010 Halamova et al.[16]
	2012 Vialpando et al.[13]
	2013 Guo et al.[17]
Itraconazole	2008 Mellaerts et al.[18]
antifungal	2011 Kinnari et al.[19]
	2012 Vialpando et al. [13]

The first patent application was filed by the company Capsulation Pharma in Berlin/Germany [20]. The drugs, e.g. candesartan cilexetil, were loaded into the mesopores of silica, e. g. Neusilin® US2. Because an **encapsulation** was performed in the **amorphous** state, registered trade name was CapsMorph® (PharmaSol/Germany). Re-analysis of about 30 formulations produced by Capsulation Pharma after more than 3 years of storage showed, that all 30 formulations were still in the amorphous state [21]. Meanwhile, this principle is also exploited by other companies for oral administration, e.g. Merck Millipore with Parteck® SLC; the Belgium company Formac Pharmaceuticals with monodisperse pores [22] and Formac Pharmaceuticals in cooperation with W. R. Grace US [23]. In the next development step – identical to the transfer of orally used nanocrystals to dermal application – the porous particle technology was transferred to the skin by PharmaSol Germany and W. R. Grace US [24] with the registered trade name smartPearls. The increased oral bioavailability resulted from increased concentration gradient between human digestive system and blood C_s-C_{blood} .

In principle, the increased concentration gradient should also promote penetration into the skin – identical to nanocrystals.

2.3. Intellectual property aspects

The transfer from oral to dermal administration route was not implemented because of the concern, that re-crystallization should occur in dermal vehicles. In oral tablets and capsules, the loaded porous particles are in a dry and solvent-free environment (i.e. a solid-gas dispersion), where in contrast dermal vehicles consist of water and/or oil. Even though the drugs are poorly soluble, the vehicle still acts as a solvent, promoting the dissolution of drugs. When supersaturated state is reached in the vehicle, re-crystallization occurs on the surface of amorphous particles, promoting further re-crystallization as an initiator.

In supersaturated solutions, crystals can also precipitate in the water phase, when heading back from the supersaturation solubility C_{ss} towards the thermodynamic equilibrium saturation solubility C_s . Against these theory-based expectations, no re-crystallization occurred in dermal vehicles after smartPearls incorporation. Even in dermal vehicles, the amorphous state in smartPearls were physically stable for up to now 1.5 years. Also, no crystal formation was observed in the vehicle itself [25]. These data against the theoretical considerations were a) new and b) one of the innovative heights of the patent application [24].

During the loading process of porous particles, it is unavoidable that small quantities of active precipitates on the surface of the porous particles, as shown by Jin et. al. [25]. In the case that this layer is very thin, and does not provide enough substance to form crystals, the precipitated active remains on the surface in amorphous state. In the case of overloading, the layer exceeds a critical thickness and crystallization occurs, detectable by X-ray diffraction (Figure 1).

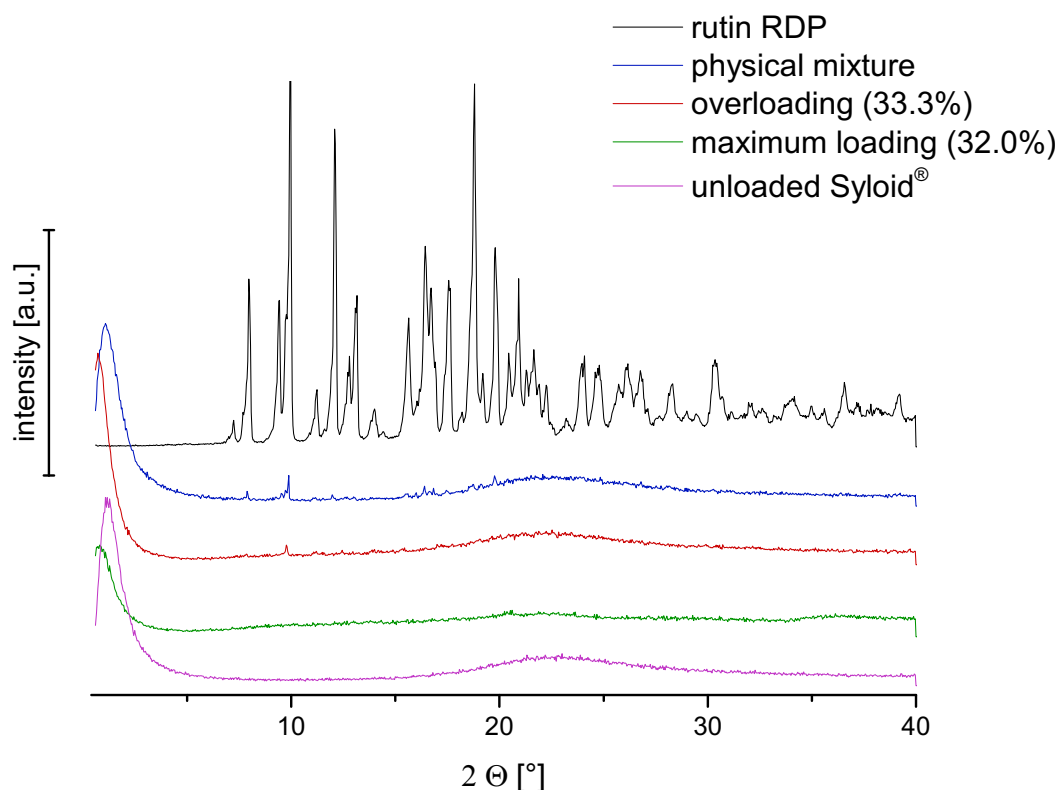


Figure 1: From top to bottom: X-ray diffraction patterns of rutin raw drug powder (rutin RDP), physical mixture of rutin and SYLOID[®], SYLOID[®] loaded with 33.3% (= overloaded, crystallization of rutin), SYLOID[®] loaded with 32% rutin (= maximum loading) and unloaded SYLOID[®] (with permission from [25]).

2.4. Mechanistic considerations

Precipitation of actives in liquid phases leads in most cases to the formation of crystalline particles, μm - or nm -sized (e. g. nanocrystals). Crystals are formed even when the particle size is in the range of 20 nm to 50 nm. This principle is applied to produce nanocrystals in the bottom-up technology [26]. Thus, only by choosing special precipitation conditions as done in the case of NanoMorph [27], amorphous nanoparticles can be generated. However, they often still have the tendency to re-crystallize. Porous particles can be loaded by various methods [28], e. g. by solvent impregnation [29-31] or solvent free by co-milling [32-34] or by supercritical carbon dioxide [30; 35; 36]. In case of the solvent impregnation method, the pores are filled with organic solution of the active. Afterwards, the solvent is evaporated and the active precipitates. Due to the small size of mesopores (2-50 nm) there is not enough space to initiate the crystal formation. This theory is called "space restriction" [18; 34]. Space restriction are effective in pores with up to 50 nm in diameters, even though crystals formed

in liquid faces without space restriction are 10-20 nm small and would theoretically fit into a 50 nm pore. In the smartPearls technology no precipitation in amorphous phase was observed even for macropores > 50 nm. Data show that the amorphous state in pores is stable for up to 3 years in dry powder form [2] and up to 1.5 years in the water phase of dermal vehicles (data by now [25], Figure 2 and 3). Investigations were performed by combining X-ray diffraction and differential scanning calorimetry (DSC). Based on this data, stable dermal formulations are feasible as products for the cosmetic and pharmaceutical market.

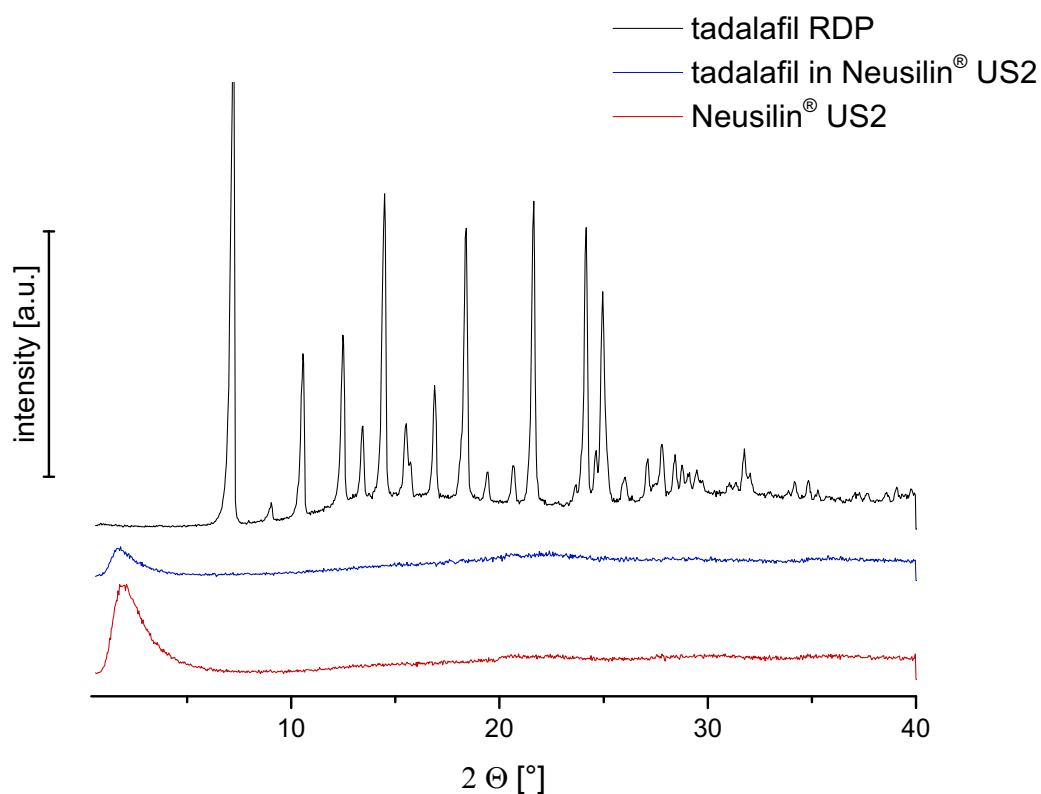


Figure 2: From top to bottom: X-ray diffraction patterns of tadafafil raw drug powder (RDP), tadafafil loaded Neusilin® US2 (after 3 years of storage) and unloaded Neusilin® US2. No crystallinity peaks were detected, thus tadafafil was efficiently preserved in amorphous state (after Grabo et. al. [37]).

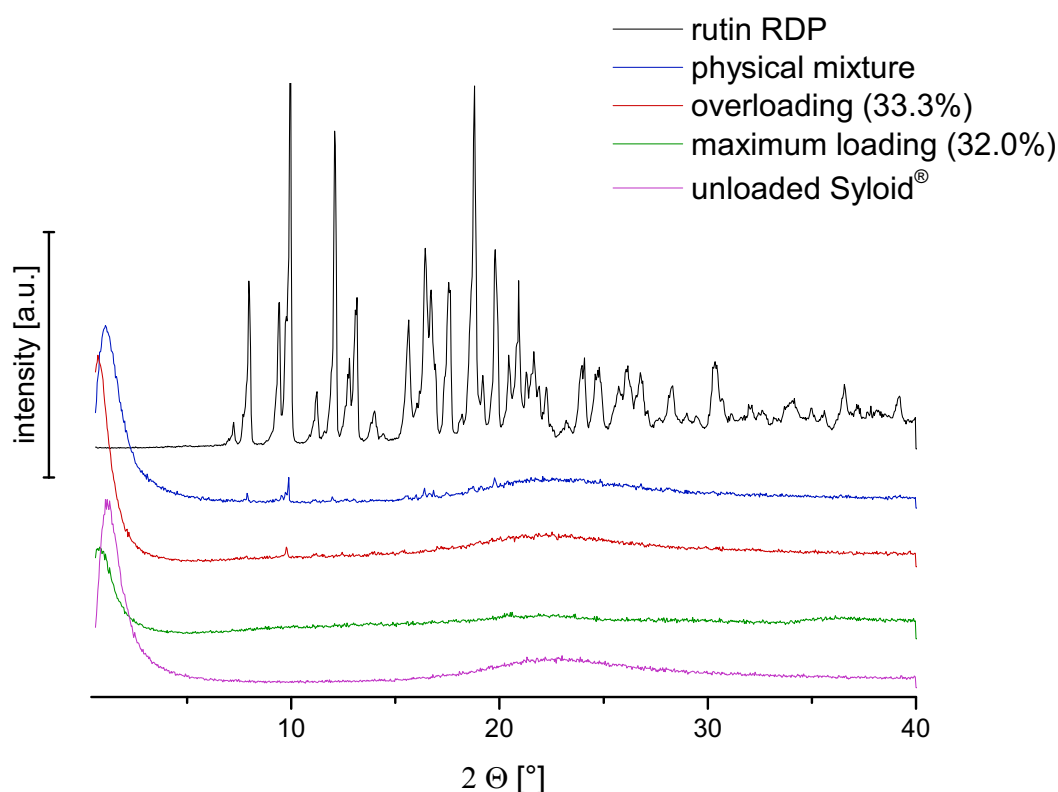


Figure 3: From top to bottom: X-ray diffraction patterns of rutin raw drug powder (RDP), physical mixture of rutin RDP and SYLOID®, amorphous rutin loaded in SYLOID® (rutin smartPearls, after 1.5 years of storage), rutin smartPearls incorporate in hydrogel (after 1.5 years of storage) and hydrogel itself. No crystallinity peaks were detected for smartPearls, whether as dry powder or in hydrogel, proving the effective preservation of amorphous state (with permission from Jin et. al. [25]).

2.5. Porous particle materials for smartPearls: technical, regulatory & marketing aspects

2.5.1. Technical aspects

Basically, any porous material can be used for producing active loaded smartPearls, inorganic but also organic materials either natural or synthetic. From the technical side, amorphization of actives can be already achieved by the interaction of active molecules with carrier surfaces. With increasing interactions between active molecule and carrier surface, also the likelihood of active amorphization increases [14]. Creating amorphous actives via this principle is thus limited to the specific surface area of the carrier. However, in addition to this surface bonded amorphous fraction of active, a large part of active can be amorphized via loading into the mesopores of the carrier [38; 39]. This can be explained by the fact that a certain space is

needed for the re-crystallization process, which is not given in the mesopores (diameter sizes of 2-50 nm). Crucial for this stabilization principle is the selection of the correct pore size in relation to the molecular weight of active. Amorphous state is preserved if the ratio of pore size to molecule size is smaller than 12 [40]. For a high amount of amorphized active, the carrier should possess a sufficiently high pore volume, preferentially in the range of 1.0 to 1.7 mL/g. Till now, around 1.7 mL/g is the highest pore volume commercially available, e.g. SYLOID® and corresponds to a maximum theoretical loading of 75% (w/w) by assuming an active density of 2.0 g/mL.

By using ordered silica, the critical carrier parameters, in particular the specific surface and number of surface silanol groups, can be individually adapted to the needs, i.e. the structure of active molecule. However, as they are tailor made, the prize is in most cases at least 10 times higher than for non-ordered silica (~1500 €/kg for ordered silica and ~150 €/kg for non-ordered silica). In addition, the majority of ordered silica have not yet been approved as pharmaceutical excipients, why the non-ordered silica are still preferred for product development. Non-ordered silica have a broader pore size distribution as the ordered silica, but long-term stabilization of amorphous state is feasible, and stabilities of even up to 7 years are reported. For the selection of a suited non-ordered silica, a safety margin of 5% on the upper limit of the pore diameter is recommended. The large number of non-ordered silica on the market possessing different properties, should allow to find a suitable one for many various actives.

Further to these properties, the carrier should have particle sizes preferentially about 1-5 µm to minimize sedimentation effect in dermal formulations. Both viscosity and rheological properties of dermal vehicle finally determine the maximum possible particle size. A sandy feeling on the skin does not even occur with particle sizes of about 50 µm [25], thus can be problem-free used in dermal formulations. A sandy feeling on the skin does not even occur with particle sizes of about 50 µm [25], thus can be problem-free used in dermal formulations.

2.5.2. Regulatory aspects

To be used in market products, the materials should be non-toxic, well tolerated by the skin and most important, are regulatory accepted. This is the case for porous silica particles but also other inorganic materials, e. g. calcium phosphate. Looking farsighted in the future,

materials should be avoided which are still regulatorily accepted at present but might lose this acceptance in the future. Examples are particles containing aluminum ions being presently heavily under discussion in deodorants [41]. Silica particles used preferentially in dermal formulations are various SYLOID[®] silica particles from W. R. Grace US and AEROPERL[®] from Evonik. Table 2 provides an overview about their most important features.

Table 2: Overview of silica particles and their relevant properties for the use as smartPearls in dermal formulations.

product name	manufacturer	average pore size [nm]	size distribution [µm]	specific surface area [m ² /g]	pore volume [mL/g]
Neusilin [®] US2	Fuji Chemical Industry, Japan	5-6	44-177	300	1.2
AEROPERL [®] 300 Pharma	Evonic Industries AG, Germany	2-20	30-40	300	1.6
SYLOID [®] SP53D-11920	Grace GmbH & Co. KG, Germany	6	12	550	0.9

2.5.3. Marketing aspects

The marketing should meet the expectations of the customers. Important is to know, that consumers expectations are different for cosmetics and pharmaceuticals even though both are dermally applied. In dermal pharmaceuticals, the patients are willing to accept products with unpleasant application properties (application feeling, smell, appearance) or critical excipients as long as the therapy of disease is effective. However, in cosmetics the consumer expects appealing product properties (pleasant application feeling, pleasant smell). Furthermore, consumers expect that modern products are for example natural or organic and not synthetic, environment-friendly and if possible, comply with ECOSERT (one of the world’s biggest organic certification organization for organic products, also cosmetics, according to ISO 17065). This excludes synthetic polymers, especially ones which are not biodegradable. Based on ecological expectations, particles from natural materials should be preferred, i.e. silica (Table 2).

Meanwhile there is an increasing reluctance of the public towards “nano”, promoted by newspaper articles how dangerous “nano” is. Nano is still fully accepted in pharma, especially if “nano”-pharmaceutics cures your cancer or solves your atopic dermatitis or psoriasis problem. “Nano” is also still accepted in cosmetics, since people accept a lot for their beauty. But in food sector, it is completely different. Like GMO (gen modified organisms), most consumers do not want “nano” in their food products. Cosmetic companies try to meet the “anti-nano” trend by developing new products being nano-free, to avoid the INCI declaration of nano on product labels.

Based on this, smartPearls are no nanoparticles according to the EU regulation ((EC) No 1223/2009). They are clearly in the μm range (EU cosmetic definition of nanoparticles: more than 50 % of particles need to be smaller than 100 nm after number distribution). Also, according to other non-cosmetic EU regulations (2011/696/EU) the silica particles are no “nanomaterial”, since they are dissolvable particles, even though they are low soluble. Nowadays, marketing does less emphasize what is in a product, but even more what is not in the product, i.e. “free of ...”. Obviously, the consumer is meanwhile focused on this – even when the advertising is completely ridiculous. For example, advertising “cholesterol-free” in products which can absolutely not contain any cholesterol at all being. To meet such consumer expectations world-wide, smartPearls can be advertised “nano-free, synthetic-free etc.”, and in addition with positive features such as “natural, eco-friendly etc.”.

2.6. smartPearls on skin – penetration performance

A pre-requisite for a successful market entry is the presence of a clear advantage whether in terms of technology, costs, or marketing. One marketing advantage can be, that a product has a “selling story” – despite being not superior compared to other marketed products. A cost advantage can be a development of a product performing identically compared to already existing products but being less costly in production or in feed material. A technical advantage can be that the products performs better compared to already existing products. In case of smartPearls this would be the increased skin penetration.

The present gold standard for improved skin penetration are nanocrystals. Another competing technology in skin penetration is the use of amorphous actives, ignoring the hurdle of limited physical stability for marketable products. To assess the performance and value of the delivery

system, the smartPearls should be therefore compared with nanocrystals and amorphous actives (μm -sized). Even more challenging would be if smartPearls would be compared to nanoparticles being at the same time amorphous (amorphous nanoparticles), since the solubility enhancing effects of nanosize and amorphous superimpose.

The ideal compound for such a study is cyclosporine A, having poor skin penetration and being available as relatively stable amorphous powder. Thus, for the study 3 formulations were prepared with cyclosporine A [25]:

- amorphous μm -crystal suspension gel
- amorphous nanoparticles (milled by high pressure homogenization)
- smartPearls loaded with amorphous cyclosporine A

Penetration was studied ex-vivo on porcine ear skin by tape stripping [42; 43], being a well-established method to differentiate various dermal formulations regarding both total amount of penetrated active and penetration depth. Freshly isolated porcine ears were obtained from local slaughterer and used on the very same day for penetration studies. Before usage, the integrity of the skin was tested by measuring its transdermal water loss. Only then defined amount of formulations were applied on defined area of porcine ear skin and removed after 20 minutes of application time. The treated skin was removed layer by layer using successively 30 adhesive tapes. As special challenge, 5% cyclosporine A were incorporated into the suspension gel and the amorphous nanoparticle gel, respectively, but only 1% in the smartPearls gel.

The penetration from the amorphous μm -crystal suspension gel is below the other 2 formulations and the smartPearls formulation is clearly superior, especially in the deeper skin layers (Figure 4). For simpler comparison, the penetrated amount in various tapes ($\mu\text{g}/\text{tape}$) are normalized by dividing them by the applied total concentration in the dermal formulation (i.e. μg per tape/%). Based on these results, the smartPearls are a promising alternative to the amorphous nanoparticles and nanocrystals, showing a better performance and having the advantage of not being nano, independent from definition used (EU regulation < 100 nm or pharmaceutical regulation $< 1,000$ nm). How can the superiority of smartPearls be explained, even being better than amorphous cyclosporine A particles? This is based on the fact that the active is in amorphous state and dispersed in the structure of the porous particles. Since the pores are between 2-50 nm in diameter, the loaded active exhibit

simultaneously the advantage of being nanosized and amorphous. Since the size in the pores are restricted to a maximum 50 nm, they are even finer dispersed than the amorphous nanoparticles, leading to higher saturation solubility and thus improved penetration. Also, with regards to cost advantages, the smartPearls are superior, since a higher penetrated amount was achieved with only one fifth of the concentration used in the nanoparticle formulation. Meaning, that for same effectiveness less amount of active is needed. Especially in cases of expensive actives, a clear cost advantage is given, e.g. cosmetic antioxidant glabridin (about 20,000 USD/kg). smartPearls were also compared to other nanocrystals of, e.g. rutin [25] and hesperidin [25]. In all cases, the smartPearls showed a superior penetration.

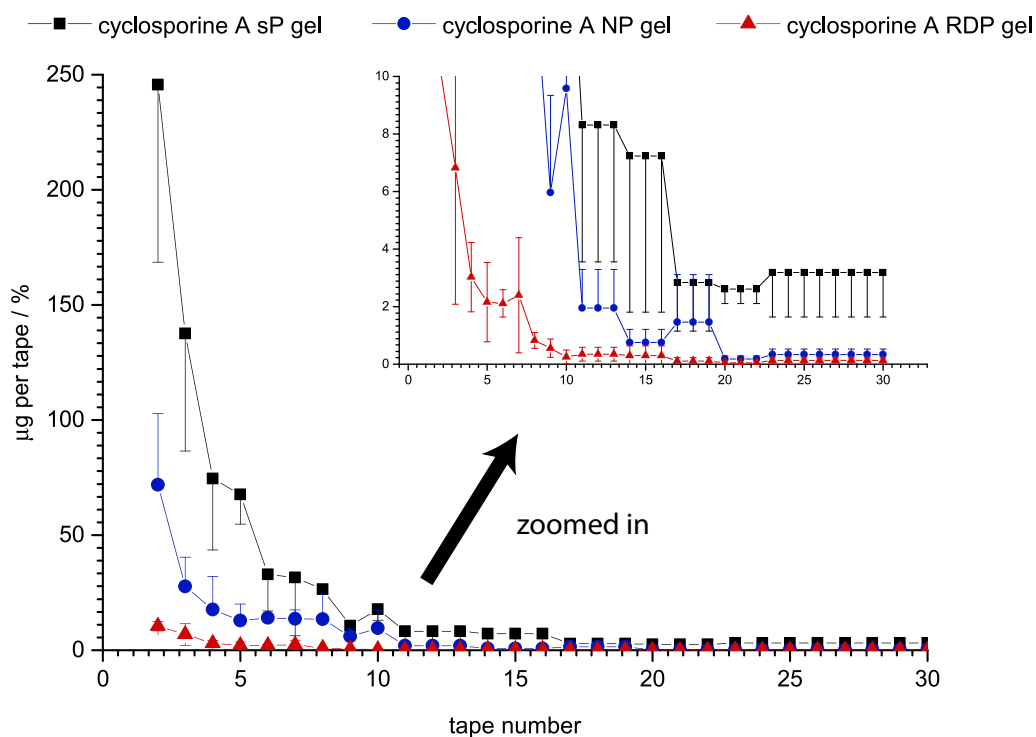


Figure 4: Penetration profiles of cyclosporine A formulations from top to bottom: amorphous cyclosporine A smartPearls in hydrogel (only 1% cyclosporine A), amorphous cyclosporine A nanoparticles in hydrogel (5% cyclosporine A) and crystalline cyclosporine A raw drug powder (5 % cyclosporine A). Data were displayed normalized by dividing the penetrated amount per tape by the cyclosporine A concentration in formulation (with permission from [25]).

2.7. Final market formulations

The final market formulations will be typically gels, o/w creams or lotions, where the smartPearls are dispersed in the water phase. Dispersing smartPearls in oils is also possible,

i.e. incorporation into water-free ointments. The particle size needs to be below 50 μm to avoid a sandy feeling on skin [24]. Another effect related to size is the potential sedimentation. According to Stokes' law sedimentation is a function of size d , particle density σ and viscosity η of the dispersion medium. The density of dry, air filled porous silica is very low ($\sigma \ll 1 \text{ g/mL}$), but increases strongly after active loading (σ average of actives around 2 g/mL) and water uptake from the dermal vehicle. Based on this, the size should be preferentially even below 5 μm . However, also distinctly larger particle sizes can be used when incorporated into a viscoelastic vehicle. Viscoelastic systems are already well known from food products, e.g. salad dressing with non-sedimenting herbs, even when they are resting for years (Figure 5, middle).

In a purely viscous system, sedimentation at a given viscosity is a function of size and particle density, being non-existent or very slow for small sized particles with low density (Figure 5, left). In a viscoelastic system a rebound effect occurs when a particle is sedimenting. Like falling on a spring, the particle is drawn back to its initial position. The related size for non-sedimenting particles depends on the yield force F_Y of the system. If F_Y is not exceeded, the particles will not sediment, and a stable, non-sedimenting particle dispersion can be obtained (Figure 5, right).

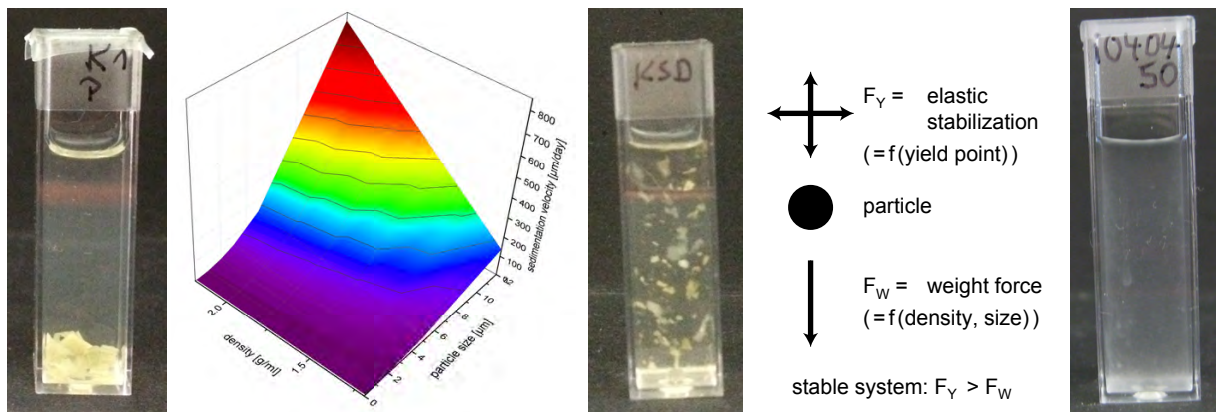


Figure 5: Normalized sedimentation velocity per day (z-axis: $\mu\text{m/day}$) in normal viscous systems as a function of particle size (y-axis: μm) and density (x-axis: g/mL) for herbs incorporated in an 1% HPC gel (left). A clear sedimentation of herbs is visible. In contrast, herbs stayed homogenous distributed in viscoelastic salad dressing (middle), as well as the 50 μm smartPearls in viscoelastic hydrogel (right). The viscoelastic stabilization takes place, when the rebound force (F_Y) of the elastic gel exceeds the weight force (F_W) of the particles ($F_Y > F_W$).

To assess the difference in suspension stabilization, unloaded smartPearls (SYLOID®) were incorporated into a classical viscous hydroxypropyl cellulose gel (HPC, 5%), in a viscoelastic gel

obtained by filtration from a viscoelastic salad dressing (KSD) and a self-made, pharmaceutically defined viscoelastic gel using ι-carrageenan at 0.35%. To challenge the systems, very large sized SYLOID® particles with mean diameters of 150 μm were used. Freshly produced gels with SYLOID® were stored in photometric cuvettes and the occurrence or absence of sedimentation was investigated by macroscopic observation and photometric measurements at a wavelength of 500 nm. In addition, rheological properties of the gels were characterized by both shear stress sweep and frequency sweep analysis. Already 1 day after, the particles sedimented in the classical viscous HPC gel formulation, with a clear supernatant phase being formed (Figure 6, left). In contrast, no sedimentation was visible in both viscoelastic gels, salad dressing and ι-carrageenan gel. Also, the photometric value stayed constant during storage time.

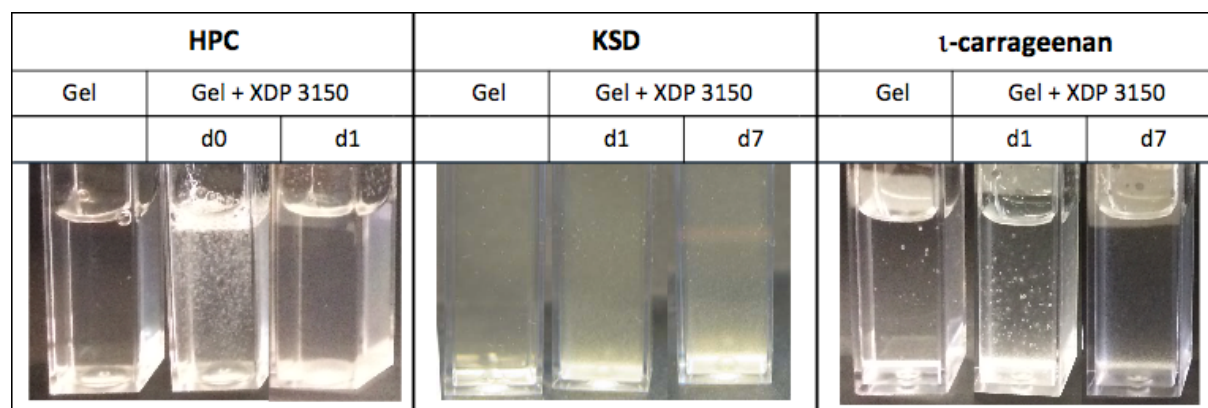


Figure 6: Macroscopic evaluation of hydrogels (viscous HPC gel, viscoelastic salad dressing and ι-carrageenan) without (left) or with 150 μm sized SYLOID® particles directly after incorporation (middle) and after storage (right). Complete sedimentation was observed already after 1 day of storage for viscous HPC gel, where in salad dressing and ι-carrageenan gel no sedimentation was observed even after 7 days of storage.

Rheological evaluation revealed a shear thinning flow behavior for the HPC gel (Figure 7, left). For the viscoelastic pharmaceutical gel, a yield point and an elastic limit was detected (Figure 7, right). Depending on the yield point and the elastic limit, respective sized particles will show no sedimentation at all, staying in abeyance as clearly visible in the macroscopic images (Figure 6). Based on this, the addition of viscoelastic gel formers to the water phase of dermal vehicles enables the incorporation of relatively large porous particles. Thus, the production physically long-term stabilized smartPearls formulations are possible.

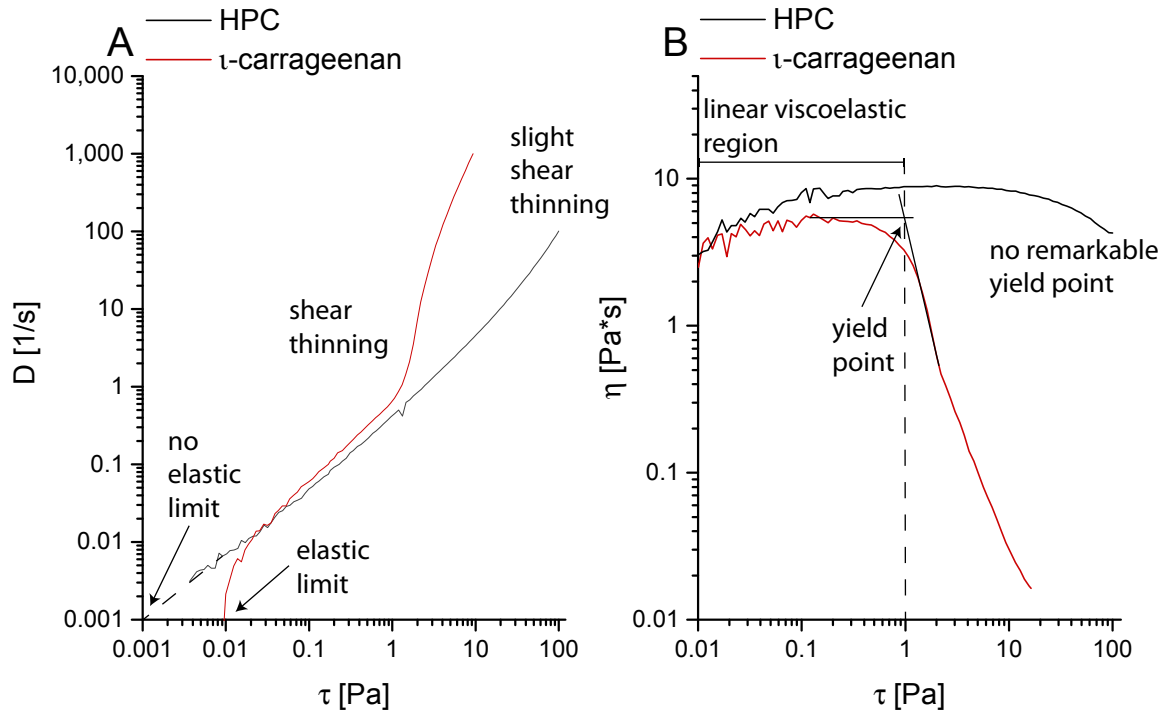


Figure 7: Rheological graphs of HPC and ι -carrageenan gel measured with a 1° cone-plate for 300 s at a rotation shear stress increasing from 0-100 Pa. A: shear velocity D (y-axis) versus shear stress τ (x-axis) is plotted, showing a stronger shear thinning behavior and an elastic limit of 0.01 Pa for the ι -carrageenan gel. B: shear viscosity η (y-axis) versus shear stress τ (x-axis) is plotted, showing almost similar viscosities for both gels in the linear viscoelastic region. For ι -carrageenan gel a yield point at 1 Pa is clearly visible.

2.8. Conclusions & Perspectives

The smartPearls technology is at least similar effective as amorphous actives, amorphous nanoparticles, and nanocrystals (crystalline nanoparticles). In contrast to amorphous actives, the amorphous state in the smartPearls is long-term preserved, and in contrast to amorphous nanoparticles and nanocrystals, the smartPearls are not “nano”, meeting the upcoming expectations of customers of nano-free products. Based on this, the smartPearls technology is a promising delivery system for dermal products, being highly efficient and providing the opportunity of market differentiation against competitors. In addition, the excipients are regulatorily accepted, commercially available for dermal application (e.g. SYLOID[®] products from W. R. Grace US, AEROPERL[®] from Evonik, etc.), and provide features such as non-synthetic and natural. Also, smartPearls is an exclusive technology in the relevant markets, not only providing many aspects for market differentiation but also showing superior performance.

References

- [1] Amri, A.; Chaumeil, J.C.; Sfar, S.; Charrueau, C.; 2012. Administration of resveratrol: What formulation solutions to bioavailability limitations? *Journal of Controlled Release* 158(2), 182-193. <http://dx.doi.org/10.1016/j.jconrel.2011.09.083>
- [2] Wei, Q.; 2016. Nanocrystals & loaded porous silica for increased oral bioavailability [doctoral thesis]. [Germany]: Freie Universität Berlin. urn:nbn:de:kobv:188-fudissthesis000000104838-8
- [3] Mithani, S.D.; Bakatselou, V.; TenHoor, C.N.; Dressman, J.B.; 1996. Estimation of the Increase in Solubility of Drugs as a Function of Bile Salt Concentration. *Pharmaceutical Research* 13(1), 163-167. <https://doi.org/10.1023/A:1016062224568>
- [4] Saar, B.G.; Contreras-Rojas, L.R.; Xie, X.S.; Guy, R.H.; 2011. Imaging Drug Delivery to Skin with Stimulated Raman Scattering Microscopy. *Molecular Pharmaceutics* 8(3), 969-975. <https://doi.org/10.1021/mp200122w>
- [5] Mauludin, R.; Müller, R.H.; Keck, C.M.; 2009. Kinetic solubility and dissolution velocity of rutin nanocrystals. *European Journal of Pharmaceutical Sciences* 36(4–5), 502-510. <http://dx.doi.org/10.1016/j.ejps.2008.12.002>
- [6] Liversidge, G.G.; Cundy, K.C.; Bishop, J.F.; Czekai, D.A., inventors; Sterling Drug Inc., assignee; 1992. Surface modified drug nanoparticles. United States patent US 5,145,684, Sep 8.
- [7] Petersen, R., inventors; Abbvie Deutschland GmbH & Co KG, assignee; 2007. Nanocrystals for use in topical cosmetic formulations and method of production thereof. United States patent US 9,114,077 B2, Nov 19.
- [8] Auweter, H.; Bohn, H.; Heger, R.; Horn, D.; Siegel, B.; Siemensmeyer, K., inventors; BASF AG, assignee; 2002. Precipitated water-insoluble colorants in colloid disperse form. United States patent US 6,494,924 B1, Dec 17.
- [9] BASF SE, 2013. Product Catalog Human Nutrition. document ENH-NEW-1201-001-02-E, Apr. http://www.ethorn.com/ssw/files/BASF_Brochures%20and%20Catalog.pdf [accessed: 2017 September 11]

- [10] Charnay, C.; Bégu, S.; Tourné-Péteilh, C.; Nicole, L.; Lerner, D.A.; Devoisselle, J.-M.; 2004. Inclusion of ibuprofen in mesoporous templated silica: drug loading and release property. *European Journal of Pharmaceutics and Biopharmaceutics* 57(3), 533-540. <https://doi.org/10.1016/j.ejpb.2003.12.007>
- [11] Fernández-Núñez, M.; Zorrilla, D.; Montes, A.; Mosquera, M.J.; 2009. Ibuprofen Loading in Surfactant-Templated Silica: Role of the Solvent According to the Polarizable Continuum Model. *The Journal of Physical Chemistry A* 113(42), 11367-11375. <https://doi.org/10.1021/jp903895r>
- [12] Shen, S.-C.; Ng, W.K.; Chia, L.; Hu, J.; Tan, R.B.H.; 2011. Physical state and dissolution of ibuprofen formulated by co-spray drying with mesoporous silica: Effect of pore and particle size. *International Journal of Pharmaceutics* 410(1–2), 188-195. <http://dx.doi.org/10.1016/j.ijpharm.2011.03.018>
- [13] Vialpando, M.; Backhuijs, F.; Martens, J.A.; Van den Mooter, G.; 2012. Risk assessment of premature drug release during wet granulation of ordered mesoporous silica loaded with poorly soluble compounds itraconazole, fenofibrate, naproxen, and ibuprofen. *European Journal of Pharmaceutics and Biopharmaceutics* 81(1), 190-198. <https://doi.org/10.1016/j.ejpb.2012.01.012>
- [14] Delle Piane, M.; Corno, M.; Ugliengo, P.; 2013. Does Dispersion Dominate over H-Bonds in Drug–Surface Interactions? The Case of Silica-Based Materials As Excipients and Drug-Delivery Agents. *Journal of Chemical Theory and Computation* 9(5), 2404-2415. <https://doi.org/10.1021/ct400073s>
- [15] Cavallaro, G.; Pierro, P.; Palumbo, F.S.; Testa, F.; Pasqua, L.; Aiello, R.; 2004. Drug Delivery Devices Based on Mesoporous Silicate. *Drug Delivery* 11(1), 41-46. <https://doi.org/10.1080/10717540490265252>
- [16] Halamová, D.; Badaničová, M.; Zeleňák, V.; Gondová, T.; Vainio, U.; 2010. Naproxen drug delivery using periodic mesoporous silica SBA-15. *Applied Surface Science* 256(22), 6489-6494. <https://doi.org/10.1016/j.apsusc.2010.04.044>
- [17] Guo, Z.; Liu, X.-M.; Ma, L.; Li, J.; Zhang, H.; Gao, Y.-P.; Yuan, Y.; 2013. Effects of particle morphology, pore size and surface coating of mesoporous silica on Naproxen dissolution rate enhancement. *Colloids and Surfaces B: Biointerfaces* 101, 228-235. <https://doi.org/10.1016/j.colsurfb.2012.06.026>

- [18] Mellaerts, R.; Jammaer, J.A.G.; Van Speybroeck, M.; Chen, H.; Humbeeck, J.V.; Augustijns, P.; Van den Mooter, G.; Martens, J.A.; 2008. Physical state of poorly water soluble therapeutic molecules loaded into SBA-15 ordered mesoporous silica carriers: a case study with itraconazole and ibuprofen. *Langmuir* 24(16), 8651-8659. <https://doi.org/10.1021/la801161g>
- [19] Kinnari, P.; Mäkilä, E.; Heikkilä, T.; Salonen, J.; Hirvonen, J.; Santos, H.A.; 2011. Comparison of mesoporous silicon and non-ordered mesoporous silica materials as drug carriers for itraconazole. *International Journal of Pharmaceutics* 414(1), 148-156. <https://doi.org/10.1016/j.ijpharm.2011.05.021>
- [20] Dahne, L.; Baude, B., inventors; Capsulation Pharma AG, assignee; 2011. Method for producing core-shell (CS) particles and microcapsules using porous templates, CS particles and microcapsules, and the use thereof. United States patent US 7,939,103 B2, May 10.
- [21] Wei, Q.; Keck, C.M.; Müller, R.H.; 2015. CapsMorph® technology for oral delivery— theory, preparation and characterization. *International Journal of Pharmaceutics* 482(1), 11-20. <https://doi.org/10.1016/j.ijpharm.2014.10.068>
- [22] Van Speybroek, M.; Verheyden, L., inventors; Formac Pharmaceuticals NV, assignee; 2013. Dry granulates of mesoporous silica powders. International patent WO 2014/013044 A1, Jan 23.
- [23] Libanati, C.; Van Speybroeck, M.; Monsuur, F.H., inventors; W. R. Grace & Co.Conn., Formac Pharmaceuticals N.V., assignee; 2013. Compositions Containing a Biologically Active Material and a Non-Ordered Inorganic Oxide Material and Methods of Making and Using the Same. United States patent US 2016/0303048 A1, October 20.
- [24] Monsuur, F.H.; Hoefer, H.H.; Keck, C.M., inventors; Grace GmbH & Co. KG, Pharmasol GmbH, assignee; 2014. Active-loaded particulate materials for topical administration. International Publication Number WO 2016/041992 A1, patent application PCT/EP2015/071138, Sep 15.
- [25] Jin, N.; 2017. Nanocrystals & loaded porous silica for increased dermal bioavailability [doctoral thesis]. [Germany]: Freie Universität Berlin. urn:nbn:de:kobv:188-fudissthesis000000105191-3
- [26] Rabinow, B.E.; 2004. Nanosuspensions in drug delivery. *Nature Reviews Drug Discovery* 3(9), 785-796. <https://doi.org/10.1038/nrd1494>

- [27] Auweter, H.; André, V.; Horn, D.; Lüddecke, E.; 1998. The funktion of gelantin in controlled precipitation processes of nanosize particles. *Journal of Dispersion Science and Technology* 19(2-3), 163-184. <https://doi.org/10.1080/01932699808913170>
- [28] Choudhari, Y.; Hoefler, H.; Libanati, C.; Monsuur, F.; McCarthy, W.; 2014. Mesoporous silica drug delivery systems, in: Shah, N.; Sandhu, H.; Choi, D.; Chokshi, H.; Malick, A. (Eds.), *Amorphous Solid Dispersions*. Springer, New York, 665-693. https://doi.org/10.1007/978-1-4939-1598-9_23
- [29] Ahern, R.J.; Hanrahan, J.P.; Tobin, J.M.; Ryan, K.B.; Crean, A.M.; 2013. Comparison of fenofibrate–mesoporous silica drug-loading processes for enhanced drug delivery. *European Journal of Pharmaceutical Sciences* 50(3), 400-409. <https://doi.org/10.1016/j.ejps.2013.08.026>
- [30] Bouledjoudja, A.; Masmoudi, Y.; Van Speybroeck, M.; Schueller, L.; Badens, E.; 2016. Impregnation of Fenofibrate on mesoporous silica using supercritical carbon dioxide. *International Journal of Pharmaceutics* 499(1), 1-9. <https://doi.org/10.1016/j.ijpharm.2015.12.049>
- [31] Qian, K.K.; Wurster, D.E.; Bogner, R.H.; 2012. Spontaneous Crystalline-to-Amorphous Phase Transformation of Organic or Medicinal Compounds in the Presence of Porous Media, Part 3: Effect of Moisture. *Pharmaceutical Research* 29(10), 2698-2709. <https://doi.org/10.1007/s11095-012-0734-4>
- [32] Mura, P.; Cirri, M.; Faucci, M.T.; Ginès-Dorado, J.M.; Bettinetti, G.P.; 2002. Investigation of the effects of grinding and co-grinding on physicochemical properties of glisentide. *Journal of Pharmaceutical and Biomedical Analysis* 30(2), 227-237. [http://dx.doi.org/10.1016/S0731-7085\(02\)00252-2](http://dx.doi.org/10.1016/S0731-7085(02)00252-2)
- [33] Gupta, M.K.; Vanwert, A.; Bogner, R.H.; 2003. Formation of physically stable amorphous drugs by milling with Neusilin. *Journal of Pharmaceutical Sciences* 92(3), 536-551. <https://doi.org/10.1002/jps.10308>
- [34] Shen, S.C.; Ng, W.K.; Chia, L.; Dong, Y.C.; Tan, R.B.H.; 2010. Stabilized amorphous state of ibuprofen by co-spray drying with mesoporous SBA-15 to enhance dissolution properties. *Journal of Pharmaceutical Sciences* 99(4), 1997-2007. <https://doi.org/10.1002/jps.21967>

- [35] Miura, H.; Kanebako, M.; Shirai, H.; Nakao, H.; Inagi, T.; Terada, K.; 2011. Influence of particle design on oral absorption of poorly water-soluble drug in a silica particle–supercritical fluid system. *Chemical and Pharmaceutical Bulletin* 59(6), 686-691. <https://doi.org/10.1248/cpb.59.686>
- [36] Cha, K.-H.; Cho, K.-J.; Kim, M.-S.; Kim, J.-S.; Park, H.J.; Park, J.; Cho, W.; Park, J.-S.; Hwang, S.-J.; 2012. Enhancement of the dissolution rate and bioavailability of fenofibrate by a melt-adsorption method using supercritical carbon dioxide. *International Journal of Nanomedicine* 7, 5565-5575. <https://doi.org/10.2147/IJN.S36939>
- [37] Grabo, M.; Dunmann, C.; Müller, R.H.; 2012. CapsMorph™ – simple, cost effective industrial process to generate amorphous state of poorly solubles for oral administration, #46, p. 62, 8th World Meeting on Pharmaceuticals, Biopharmaceutics and Pharmaceutical Technology, Istanbul, Turkey, March 19-22.
- [38] Heikkilä, T.; Salonen, J.; Tuura, J.; Kumar, N.; Salmi, T.; Murzin, D.Y.; Hamdy, M.S.; Mul, G.; Laitinen, L.; Kaukonen, A.M.; 2007. Evaluation of mesoporous TCPSi, MCM-41, SBA-15, and TUD-1 materials as API carriers for oral drug delivery. *Drug Delivery* 14(6), 337-347. <https://doi.org/10.1080/10717540601098823>
- [39] Preisig, D.; Haid, D.; Varum, F.J.O.; Bravo, R.; Alles, R.; Huwyler, J.; Puchkov, M.; 2014. Drug loading into porous calcium carbonate microparticles by solvent evaporation. *European Journal of Pharmaceutics and Biopharmaceutics* 87(3), 548-558. <https://doi.org/10.1016/j.ejpb.2014.02.009>
- [40] Sliwinska-Bartkowiak, M.; Dudziak, G.; Gras, R.; Sikorski, R.; Radhakrishnan, R.; Gubbins, K.E.; 2001. Freezing behavior in porous glasses and MCM-41. *Colloids and Surfaces A: Physicochemical and Engineering Aspects* 187–188, 523-529. [http://dx.doi.org/10.1016/S0927-7757\(01\)00637-9](http://dx.doi.org/10.1016/S0927-7757(01)00637-9)
- [41] Darbre, P.D.; 2009. Underarm antiperspirants/deodorants and breast cancer. *Breast Cancer Research* 11(3), S5. <https://doi.org/10.1186/bcr2424>
- [42] Teichmann, A.; Jacobi, U.; Ossadnik, M.; Richter, H.; Koch, S.; Sterry, W.; Lademann, J.; 2008. Differential Stripping: Determination of the Amount of Topically Applied Substances Penetrated into the Hair Follicles. *Journal of General Internal Medicine* 20(5), 264-269. <https://doi.org/10.1111/j.0022-202X.2005.23779.x>

- [43] Weigmann, H.J.; Lademann, J.; Schanzer, S.; Lindemann, U.; von Pelchrzim, R.; Schaefer, H.; Sterry, W.; Shah, V.; 2001. Correlation of the Local Distribution of Topically Applied Substances Inside the Stratum corneum Determined by Tape-Stripping to Differences in Bioavailability. *Skin Pharmacology and Physiology* 14(Suppl. 1), 98-102. <https://doi.org/10.1159/000056397>

Results and Discussion

3. smartPearls for dermal bioavailability enhancement – Long-term stabilization of suspensions by viscoelasticity²

Abstract

smartPearls are a novel dermal delivery system based on mesoporous (pores 2-50 nm) particles, developed in 2014. Their pores can be loaded with active which is long-term stabilized in its amorphous state. The increased saturation solubility by the amorphous state leads to an increased dermal bioavailability of poorly soluble actives. To avoid sedimentation of the porous particles (3-50 μm) in dermal formulations, viscoelastic gels were developed using ι -carrageenan, polyacrylate and the viscoelastic Kühne salad dressing as a reference from food industry. Silica particles (company Grace/US, 50 and 150 μm) were loaded into the gels and long-term stability was assessed by a VIS sedimentation test. Furthermore, the gels were characterized by analytical centrifugation (LUMiSizer[®]) to assess the critical rpm/g values, allowing to order them after their absolute viscoelastic stabilizing ability. Characterization was complemented by rotation rheology, amplitude sweep, and a frequency sweep analysis for the determination of elastic and viscous moduli G' and G'' at varying conditions. Based on the throughout characterization, polymers can be selected to sufficiently stabilize dermal formulations even with large sized smartPearls – the prerequisite for using this delivery system in dermal products.

² This chapter has been published as:

Hespeler, D.; Knoth, D.; Keck, C.M.; Müller, R.H.; Pyo, S.M.; 2019. smartPearls[®] for dermal bioavailability enhancement – Long-term stabilization of suspensions by viscoelasticity. *International Journal of Pharmaceutics* 562, 293-302.
<https://doi.org/10.1016/j.ijpharm.2019.03.016>

3.1. Introduction

One approach to increase the bioavailability of poorly soluble actives is their transfer from crystalline into amorphous state. Amorphous actives possess a higher saturation solubility C_s [1; 2], thus an increased concentration gradient $C_s - C_a$ between donor and acceptor compartment, leading to an increased diffusive flux [3]. However, the problem is the limited physical stability of amorphous state [4-6], having the tendency to re-crystallize during the shelf life of a product.

In 2009 the German company Capsulation Pharma from Berlin developed the CapsMorph technology for oral administration [7; 8]. Drugs are kept in the amorphous state by loading them into the mesopores (2-50 nm diameter) of porous materials, e.g. the silicate NEUSILIN® US2. Loading was performed by e.g. the solvent impregnation method [9; 10], where drug solidifies in the amorphous state after evaporating the solvent. The space restriction in the pores effectively hinders crystal formation and also re-crystallization during storage for more than 6 years [11]. Beside the space restriction, also physical interactions between the active and the matrix are discussed as influencing factors [12; 13]. With regards to regulatory aspects, the mesoporous silica particles have a high regulatory acceptance [14], being approved as “natural” e.g. after ECOCERT standards.

As next step, the technology was transferred from the oral administration route to dermal application [15; 16]. In a tablet or capsule, the porous particles are in the dry and solvent-free state. Being in the water phase of a dermal formulation, the amorphous drug is in contact with a liquid. Water is a poor solvent, but still a solvent and therefore a triggered re-crystallization was expected. Surprisingly and against the theoretical expectation, the actives in the pores remained stable in the amorphous state even in the water phase of dermal formulations [17]. After application to the skin, identical to oral delivery, a clear bioavailability enhancement in the skin compared to other delivery systems was achieved [17; 18]. Thus, this dermal delivery technology – the so called smartPearls – is meanwhile in development with various cosmetic and pharma actives to increase their penetration into the skin.

The technology is in competition with dermal nanocrystals. They are nm-sized crystalline drug powders and also provide an increased saturation solubility C_s compared to μm -sized crystalline drug powders [19]. However, the increase in C_s by the amorphous state is typically

higher than the increase in C_s by nanoization. Thus, the smartPearls have the chance to be the successor or at least the alternative technology for poorly soluble drugs or cosmetic actives. The nanocrystals have the advantage, that they do not sediment in dermal formulations because of their small size. In contrast, the porous smartPearls possess mean sizes between a few μm and about 50 μm (being the upper size limit to avoid a sandy feeling on skin), leading to sedimentation in “normal” dermal formulations, e.g. conventional creams or gels.

The aim of this study was to develop formulations preventing the sedimentation. This is the prerequisite for the practical realization of smartPearls containing dermal products. Role model for this development is the viscoelastic salad dressings from food industry. They can stand for months, nonetheless the herbs in the dressing stay nicely dispersed without any signs of sedimentation. The principle of viscoelastic stabilization is, that the elastic modulus G' surpasses the viscous modulus G'' . Further, the flow point of the formulation must exceed the sedimentation force of the particles. Various polymers were screened, which yield classical viscous systems (cellulose ethers) and polymers which generate viscoelastic gels (ι -carrageenan, polyacrylate). The rheological properties were investigated, and traditional VIS analysis performed to assess the ability of preventing sedimentation (long-term stabilization). This test provides typically a yes or no answer but cannot assess the drag forces provided by the different viscoelastic gels. Thus, analytical centrifugation was additionally applied to place the viscoelastic gel forming polymers in an order of increasing stabilization ability. To challenge the system, large silica particles of 50 μm and 150 μm were used.

3.2. Materials and methods

Hydroxypropyl cellulose, Klucel™ GF Pharma (HPC with a Brookfield viscosity of 400 (2% at 25°C, 60 rpm) and a molecular weight of 370,000 g/mol was provided from Ashland (Schaffhausen, Switzerland). The polyacrylate gelling agent Carbopol® ETD 2020 NF (polyacrylate) was provided by Lubrizol (Brussels, Belgium), the ι -carrageenan GENUVISCO® CG-131 (ι -carrageenan) by CP Kelco (Lille Skensved, Denmark). Kühne salad dressing was purchased from a local supermarket.

Silica particles Syloid® XDP 3150 (150 μm) and Syloid® XDP 3050 (50 μm) were provided by Grace (Worms, Germany). Microcare® PEHG (liquid blend of ethylhexyl glycerin in phenoxyethanol) as preservative was obtained from Thor GmbH (Speyer, Germany).

Potassium chloride (KCl) and sodium hydroxide (NaOH) were purchased from Caelo (Hilden, Germany). Water was purified with a Millipore System from Merck (Darmstadt, Germany).

3.2.1. Production of hydrogel bases

Cellulose ether

Klucel™ GF Pharma (HPC), HPC-M and HEC powder was spread on aqueous 1% Microcare PEHG solution in an ointment bowl and stored below 8°C for swelling. After a swelling time of 24 hours the gel was stirred with a pestle and stored for further 24 hours. The gel was produced in a concentration of 5% polymer.

Dressing

Kühne salad dressing (dressing) was vacuum filtered with a Whatman® filter type 598 to remove the herbs and obtain the gel base. According to the manufacturer specification, the dressing contains carrageenan and locust bean gum as gelling agent. Since lambda(λ)-carrageenan act just as a thickener and kappa-(κ)carrageenan forms firm and brittle gels, the contained carrageenan is concluded as iota-(ι)carrageenan. Further contains the dressing spirit vinegar, white wine vinegar, glucose-fructose syrup, salt, spices, sugar, sodium acetate, herbs, saccharin, and yeast extract.

ι -carrageenan

ι -carrageenan is a natural product made from red algal species or Irish moss. ι -carrageenan dispersed in an aqueous 1% Microcare PEHG solution and heating up to 80°C for 10 minutes lead to a ι -carrageenan solution. To form a viscoelastic gel, 10% KCl solution was added until the final concentration of either 0.35% (for rheological investigations c.f. section 2.5) or 0.40% (for all other measurements) was reached [20]. The gel was cooled under agitation and replenished to 100 g afterwards.

Polyacrylate

Carbopol® ETD 2020 NF (polyacrylate) was dispersed in an aqueous 1% Microcare PEHG solution while stirring for at least 15 minutes to ensure a swelling of the gelling agent. Afterwards the pH-level was adjusted to 5.5 ± 0.5 with 1 molar sodium hydroxide solution to obtain the final gel. Polyacrylate gels were produced at 0.125% for rheological investigations (c.f. section 2.5). For all other measurements polyacrylate gels at 0.250% were prepared.

3.2.2. Production of silica loaded hydrogels

smartPearls without drug loading and sizes of 50 and 150 μm were incorporated into all the different gels. To avoid a destruction of the incorporated particles a flexible plastic card was used instead of a melamine pestle for blending the gel base and the particles in an ointment bowl. For VIS investigations, about 30-60 mg smartPearls were incorporated per cuvette filling to achieve a transmission below 50%. For the investigation by the analytical centrifuge a particle concentration of 1% was favored to avoid possible interactions of the particles and influences on the viscosity [21].

When incorporating the loaded silica particles into gel, drug will be released into the hydrogel – but only to a minor part. Drug dissolves from the pores until a supersaturated solution is formed in gel. Because more drug is contained in the pores than it can be dissolved in the gel, a major part will remain in the pores. After application to the skin, the drug in the pores acts as a depot. When drug from the gel is penetrated into the skin, it will be immediately replaced in the gel by new drug dissolving from the pores. To make sure, that drug remains in the pores, a sufficiently high drug amount needs to be incorporated into the gel, i.e. multiple of supersaturation concentration.

3.2.3. Sedimentation behavior investigation by VIS analysis and macroscopic observation

Transmission of the loaded smartPearls gels was determined at 500 nm using a PharmaSpec UV-1700 (Shimadzu, Japan). The smartPearls loaded gels were filled in 10 mm cuvettes and measured directly after preparation. Transmission of the smartPearls gels were normalized compared to the pure gel. The transmission approximates to 100% if sedimentation appears. The measurements were repeated for stability investigation after one, three, seven and thirty days.

3.2.4. Sedimentation behavior investigation by analytical centrifugation

Accelerated sedimentation analysis was performed with the LUMiSizer[®] (LUM GmbH, Berlin, Germany). The **STEP**-technology measures **S**pace and **T**ime related **E**xinction **P**rofiles, in relation to the sedimentation of dispersed particles. Analytical centrifugation was performed with 50 and 150 μm smartPearls at low acceleration (250 rpm \triangleq 7.8 g) up to high acceleration (4000 rpm \triangleq 1970 g) to differentiate between viscous and viscoelastic stabilization of the

particles, and to assess the critical rpm/g number at which sedimentation occurs in viscoelastic systems. The measurement of the transmission was performed at a wavelength of 865 nm. 120 profiles were recorded with a five second interval and afterwards 120 profiles with a 10 second interval, i.e. a total of 300 scans. For evaluation, all profiles are plotted in one overview graph, where the number of scans to be plotted can be selected (e.g. in case of 300 profiles, each 20th profile can be plotted, corresponding to 15 profiles in total). The software displays the time dependence of a single measurement by a change of the color from red (first measurement) to green (last measurement).

3.2.5. Rheological behavior of unloaded and silica loaded hydrogels

All rheological measurements were performed at a RheoStress RS 100 (Haake, Karlsruhe, Germany) with a 60 mm, 1° cone plate geometry and a gap of 1000 μm at $25\pm 1^\circ\text{C}$. A sample amount of 4 mL was filled with a syringe between cone and plate. Shear stress controlled rotation rheology, shear stress amplitude sweep rheology and shear stress frequency sweep rheology were measured. The measurement routine started with a low shear rate (5 s^{-1}) for two minutes to stress all samples similar before measurement. Followed by five minutes' rest time to rebuild the gel matrix. First measurement was the shear stress controlled rotation rheology with a shear stress ramp from 0 to 100 Pa, which stopped at 100 Pa or a rotation speed of 1000 rpm. Viscous behavior was evaluated from the measured shear rate related to the applied shear stress. After a second time of rest for five minutes the shear stress (τ) amplitude sweep rheology was performed at an angular frequency (ω) of 6.28 rad/s (1 Hz) from 0 to 100 Pa. The linear viscoelastic area and the flow point were determined based on the amplitude sweep test. Afterwards shear stress frequency sweep tests at frequencies ω from 0.01 up to 100 rad/s were performed at a constant shear stress of 0.2 Pa (1-carrageenan gel, polyacrylate gel and dressing) or 0.5 Pa (HPC) which was in the linear viscoelastic area, determined from the amplitude sweep analysis. The frequency sweep analysis enabled the evaluation of the viscoelastic behavior of gels at low shear stress and frequencies, to predict the viscoelastic behavior in the rest state, which is fundamental for the interpretation of physical stabilization effects on smartPearls.

3.3. Results and discussion

3.3.1. Light microscopy

Incorporation of particles into a gel can lead to particle agglomeration or aggregation, e.g. by polymer bridging or reduced electrostatic stabilization. Reduction in electrostatic stabilization can be caused by particle coating with uncharged polymers (cellulose ethers), or by electrolytes being present in a gel (e.g. high concentrations in the ι -carrageenan and the polyacrylate gels). A simple and efficient tool to assess the even distribution of particles is the light microscopy analysis, preferably by low magnifications to screen larger areas for aggregates. Light microscopy was preferred to the particle size analysis by laser diffraction (LD), since the dilution procedure of the gel being required for performing LD measurements might change the dispersion state of the particles.

Light microscopy images were taken showing the even distribution of the silica particles in all gels, exemplarily the cellulose ether HPC, ι -carrageenan and polyacrylate gels are shown in Figure 1. The images also give an impression of the size distribution of the particles, being relatively homogenous.

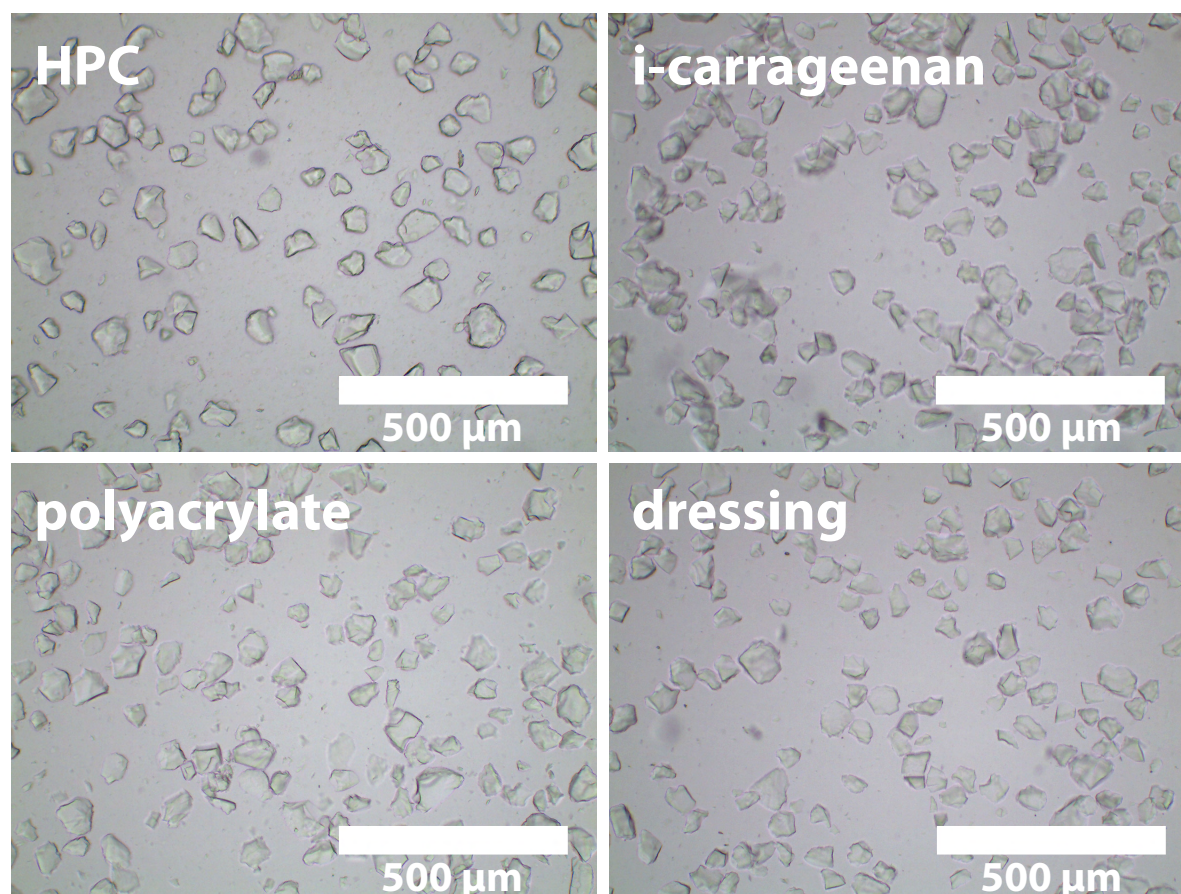


Figure 1: Light microscopy images of silica (50 μm) in gels, prepared with HPC, ι -carrageenan, polyacrylate and salad dressing as reference at 100-fold magnification (scale bar: 500 μm).

3.3.2. Sedimentation behavior investigation by VIS analysis

Following the Stokes law of sedimentation, the sedimentation velocity is proportional to the particle size and the density difference between particle and dispersion medium. Thus, the silica particles undergo sedimentation due to their large size (up to 150 μm), in combination with a density being distinctly higher than the aqueous gel phase. The unloaded smartPearls possess a density of around 1.24 g/mL in water, resulting from the density of silica (2.2 g/mL) and the water (1.0 g/mL) in the pores (pore volume 1.8 mL/g). smartPearls loaded with active pharmaceutical ingredient (API) can exhibit a density of about 2.0 g/mL, assuming an API density of 1.95 g/mL.

Force F is $F=m \cdot g$ (m – mass, g – gravitational acceleration). The sedimentation force F_G depends on the density difference of the continuous phase of the formulation ρ_f and the particles ρ_p , and on their radius r (3rd power) and the gravitational acceleration g .

$$F_G = (\rho_p - \rho_f)g \frac{4}{3}\pi r^3 \quad (1)$$

For example, the sedimentation force of loaded 50 μm sized smartPearls with a density of 2.0 g/mL are less than one/tenth of the force of unloaded 150 μm sized particles with a density of 1.24 g/mL. Thus the 150 μm particles with pronounced sedimentation were used in this study as “challenge test” to identify the gelling agents with the best sedimentation prevention. In dermal formulations, only smartPearls with a size of 50 μm or below will be relevant since larger particles have a sandy skin feeling [18]. Therefore, if the 150 μm particles do not sediment, the practically relevant particles with a size of 50 μm or less will definitely not sediment.

In viscous gels, the sedimentation velocity will only be slowed down by increasing the viscosity of the gel phase. Increase of velocity is limited, because good spreadability on the skin must remain. In viscoelastic gels, no sedimentation takes place at all if the sedimentation force F_G is lower than the drag force F_D , due to the viscoelastic properties.

The monitoring of sedimentation behavior was performed by transmission measurements at 500 nm – a wavelength with high extinction coefficient for particles. Particle concentrations in gels were adjusted to obtain a transmission of about 50%, corresponding to about 30 to 60 mg silica per cuvette. The 50% transmission allowed to monitor both increase due to sedimentation and decrease due to potential particle aggregation. In the study no particle aggregation took place, as shown by preceding microscopy examination of the gels after 30 days of storage. Observed increases in the transmission value were thus only due to particle sedimentation.

Measurements to determine the sedimentation behavior only caused by gravity force were performed as described in section 2.3. Exemplarily, normalized results for dressing, polyacrylate, HPC, and ι -carrageenan are shown in Figure 2. No increase in transmission was found for the viscoelastic gels, where in contrast, an increase of up to about 95% transmission occurred for the viscous HPC gel. The transmission did not reach 100% which was attributed to fine silica particles which were formed by erosion from the silica particles during the incorporation process (mechanical stress).

In this challenge test with very large silica size of 150 μm , the viscoelastic gels showed one month stability. F_D was higher than the F_G , thus a long-term stability is given, especially when

using the practically relevant smaller particles. According to Mezger [22], the shear rate D is below 0.01 s^{-1} in case of sedimentation. Gel bases being able to efficiently inhibit the particle sedimentation have to exhibit viscoelastic properties already at this shear rate up to shear stresses equivalent to the sedimentation force.

A concentration of 0.35% ι -carrageenan with 0.2% KCl was suitable to stabilize the large silica particles, with the advantage of exhibiting liquid like properties, being favorable for good spreadability on skin. In contrast, the polyacrylate gel, also sufficient stabilizing properties, exhibits a higher viscosity.

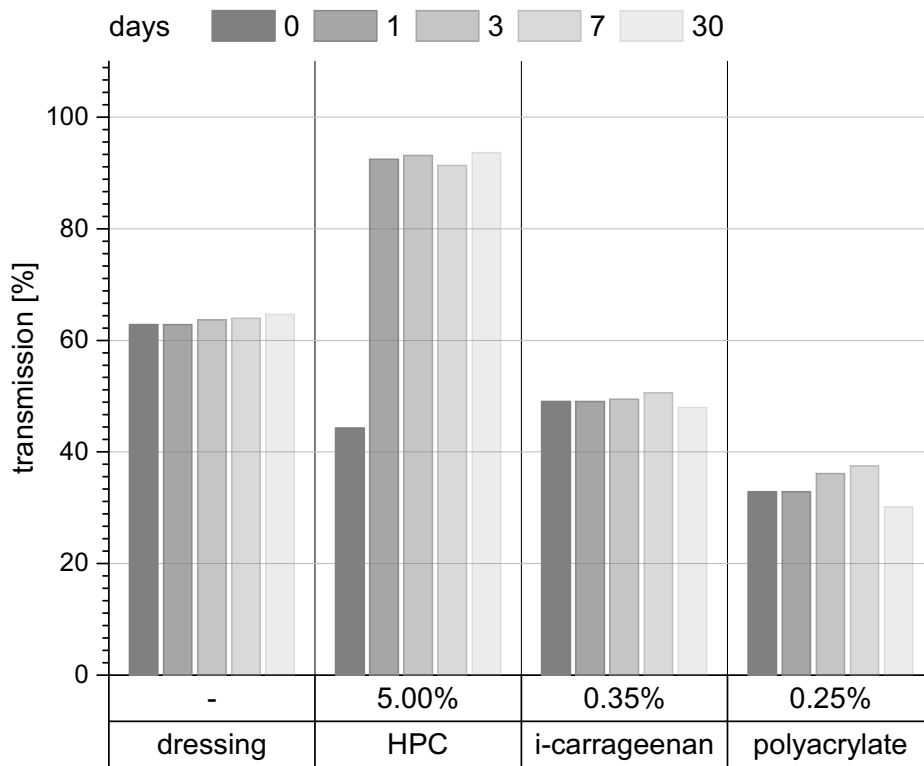


Figure 2: Normalized transmission of Syloid® XDP 3150 ($150 \mu\text{m}$) in commercially available salad dressing, 5.0% HPC, 0.35% ι -carrageenan and 0.25% polyacrylate gel measured after production and 1, 3, 7 and 30 days storage at room temperature.

Photos of the cuvettes taken directly after VIS measurements on the day of preparation (day 0) and after 7 days of storage are shown exemplarily. Figure 3 shows sedimentation occurring in the HPC gel already within 7 days, but a uniform turbidity in the 3 viscoelastic formulations, which remained throughout the study (30 days).

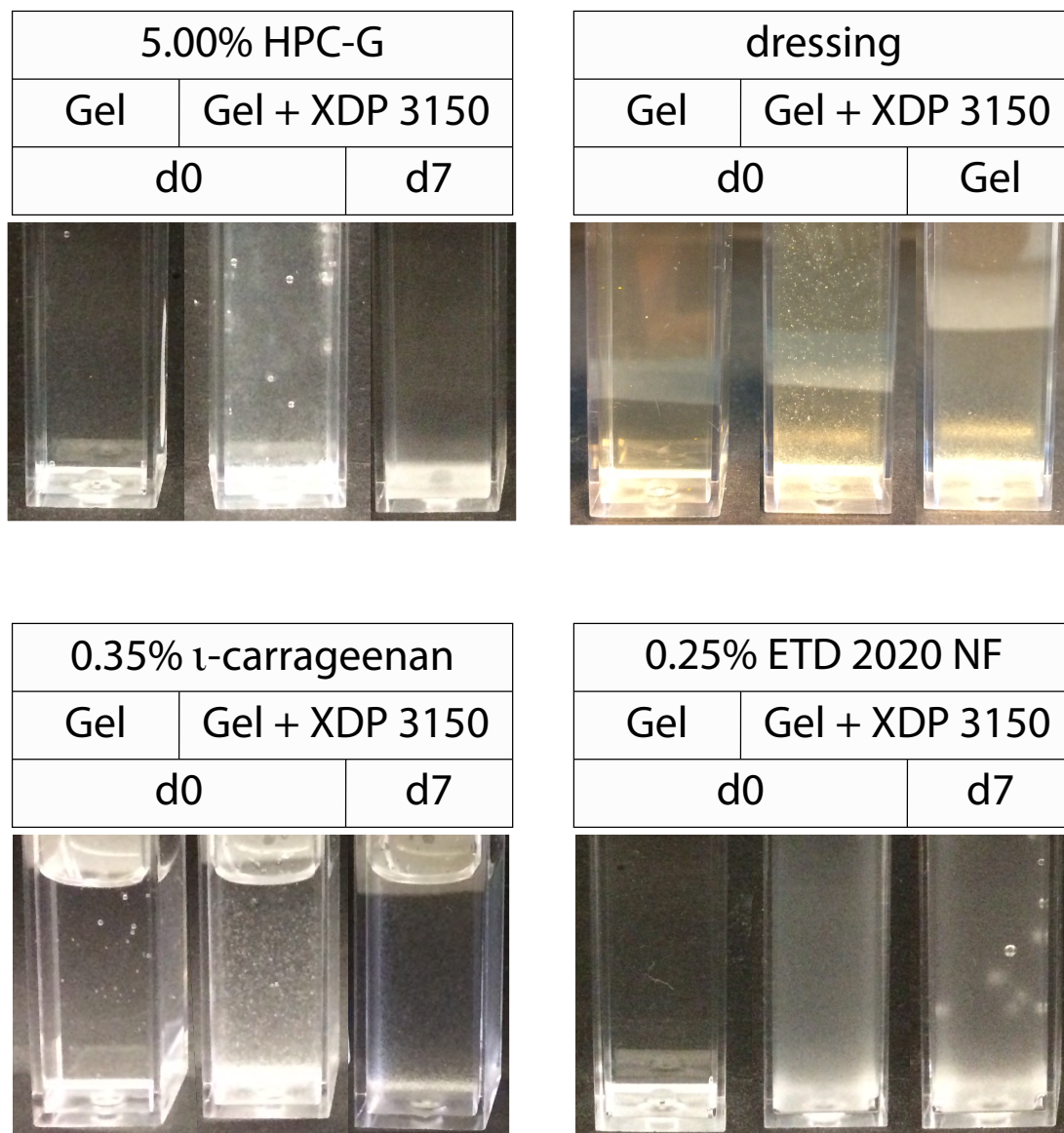


Figure 3: Photos of gels from 5% HPC gel, commercially available salad dressing, 0.35% ι-carrageenan gel and 0.25% polyacrylate gel without (left, resp.) and with 1% Syloid® XDP 3150 (150 μm) directly after production (d0) and after 7 days of storage (d7, right, resp.). Sedimentation only occurred in the HPC gel. In the other formulations, the particles remained evenly distributed.

3.3.3. Sedimentation behavior of smartPearls in selected gels introduced by centrifugal forces

Theoretical considerations

The analytical centrifugation provides information about the correlation between:

- a) applied centrifugal force (controlled via selected rounds per minute (rpm) of the centrifuge, 250 rpm \triangleq 7.8 g; 4000 rpm \triangleq 1970 g), and
- b) the sedimentation behavior (sedimentation yes or no; in case of sedimentation about the sedimentation profile and the sedimentation kinetics).

Important parameter for viscoelastic gels is the centrifugal force g at which sedimentation starts, i.e. the sedimentation force F_G is larger than the drag force F_D of the system. This information can be obtained from the sedimentation profiles, being taken by the LUMiSizer[®] (LUM GmbH, Berlin, Germany).

The homogenously dispersed sample is placed in a cuvette, then sedimentation starts which is monitored in the different Spaces of the cuvette as a function of Time, yielding Extinction Profiles (so called **STEP**-technology). In graphical presentation the extinction or alternatively the transmission values can be plotted on the y-axis. In this study the transmission was plotted on the y-axis, to have increasing values at increasing sedimentation.

Figure 4 shows the principle set up and sequence of the measurements. The sample filled cuvette is placed in the instrument and at time $t=0$ an extinction (transmission) scan is performed over the whole cuvette (Figure 4, upper left). From this scan, an extinction profile result (upper right). In the space of the cuvette filled with air, the transmission is 100%, then the interface air-liquid (meniscus) is passed, which typically generates a transmission peak. After entering the liquid (suspension) phase, a transmission value results depending on the turbidity of the suspension. Typically, the particle concentration in the suspension is adjusted to about 30-50% transmission for measurement.

After certain time intervals, the scan is repeated and yielding the profile of the respective time-dependent state of sedimentation. In Figure 4 particle sedimentation in a viscous system is exemplarily shown, with a clear supernatant, a still turbid medium phase, and a sediment which yields almost 0% transmission. In graphs, the extinction (transmission) profile is not plotted vertically, but horizontally (Figure 5). In a summarizing graph, all scans taken at

different time points are plotted in one graph for better visualization, changing the graph color from red (1st measurement) to green (last measurement) (Figure 6). In this study 240 subsequent scans were performed within one analysis per selected rpm value. Analyses were performed at increasing rpm values, i.e. from 250 rpm to 4000 rpm.

This allows to identify the critical rpm/g value at which sedimentation starts. The higher the critical g value is, the higher is the stabilizing ability of the viscoelastic system. The viscoelastic systems investigated in this study can thus be placed in order of increasing stabilizing ability.

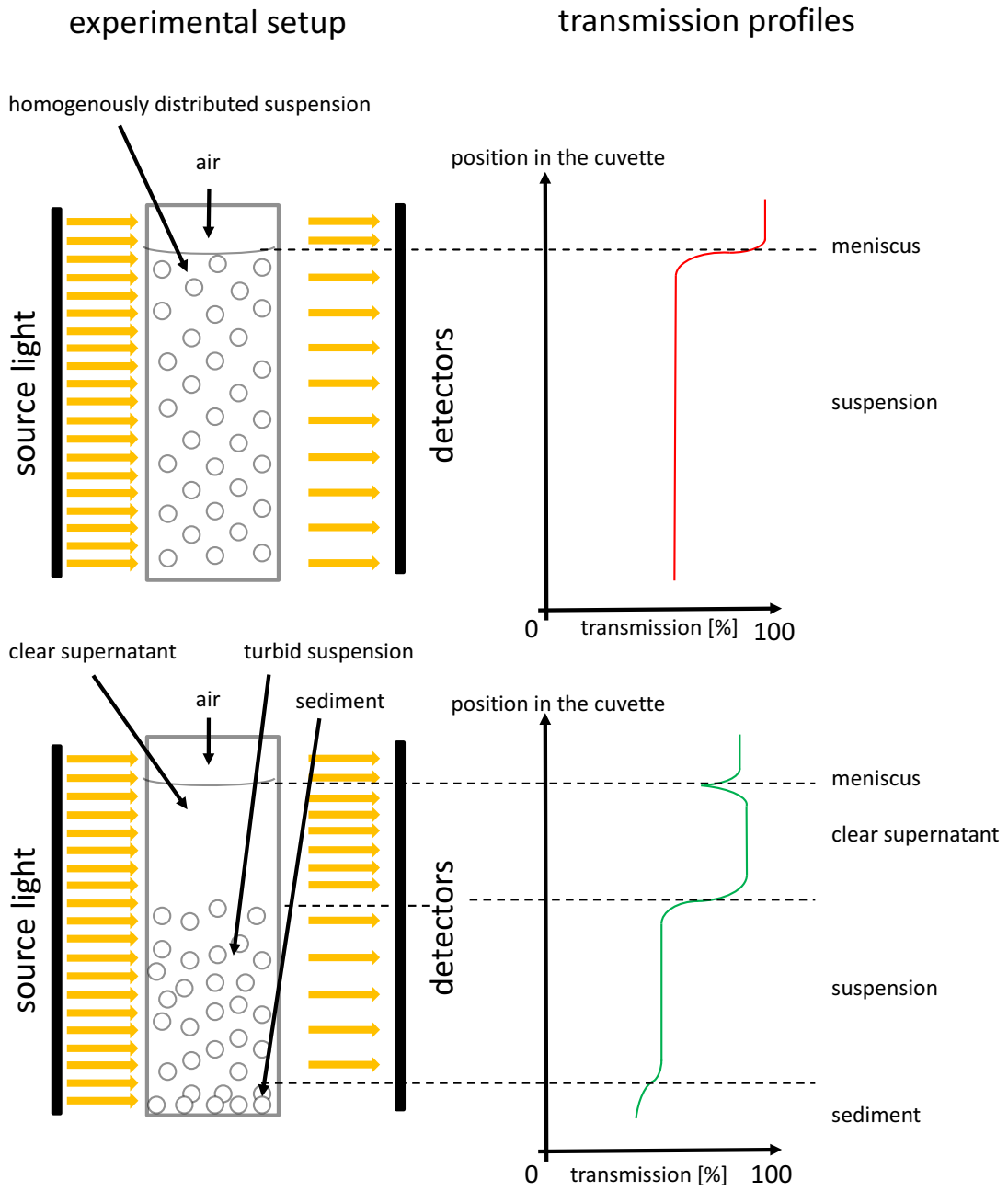


Figure 4: Principal setup of analytical centrifuge measurement (upper left) and resulting transmission profile at time $t=0$ of the measurements sequence (upper right). After certain sedimentation times, the scan is repeated (lower left and right).

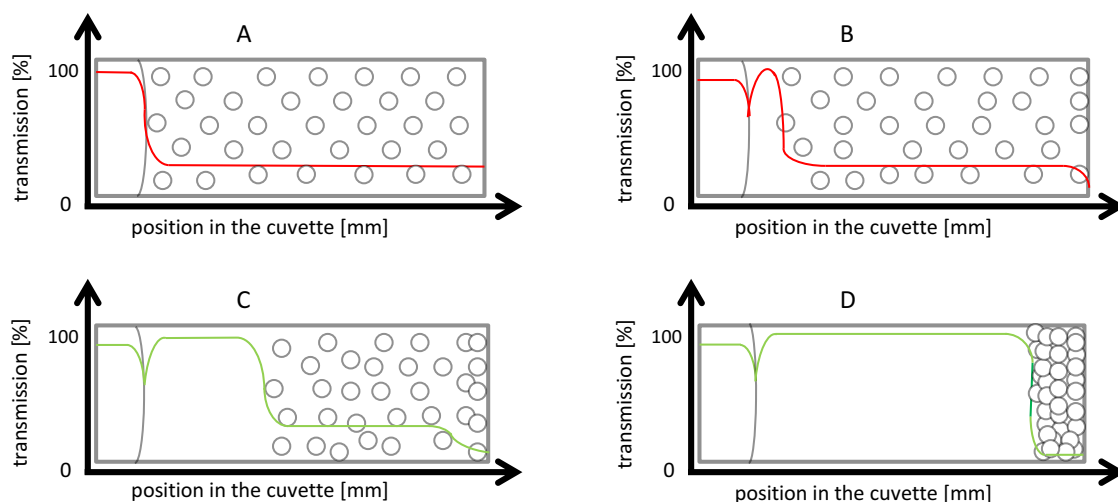


Figure 5: Measuring profiles in horizontal plot: At the first measurement (A) the particles are homogeneously distributed, and the transmission is constant over the whole liquid phase in the cuvette. With increasing time of centrifugation, the particles begin to sediment (B), and the upper part of the cuvette is clearing up (increase in transmission). The sedimentation process proceeds (C) under a continuing deposition of particles at the bottom of the cuvette (sediment). The end of the analysis is indicated by a constant high transmission throughout the liquid phase except for the dense sediment at the bottom (D). The sediment blocks off most of the incoming light, which leads to a very low transmission close or equal to zero in this space of the cuvette.

For Newtonian liquids (the cellulose derivatives) the sedimentation speed depends on the particle size, density of the particles, viscosity of the dispersion medium and the gravitational acceleration g (Stokes's equation). In viscoelastic liquids the sedimentation process is much more complex.

In a viscous Newtonian liquid, the sedimentation velocity v increases linearly with the rotation speed, starting at the zero point in the coordinate system. In non-Newtonian liquids, the correlation is not linear and strongly depends on the respective gel structure (e.g. pseudoplastic, plastic, dilatant). In contrast, viscoelastic systems have a flow/yield point above which sedimentation occurs (shear thinning). Below this point, no sedimentation occurs, and the suspensions are long-term stable. Above this point, the gel structure is changed or even destroyed because of the high g force onto the particles, resulting in higher particle weights. The physical stabilization of the particles above this point only rests upon the viscosity of the dispersion medium. Aim of this study was to assess if the viscoelastic polymers can stabilize under normal storage conditions, and to classify them regarding stabilization at increasing stress conditions (i.e. order them after their critical rpm/g number).

Analytical centrifugation – data interpretation

Analytical centrifugation was performed starting with a rotation speed of 200 rpm. After each measurement, the speed was increased stepwise up to the maximum possible 4000 rpm. The instrument is preferably recommended to be used for suspensions with particle sizes in the range 20 nm to about 100 μm . Particle sizes or sedimentation velocities can then precisely be calculated from the profiles. This is not the case when analyzing the relatively large particles as the silica, because of the increased transmission fluctuation in the profiles (effect of light detector dimensions).

For such particle populations not a quantitative but a qualitative evaluation of the results can be made. Larger particles (size close to or larger than the light sensors in the instrument) yield extinction/transmission time profiles with higher fluctuations in the values, excluding a quantitative analysis. However, the changes in the profiles (moving up of the transmission profiles to higher transmission values) can be easily seen in the graphs, being sufficient for placing the viscoelastic gels in an order of stabilizing ability. Also, easily detectable is the beginning of the sediment formation, occurring when the stabilizing ability is exceeded, and sedimentation starts in the viscoelastic systems.

Transmission profiles are shown for the 3 viscoelastic systems (ι -carrageenan gel (Figure 6), salad dressing (Figure 7) and polyacrylate gel (Figure 8)) and exemplarily for one selected viscous system, the HPC gel (Figure 9). In the Figures 6-9, transmission profiles are plotted to allow an easy visual comparison. The last profile shown is the one at which pronounced sedimentation in the respective gel occurs (being either 2000 rpm or 4000 rpm). Pronounced sedimentation means, that full sedimentation takes place within the first 10 intervals of sedimentation profiling (i.e. equal to $10 \times 5\text{s} = 50$ seconds). Table 1 lists the rpm values at which rotation speed sedimentation was clearly visible (= critical rpm/g value, e.g. 600 rpm for the ι -carrageenan gel).

CHAPTER 3

Table 1: Overview of critical rpm values, corresponding g numbers and the required rpm for pronounced sedimentation (within less than 10 profiles) of the investigated viscoelastic gels and as comparison viscous HPC gel.

gelling agent	polymer concentration	critical rpm value	corresponding g number	max. rpm for fast sedimentation
ι-carrageenan	0.35%	600	47	4000
salad dressing	-	300	12	2000
polyacrylate	0.25%	not reached >4000	>2100	not reached
HPC	5.00%	viscous system, sedimentation starts at 250 rpm = 8 g		

The smartPearls showed no movement in the ι-carrageenan gel at 250 rpm. They are immobilized by the viscoelastic gel. Hence, a physical stabilization is achieved. The corresponding g number is 7.8; meaning that they do not sediment when even about 8 times of the gravitational force is applied. Based on this data obtained with 150 μm particles, ι-carrageenan is a suitable polymer to easily stabilize silica particles of 50 μm.

At 500 rpm a slight sedimentation could be observed, where at 600 rpm the particles began to sediment fast and a complete clearance was nearly achieved. Thus 600 rpm was identified as the critical rpm/g values, corresponding to 44 g. At 1000 rpm the sedimentation is pronounced. A complete sedimentation would be possible by applying a longer running time (i.e. > 3000 s). The fastest acceleration with 4000 rpm showed a complete sedimentation of the smartPearls after running just 3 profiles (= 15 s, Figure 6).

Analytical centrifugation of the salad dressing showed a very slight sedimentation already at 250 rpm (sedimentation comparable to ι-carrageenan gel at 500 rpm). At 500 rpm a visible sedimentation occurs, being more pronounced than in the ι-carrageenan gel at 500 rpm. Thus, this viscoelastic gel has clearly less stabilization ability than ι-carrageenan. For the salad dressing 300 rpm was identified as critical rpm value, corresponding to 12 g. At 1000 rpm the particles fully sedimented within the analysis time, and at 2000 rpm sedimentation was completed already after running 2 profiles (= 10 s). In contrast, in the ι-carrageenan gel 4000 rpm was required for such a fast sedimentation – clearly showing its higher stabilizing ability. However, the salad dressing can still be used for long-term stabilization, because 1 g

at normal storage condition is distinctly away from 8 g, where first signs of sedimentation were noted. This salad dressing is on the market with herbs as particles, and stable as a food product. Its stabilizing ability has also been confirmed by the VIS measurements in the sedimentation study at normal storage conditions.

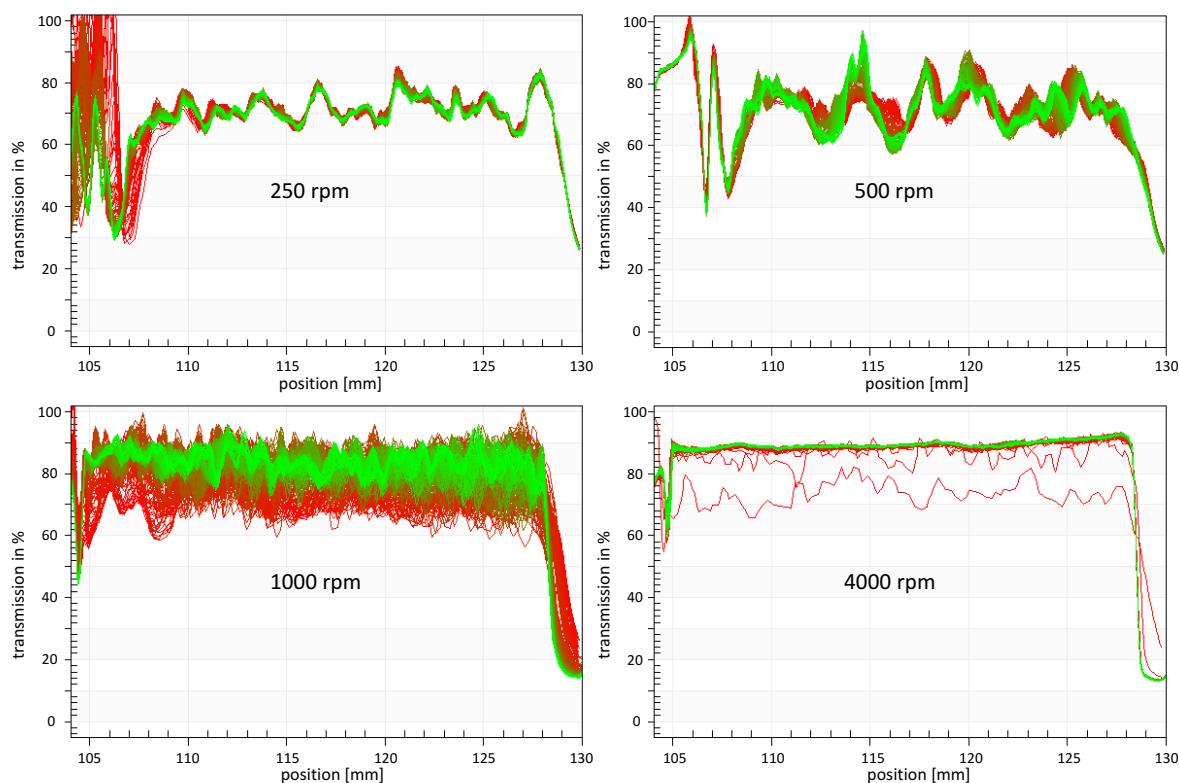


Figure 6: Sedimentation profiles (transmission vs. position in cell) of 50 μm sized smartPearls incorporated in ι -carrageenan gel. Very slight sedimentation is recognizable at 500 rpm. For pronounced sedimentation, 4000 rpm are required (i.e. in this case within 3 profiles \triangleq 15 s).

In summary, based on the analytical centrifugation, the purely viscous gels are not suitable to stabilize smartPearls. The viscoelastic gels can be placed in following order of increasing stabilization ability: salad dressing, ι -carrageenan gel, polyacrylate gel. The ι -carrageenan gel is relatively low viscous. Thus, it should be preferred to produce dermal formulations with good spreading ability on the skin. It is also suitable, when compounds are incorporated into the dermal formulations which themselves increase the viscosity (e.g. oil in o/w creams). With a stability of up to almost 8 g sedimentation of smartPearls will not occur during processing, packaging, or transporting the formulation. The polyacrylate used in the study was relatively viscous and suitable for even larger sized silica particles due to its pronounced viscoelasticity. In case particles $< 50 \mu\text{m}$ are incorporated, the polyacrylate concentration in the gel can be

reduced distinctly below 1% (as used in this study) to make it less viscous, and better spreadable. The gel will still have sufficiently high viscoelastic property for long-term stabilization. Therefore, both the ι-carrageenan and the polyacrylate gels can be used for dermal formulations with silica particles.

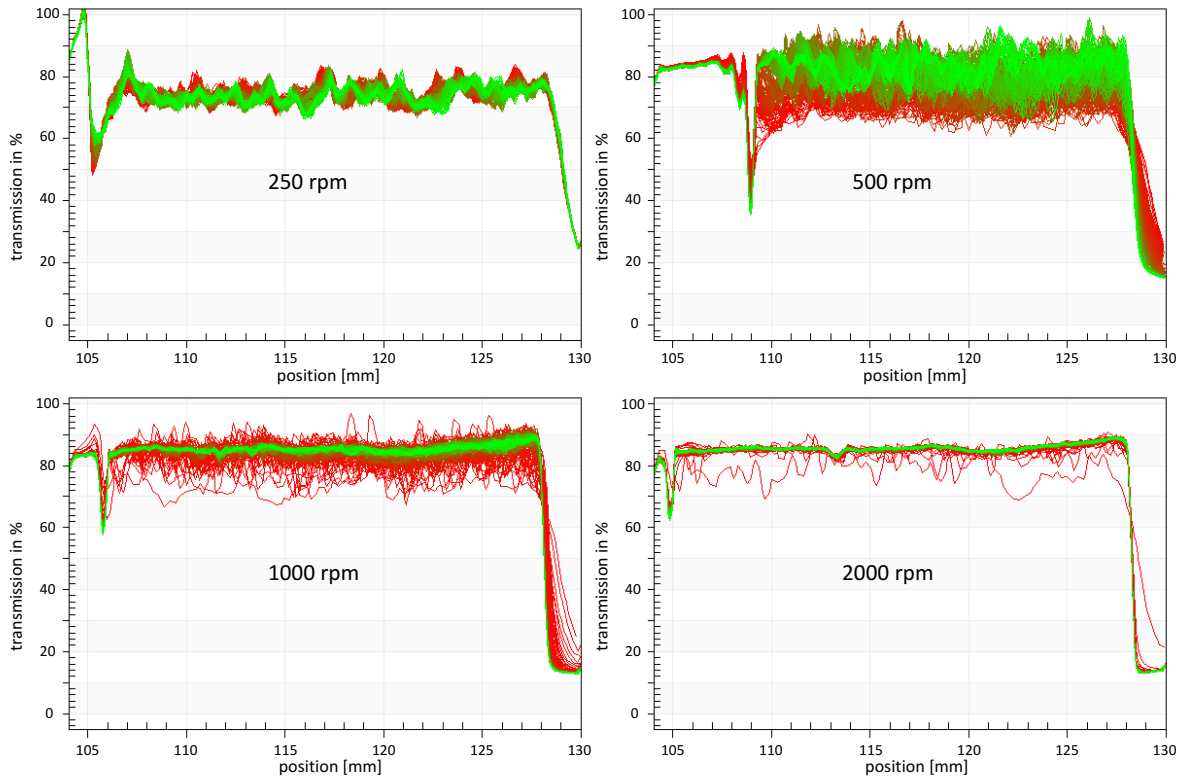


Figure 7: Sedimentation profiles (transmission vs. position in cell) of 150 μm sized smartPearls incorporated in the salad dressing. First very slight sedimentation is recognizable at 250 rpm, where clear sedimentation occurs at 500 rpm, and pronounced sedimentation already at just 2000 rpm (i.e. in this case within running 2 profiles = 10 s).

It is remarkable, that the polyacrylate gel showed no signs of sedimentation until the highest possible acceleration of 4000 rpm was applied (Figure 8). The change in the top of the cuvette can be explained by the particles sedimenting in the upper part. Particles sediment also in the lower part of the cuvette but are replaced by particles moving from the upper to the lower part. Thus, the transmission stays unchanged in the lower part within the running time of the analysis (1,800 s). Critical rpm number of this system is 3600. Based on these profiles, the polyacrylate gel is highly suitable for the stabilization of 150 μm smartPearls, and even distinctly larger particles can be stabilized when considering the g value 1970.

The ι -carrageenan gel shows at lower acceleration similar results to the polyacrylate gel at 4000 rpm. The fast sedimentation of the ι -carrageenan gel at higher rotation speeds (2000 or 4000 rpm) is based on the thinning behavior after the viscoelastic gel overcoming the yield point and the viscoelastic structure breaks.

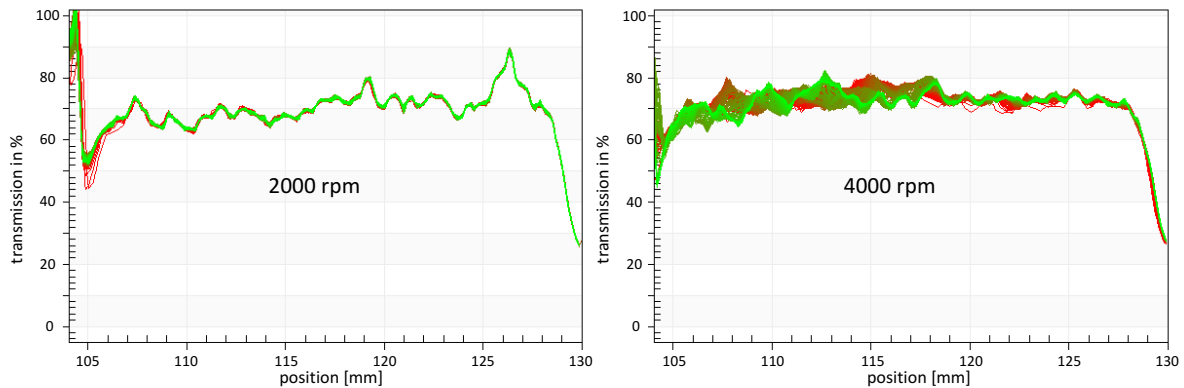


Figure 8: Sedimentation profiles (transmission vs. position in cell) of 50 μm sized smartPearls incorporated in polyacrylate gel. No sedimentation was observed for up to 2000 rpm. Slight sedimentation at the upper part of the cuvette (cell position 106-118) was visible at a rotation speed of 4000 rpm.

Figure 9 shows the profiles of the viscous HPC gel as a comparison to the viscoelastic gels. It shows that the sedimentation occurs already at 250 rpm and increases distinctly with increasing rpm number. Sedimentation is already very pronounced at 2000 rpm. This agrees with the theory that purely/dominantly viscous systems show continuously increasing sedimentation with increasing g number, according to the sedimentation law by Stokes. Complete sedimentation within less than 10 running profiles was not reached at 4000 rpm (maximum selectable rpm in the instrument). This can be explained by the relatively high viscosity of the 5% HPC gel system. At the end of the analysis time, complete separation was reached, as shown by the high transmission. Based on this data, the viscous gel is not suited for a long-term stabilization, agreeing with the fast sedimentation observed in the VIS sedimentation study. Comparable results were obtained for the other viscous gels (data not shown).

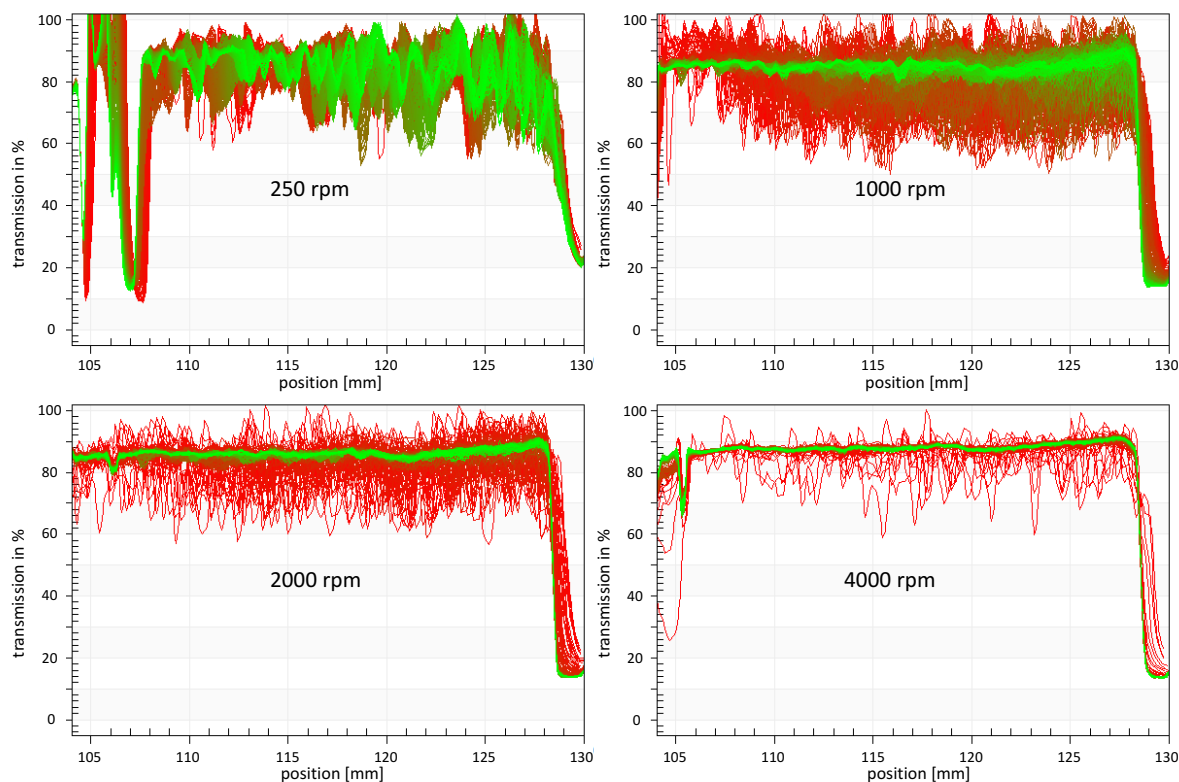


Figure 9: Sedimentation profiles (transmission vs. position in cell) of $150\ \mu\text{m}$ sized smartPearls incorporated in HPC gel. Sedimentation occurred already clearly at 250 rpm. At higher rotation speeds of 1000 and 2000 rpm the sedimentation is much faster, and the sample is nearly cleared up. Complete sedimentation was observed at 4000 rpm, displayed by a constant high transmission over the whole cuvette at the end of the analysis time (green lines). The complete sedimentation took distinctly longer compared to the viscoelastic gels.

3.3.4. Rheological behavior of unloaded and smartPearls loaded hydrogels

Rheological investigations were performed by applying a stress ramp τ up to 1000 Pa, and a shear rate D up to 1000 [1/s]. Figure 10 shows the rheograms obtained for the 3 viscoelastic gels and the viscous gel HPC. For HPC, the relationship D - τ is practically linear in the log-log plot and the flow behavior is almost Newtonian. In contrast, ι -carrageenan shows shear thinning as seen by the positive deviation to higher D values in the plot. ι -carrageenan and polyacrylate gels have flow points at about 0.01 Pa and 1 Pa, respectively, and show more pronounced shear thinning (steeper increase in D vs. τ), thus showing a plastic flow behavior. A relatively high viscosity of the suspension in rested mode, and shear thinning under stress conditions is desirable. Then, the suspension is well stabilized during storage but also flows well after shaking (application of stress) before dispensing and application on skin. The dressing shows less pronounced shear thinning at higher stress.

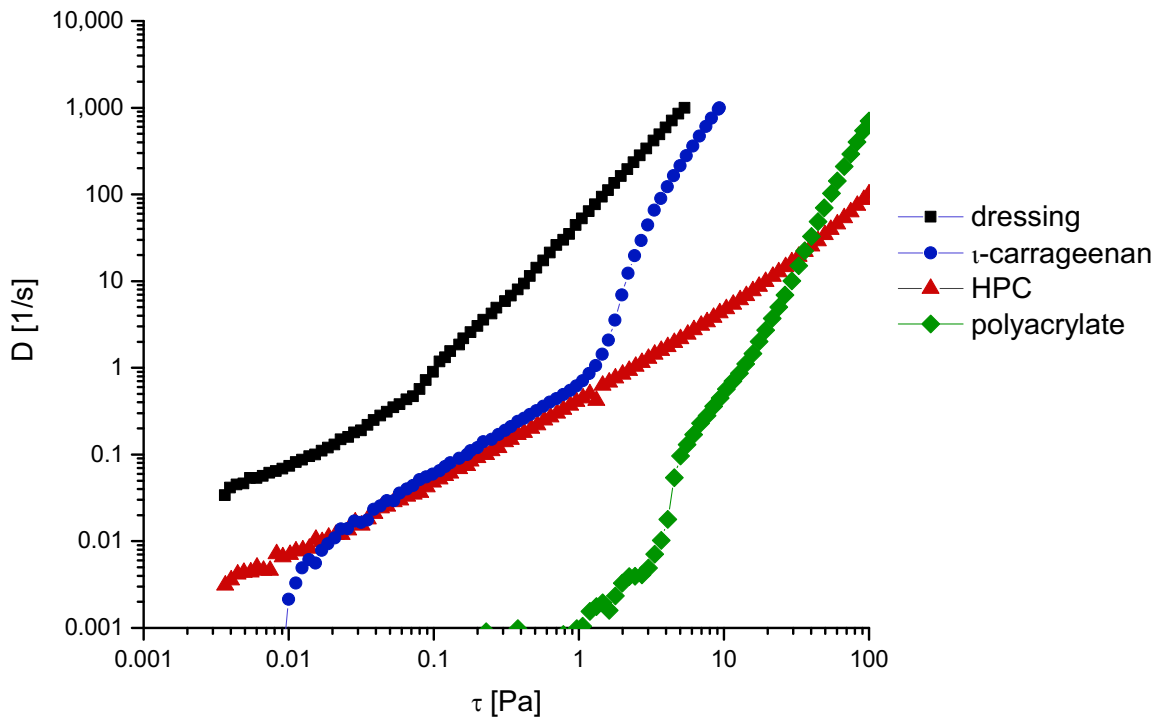


Figure 10: Rheograms of shear rate D (1/s) in dependency of the shear stress (0-100 Pa) of the salad dressing, 0.4% ι -carrageenan, 5% HPC and 0.125% polyacrylate gel.

Figure 11 (upper) shows the curves obtained by amplitude sweep measurement. G' and G'' were plotted versus the shear stress τ , where modulus G' represents the elastic fraction and modulus G'' the viscous fraction. Depending on the modulus dominating, the system has more elastic or dominantly viscous properties.

Between 0.1 and 1000 Pa the viscous modulus G'' is about twice the elastic modulus G' , showing that the HPC gel has dominantly viscous property (Figure 11 A, upper curve). This agrees with the VIS investigation (sedimentation of the silica within less than 7 days), and the results of the analytical centrifuge. The elastic G' modulus below 0,1 Pa shows high fluctuation, thus no reliable interpretation can be given.

The polyacrylate gel (Figure 11 B, upper curves) shows dominantly elastic properties up to a shear stress of around 30 Pa. This confirms the assumption of the VIS investigation of a highly viscoelastic gel, being able to stabilize silica particles at least up to 150 μm . On the other hand, the spreadability is affected by the viscoelasticity at high shear stress.

ι -carrageenan shows a more complex relationship (Figure 11 A, lower curves). G' and G'' are similar up to 1 Pa (linear regions), then up to about 10 Pa G' is lower with a minimum at about 5 Pa. Above 10 Pa, G'' is higher, i.e. the system is dominantly elastic.

The salad dressing shows a similar complex profile. Only the minimum is shifted to lower stress of 1 Pa (Figure 11 B). This might be desirable for a dressing, since the consumer expects a good flowability when pouring the dressing from a bottle. At values > 10 Pa, the salad dressing possesses identical elasticity as ι -carrageenan, having similar G' .

In summary, the amplitude sweep measurements revealed dominant viscous structure for the HPC gel. In contrast, the other polymers showed similar viscous and elastic properties at low stress (Pa), and dominantly elastic properties at high shear stress, being equivalent to the situation when large particles (= high weight force F) want to sediment in the gel. This property is very favorable for incorporating large silica particles of 50 μm or larger. The magnitude of the G' moduli is similar for all viscoelastic gels. Based on these properties all 3 viscoelastic gels are suitable for silica containing formulations, and the final selection will depend on other rheological properties contributed by other compounds (e.g. oil or other polymers) in the final formulation.

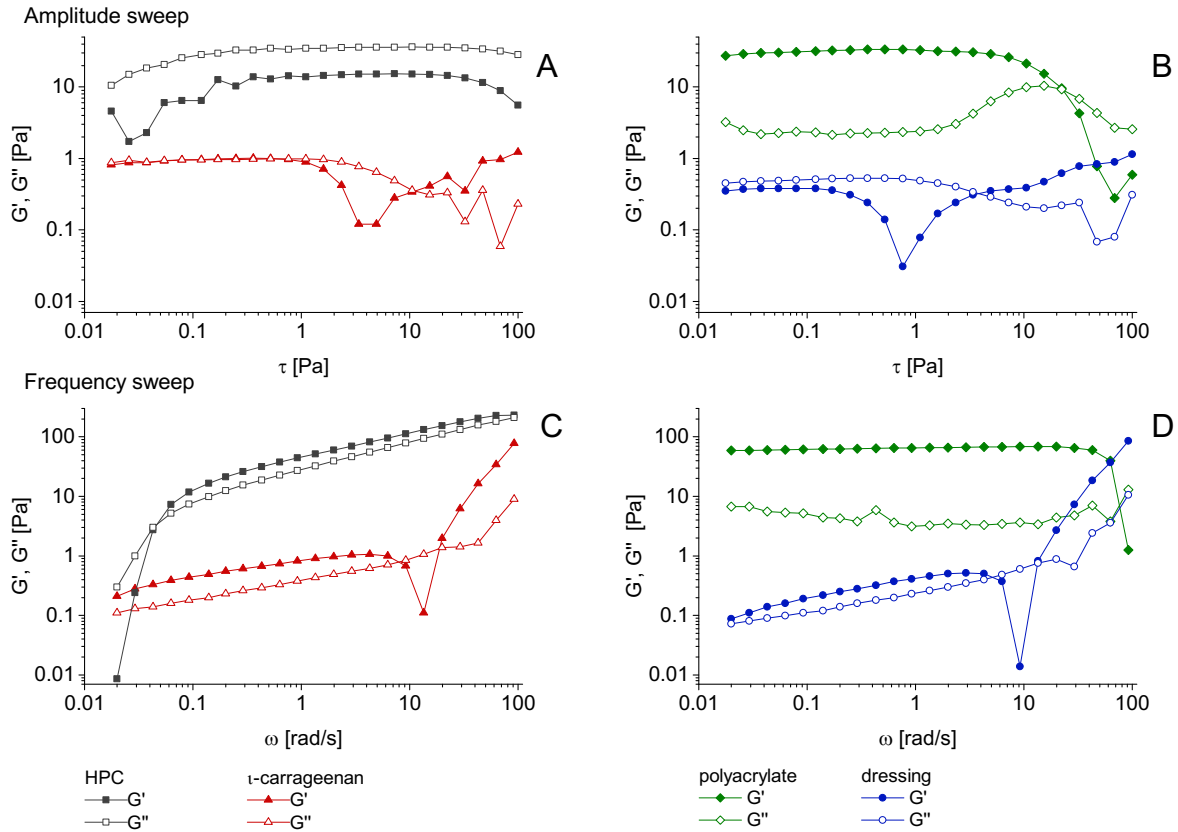


Figure 11: A/B: Amplitude sweep measurements from 0.01 up to 100 Pa show the linear viscoelastic area (LVA) for the elastic modulus G' (filled symbols) and the viscous modulus G'' (blank symbols) at a frequency of 6.28 rad/s. C/D: Elastic modulus G' and viscous modulus G'' measured by a frequency sweep test at controlled shear stress of $\omega=0.01$ up to 100 rad/s. Measurements were conducted for 5% HPC (squares), 0.35% ι -carrageenan (triangles), 0.25% polyacrylate ETD 2000 NF (rhombus) and dressing sample (dots).

The frequency sweep analysis clarifies the influence of the frequency on the measured elastic and viscous modulus [22]. In the frequency sweep analysis, except for the HPC gel, all measurements were performed at 0.2 Pa, i.e. in the linear viscoelastic area (LVA). Due to non-linearity of the HPC sample at $\tau=0.2$ Pa, a higher value of 0.5 Pa was chosen for the frequency sweep analysis.

Apart from below 0.03 rad/s, the HPC gel showed similar values for both moduli at all applied shear stresses of up to 1000 rad/s (Figure 11 C). This means, at low stress (e.g. a suspension at resting state) the viscous part dominates with only little contribution of elastic stabilization. The G' value at 0.02 rad/s is below 0.01 Pa. In contrast, the ι -carrageenan shows roughly twice as high elastic modulus over the whole frequency range (please note logarithmic axis), apart from a minimum at about 10 rad/s. This is in agreement with the minimum observed in the

amplitude sweep test performed with 6.28 rad/s. These data show nicely the viscoelastic stabilization capacity of the ι-carrageenan.

The dressing shows a similar behavior as the ι-carrageenan in the frequency sweep analysis (Figure 11 D). The shape of the curve is comparable as well as the absolute values measured. There is also a minimum for G' at about 10 rad/s, at which the elastic modulus drops below the viscous modulus. This crossover point of the G' and G'' curve (= both moduli are similar) is at about 6 rad/s, the frequency at which the amplitude sweep analysis was performed. That means, that this crossover point is an exceptional situation (at all other frequencies G' is higher than G''). Thus, to obtain an overall picture, it is meaningful to run both the amplitude sweep and the frequency sweep analysis.

The polyacrylate shows a pronounced viscoelastic behavior with almost 10 times higher values for the elastic modulus G' than the viscous modulus G'' for the entire range till 60 rad/s (Figure 11 D). The crossover point of both moduli is at around 80 rad/s, meaning that the stabilization with the polyacrylate gel can be realized for almost the entire observed measurement range.

In summary, the 3 different rheological analyses showed that the elastic contributions were at most conditions of shear stress (Pa) and shear frequency (rad/s) dominant, which makes the 3 viscoelastic polymers suitable for the stabilization of large silica particles in suspensions. The absolute values of G' and G'' were much higher for the HPC gel, which is attributed to the distinctly higher polymer concentration of 5% compared to e.g. 0.35% in the ι-carrageenan gel. For the overall stabilization ability, the ratio of G' and G'' is important.

3.4. Conclusion

As predictable, pure viscous or predominantly viscous systems such as HPC are not able to sufficiently stabilize smartPearls suspensions. In contrast, viscoelastic systems are an elegant way to avoid sedimentation in dermal formulations, even for 150 μm large particles.

Stability tests such as the employed sedimentation test can predict long-term stability under normal storage conditions, but not in case of special stress which may occur during storage. To select a polymer system which has a certain “reserve capacity” for such physical stresses, an analytical centrifuge, in this case the LUMiSizer[®], proved to be very helpful. The viscoelastic

polymers could be placed in increasing order of yield point, representing the point where the viscoelastic capacity collapses. Thus, a polymer with desired reserve capacity can be selected.

The characterization should be completed by rheological investigations to determine the elastic modulus G' and viscous modulus G'' , for the selection of predominantly viscoelastic systems. Polymers, such as ι -carrageenan, with a low viscosity are preferred to provide a good spreadability on the skin. Low viscous systems also have the advantage, that they can be “problem-free” added to creams with already high viscosities due to e.g. relatively high content of oil droplets. In case that the polymers are relatively viscous (as in this study the 5% HPC gel and the polyacrylate gel), the problem might be solved by reducing the polymer concentration. With this characterization approach, dermal gels and also creams with smartPearls can be formulated with sufficient long-term stability.

References

- [1] Saal, C.; Petereit, A.C.; 2012. Optimizing solubility: Kinetic versus thermodynamic solubility temptations and risks. *European Journal of Pharmaceutical Sciences* 47(3), 589-595. <https://doi.org/10.1016/j.ejps.2012.07.019>
- [2] Hancock, B.C.; Parks, M.; 2000. What is the True Solubility Advantage for Amorphous Pharmaceuticals? *Pharmaceutical Research* 17(4), 397-404. <https://doi.org/10.1023/A:1007516718048>
- [3] Moser, K.; Kriwet, K.; Naik, A.; Kalia, Y.N.; Guy, R.H.; 2001. Passive skin penetration enhancement and its quantification in vitro. *European Journal of Pharmaceutics and Biopharmaceutics* 52(2), 103-112. [https://doi.org/10.1016/S0939-6411\(01\)00166-7](https://doi.org/10.1016/S0939-6411(01)00166-7)
- [4] Lin, X.; Hu, Y.; Liu, L.; Su, L.; Li, N.; Yu, J.; Tang, B.; Yang, Z.; 2018. Physical Stability of Amorphous Solid Dispersions: a Physicochemical Perspective with Thermodynamic, Kinetic and Environmental Aspects. *Pharmaceutical Research* 35(6), 125. <https://doi.org/10.1007/s11095-018-2408-3>
- [5] DeBoyace, K.; Wildfong, P.L.D.; 2018. The Application of Modeling and Prediction to the Formation and Stability of Amorphous Solid Dispersions. *Journal of Pharmaceutical Sciences* 107(1), 57-74. <https://doi.org/10.1016/j.xphs.2017.03.029>

-
- [6] Khougaz, K.; Clas, S.D.; 2000. Crystallization Inhibition in Solid Dispersions of MK-0591 and Poly(vinylpyrrolidone) Polymers. *Journal of Pharmaceutical Sciences* 89(10), 1325-1334. [https://doi.org/10.1002/1520-6017\(200010\)89:10<1325::AID-JPS10>3.0.CO;2-5](https://doi.org/10.1002/1520-6017(200010)89:10<1325::AID-JPS10>3.0.CO;2-5)
- [7] Nolte, M.; Mayer, J.; Ferreiro, M.G.; Assogba-Zandt, A.; Fehring, V.; Kröhne, L.; Voigt, A.; Dunmann, C., inventors; 2009. Stabilization of amorphous drugs using sponge-like carrier matrices. International Publication Number WO 2009/153346 A2, patent application PCT/EP2009/057688
- [8] Wei, Q.; Keck, C.M.; Müller, R.H.; 2015. CapsMorph® technology for oral delivery—theory, preparation and characterization. *International Journal of Pharmaceutics* 482(1), 11-20. <https://doi.org/10.1016/j.ijpharm.2014.10.068>
- [9] Hong, S.; Shen, S.; Tan, D.C.T.; Ng, W.K.; Liu, X.; Chia, L.S.O.; Irwan, A.W.; Tan, R.; Nowak, S.A.; Marsh, K.; Gokhale, R.; 2016. High drug load, stable, manufacturable and bioavailable fenofibrate formulations in mesoporous silica: a comparison of spray drying versus solvent impregnation methods. *Drug Delivery* 23(1), 316-327. <https://doi.org/10.3109/10717544.2014.913323>
- [10] Limnell, T.; Santos, H.A.; Mäkilä, E.; Heikkilä, T.; Salonen, J.; Murzin, D.Y.; Kumar, N.; Laaksonen, T.; Peltonen, L.; Hirvonen, J.; 2011. Drug delivery formulations of ordered and nonordered mesoporous silica: comparison of three drug loading methods. *Journal of Pharmaceutical Sciences* 100(8), 3294-3306. <https://doi.org/10.1002/jps.22577>
- [11] Wei, Q.; Keck, C.M.; Müller, R.H.; 2015. CapsMorph – amorphous oral delivery technology in porous particles, W4224, AAPS Annual Meeting, Orlando, 25.-29. Oktober.
- [12] Qian, K.K.; Bogner, R.H.; 2012. Application of Mesoporous Silicon Dioxide and Silicate in Oral Amorphous Drug Delivery Systems. *Journal of Pharmaceutical Sciences* 101(2), 444-463. <https://doi.org/10.1002/jps.22779>
- [13] Laitinen, R.; Löbmann, K.; Strachan, C.J.; Grohgan, H.; Rades, T.; 2013. Emerging trends in the stabilization of amorphous drugs. *International Journal of Pharmaceutics* 453(1), 65-79. <https://doi.org/10.1016/j.ijpharm.2012.04.066>

- [14] Charnay, C.; Bégu, S.; Tourné-Péteilh, C.; Nicole, L.; Lerner, D.A.; Devoisselle, J.-M.; 2004. Inclusion of ibuprofen in mesoporous templated silica: drug loading and release property. *European Journal of Pharmaceutics and Biopharmaceutics* 57(3), 533-540. <https://doi.org/10.1016/j.ejpb.2003.12.007>
- [15] Monsuur, F.H.; Hoefer, H.H.; Keck, C.M., inventors; Grace GmbH & Co. KG, Pharmasol GmbH, assignee; 2014. Active-loaded particulate materials for topical administration. International Publication Number WO 2016/041992 A1, patent application PCT/EP2015/071138, Sep 15.
- [16] Müller, R.H.; Monsuur, F.; Höfer, H.H.; Jin, N.; Staufenbiel, S.; Keck, C.M.; 2014. smartPearls - novel amorphous delivery system based on porous materials to increase skin penetration of anti-oxidants, Workshop NutriOX, Metz, 1-3 October.
- [17] Jin, N.; 2017. Nanocrystals & loaded porous silica for increased dermal bioavailability [doctoral thesis]. [Germany]: Freie Universität Berlin. urn:nbn:de:kobv:188-fudissthesis000000105191-3
- [18] Keck, C.M.; Monsuur, F.; Höfer, H.H.; Jin, N.; Staufenbiel, S.; Müller, R.H.; 2014. smartPearls - new dermal injection-like delivery system without use of a needle, p. 10, Menopause, Andropause, Anti-aging, Vienna, 10-13 December.
- [19] Hecq, J.; Deleers, M.; Fanara, D.; Vranckx, H.; Amighi, K.; 2005. Preparation and characterization of nanocrystals for solubility and dissolution rate enhancement of nifedipine. *International Journal of Pharmaceutics* 299(1), 167-177. <https://doi.org/10.1016/j.ijpharm.2005.05.014>
- [20] Watase, M.; Nishinari, K.; 1982. Effect of alkali metal ions on the viscoelasticity of concentrated kappa-carrageenan and agarose gels. *Rheologica Acta* 21(3), 318-324. <https://doi.org/10.1007/BF01515719>
- [21] Mezger, T.G.; 2016. *Das Rheologie Handbuch*, 5th ed. FARBE UND LACK // BIBLIOTHEK. Vincentz Network GmbH & Co. KG, Hannover. ISBN: 9783866306332

4. Dermal smartPearls – Optimized silica particles for commercial products & mechanistic considerations³

Abstract

The amorphous state of actives can be long-term stabilized by incorporation into mesoporous particles, thus the increase in the saturation solubility by amorphicity can be exploited to improve the bioavailability. In this study 5 different silica particles were investigated regarding loading capacity and long-term stability of the amorphous form. Five different silica were used ranging in pore mean size from 3 to 25 nm, pore volume 0.4 to 1.8 mL/g, and BET surface from 740 to 320 m²/g. As model active avobenzone was used, because it is a challenging molecule by its high crystallisation tendency. To be industrially feasible, a loading capacity of about 50% pore volume was investigated. The particles were loaded by an immersion evaporation method, being able to be used in industrial production. A theory of the active precipitation in the pores was developed based on the Ostwald-Miers range. The 25 nm pore-sized particles showed a crystalline fraction directly after loading, the 3 nm and 17 nm pore-sized particles after 1 month of storage. Long-term stability of 1 year had the silica with 6 nm and 10 nm pore size, thus being ideal for products. By nitrogen sorption studies, primarily filling of the pores from bottom to top was identified as loading mechanism. HPLC analysis showed some active remaining in the pores due to strong interaction with the pore surface, which needs to be considered when developing dermal products. Interestingly, the increase in saturation solubility C_s – determined in carrageenan gels – remained also for silica particles showing a minor partial crystalline avobenzone fraction. Thus, limited crystallinity does not impair the shelf-life and performance of dermal formulations.

³ This chapter has been submitted for publication as:

Hespeler, D.; Pyo, S.M.; Müller, R.H.; 2019. Dermal smartPearls – Optimized silica particles for commercial products & mechanistic considerations. *International Journal of Pharmaceutics*, *submitted [Manuscript ID: IJP-S-19-01888]*.

4.1. Introduction

The bioavailability of poorly soluble actives can be increased by converting them from the crystalline into the amorphous state, i.e. generating supersaturated solutions C_{ss} [1]. This leads to an increased concentration gradient across biological membranes, thus to an increased diffusional flux and higher concentration in the biological target compartment [2; 3]. However, for commercial products with defined shelf life, the instability of the amorphous state is a problem [4]. Re-crystallization is a statistical event, and might happen after a few days, months, or years of the shelf life. The only solution is to use a reliable technology to effectively stabilize the amorphous state [5].

One of the technologies is the loading of mesoporous particles (preferentially silica with non-ordered pores, being already regulatory accepted) with the active, for example the so called CapsMorph technology [6; 7] – originally developed for oral administration. The actives are loaded inside the pores and stay amorphous because the space restriction inside the 2-50 nm pores inhibits crystallization. Thereby the re-crystallisation is thermodynamically completely suppressed below a certain pore diameter, or is at least slowed down due to surface effects and changes in the nucleation mechanism [8]. Physical stability of the amorphous state of candesartan cilexetil was proven for up to 4 years [9]. Maleki et al. gives an extensive overview of studies using this principal with different silica, loading methods, and actives [10].

Most of the silica research development focussed on the oral administration route, dermal was neglected [11; 12]. In 2014, as novel approach the technology was transferred from the oral administration route to dermal application, the so called smartPearls technology [13; 14]. Incorporation of the loaded silica particles into dermal formulations (e.g. gels) created supersaturated solution and increased penetration into the skin, being superior even to nanocrystals [15] – which can be considered as the dermal gold standard for delivering poorly soluble actives.

The patent application for oral silica (CapsMorph) uses as loading procedure the impregnation of particles. The pores are soaked with drug solution, then the solvent from the silica powder is evaporated in a rotary evaporator. To achieve a higher loading, multiple soaking and evaporation steps are needed – being not an industrially efficient/friendly process. Loading can alternatively be performed e.g. with supercritical carbon dioxide [16], but this process

requires special equipment and is costly. It is not applicable in an “average” dermal company. Thus, in a previous study a one-step loading process was developed, the immersion evaporation method [17]. The particles are dispersed in an organic solution of the active, and then the solvent is evaporated from the suspension in a rotary evaporator. Volume and concentration in the solution are adjusted this way, that in one evaporation step the target loading of the silica is achieved. In the development of this method, previously rutin was used as model active, being an antioxidant and thus having high relevance for dermal application (e.g. intercept radicals formed by IR/blue light in an anti-pollution strategy).

In this study, avobenzene was used as model active, a UV absorber with high crystallization tendency. Thus, it is a suitable, challenging compound to assess the ability of porous silica to preserve the amorphous state. Systematically 5 different commercial silica were investigated to identify the most suitable silica type for loading varying in particle size (3 to 50 μm), pore diameter (3 to 25 nm) and pore volume (0.4 to 1.8 mL/g). Most suitable being defined as maintaining the amorphous state the longest time, and at the same time allowing a sufficient loading. Many previous studies [18; 19] focus on ordered silica (e.g. to have well defined systems). However, they are too expensive for many products. Having the use in cosmetic and pharmaceutical products in mind, cost-effective non-ordered silica were used. In addition, non-ordered silica particles were selected which are commercially available and are at the same time regulatorily accepted, especially for dermal application.

4.2. Materials and Methods

4.2.1. Materials

Silica particles (Table 1) with mesopores of 3, 6, 10, 17 and 25 nm were provided by Grace GmbH & Co. KG (Worms, Germany). Avobenzene and ethyl acetate (HPLC grade) were purchased from Symrise AG (Holzminden, Germany) and VWR international GmbH (Darmstadt, Germany), respectively. Purified water was obtained using a Milli-Q system from Merck Millipore GmbH (Darmstadt, Germany).

Table 1: Properties of silica particles according the certificate of analysis by the supplier

name	pore width [nm]	pore volume [mL/g]	BET surface [m ² /g]	calculated surface [m ² /g]	particle size [μm]
Syloid® XDP 3050	25	1.8	320	288	48-66
Syloid® 244 FP	17	1.6	380	376	2.5-3.7
Syloid® 72 FP	10	1.2	370	480	4.6-5.8
Davisil® LC60A	6	0.9	550	600	12
Syloid® AL-1 FP	3	0.4	740	533	6.5-8.1

4.2.2. smartPearls loading procedure for avobenzonone

All different silica particles were loaded with the immersion evaporation method. Loading of 48.8% (v/v) of the pore volume was performed. The 48.8% were selected for comparison reasons with a loading method used by Jin et. al using the impregnation method with multiple loading steps [15]. The resulting theoretical mass fraction in g was calculated by dividing the pore volume through the density of the crystalline active. Example (Syloid® 72PF): 1.2 mL/g multiplied by avobenzonone density of 1.1 g/mL yielding 1.32 g avobenzonone (=100 % pore filling). The 48.8% correspond to 0.64 g avobenzonone per 1 g silica, i.e. 38.72% avobenzonone mass fraction.

For the loading of the pores, a 20% avobenzonone ethyl acetate solution was prepared. The respective volume of this solution (containing the required amount for loading) was added to each type of silica particles. For example, in case of Syloid® XDP 3050 this was 9.13 g of 20% avobenzonone ethyl acetate solution added to 2 g of silica. The silica was placed in a 250 mL round bottom powder flask equipped with baffles, afterwards ethyl acetate solution was added. The ethyl acetate was slowly removed from this homogeneous silica dispersion under rotation by a rotary evaporator at 40°C and 350 mbar. When a dry powder was obtained, the collected solvent in the rotary evaporator was removed, and a post-treatment applied. The pressure was slowly reduced over a time period of 10 minutes to 50 mbar to minimize solvent residues. In a final step, the flask with the loaded silica was placed into a desiccator at 50 mbar for 24 hours.

4.2.3. Avobenzone smartPearls characterization and stability determination

Light microscopy and scanning electron microscopy (SEM)

Light microscope imaging was performed using a Motic Microscope BA210 (Motic Deutschland GmbH, Germany) with a Moticcama camera and the Software Motic Images Plus at 100, 400, and 1,000-fold magnification. Scanning electron microscopy (SEM) was performed at 10,000-fold magnification using a Zeiss DSM950 (Carl Zeiss AG, Germany). Samples were sputter-coated with gold-palladium in an argon atmosphere with 15-20 kV at 0.05 mbar for four minutes.

Crystallinity investigation by DSC (differential scanning calorimetry)

Differential scanning calorimetry was performed using a DSC 1 (Mettler Toledo GmbH, Germany) for the determination of crystalline fraction within the samples. A defined amount of about 5 mg (precisely weighted) was sealed in a pierced 40 μ l aluminum pan. Measurements were conducted with a heating rate of 20 K/min between 25 and 125 °C under 80 mL/min nitrogen purge. Melting point of avobenzone is 81 °C.

Confirmation of amorphous state by XRD (X-ray diffraction)

X-ray diffraction was performed using a Bruker D8 (Bruker Co., USA) to determine the amorphous state and potential crystalline fractions of avobenzone in smartPearls. A scan rate of 0.02° was used between $2\theta = 2-60^\circ$. The goniometer was equipped with a Cu-anode ($K\alpha=0.15406$ nm) with a voltage of 40 kV and current of 35 mA.

Pore and surface specification by nitrogen ad- and desorption

The samples were outgassed at 30 °C for 24 hours prior the measurement. Nitrogen physisorption isotherms with 20 adsorption points between a relative pressure of 0.05-0.99 and 27 desorption points between 0.99-0.30 were recorded after production with a NOVA Quantachrome 4000e (Quantachrome GmbH & Co. KG, Germany) at 77 K (liquid nitrogen). Calculations were performed by the provided software NOVAwin 11.0. Pore widths and pore volumes were determined after the density functional theory (DFT) and surface analysis after the Brunauer-Emmett-Teller (BET) method [20].

Avobenzene content determination by HPLC (high performance liquid chromatography)

Avobenzene content was determined by a Kontron 400 System (Kontron Instruments GmbH, Germany) equipped with a 20 µl loop and a Nucleosil® 100-5 C18 (250x4 mm) column. Mobile phase was methanol:water 85:15 with a flow rate of 0.75 mL/min. UV/VIS detection was performed at 355 nm and peak evaluation by the supplied KromaSystem 2000 software. For sample preparation a defined amount of about 50 mg were suspended in 25 ml ethyl acetate and shaken for 10 minutes. The suspension was centrifugated for 10 minutes at 10,000 rpm. An aliquot of the supernatant was diluted by a factor of 200 in mobile phase prior determination.

4.2.4. Determination of the saturation solubility via UV/VIS

Saturation solubility was determined by a UV/VIS spectrometer PharmaSpec UV-1700 (Shimadzu, Japan) at room temperature. The raw drug powder and avobenzene smartPearls were dispersed in a 0.4% carrageenan gel. The added amount of avobenzene was 10 times above the saturation solubility of its raw drug powder. Determination of the saturation solubility compared to the avobenzene raw drug powder was conducted one, three and seven days after production, and the mean calculated. Concentrations of samples analyzed in the spectrometer were adjusted to achieve a spectrum with absorption values between 0.1 and 2.0. Increase in adsorption due to presence of particles was corrected by evaluation of the area under the curve (AUC) instead of the absolute absorption value. Thus, the peak area correlates with the concentration. Results obtained with the smartPearls are displayed as a multiple of reading measured with avobenzene powder in water (= measure for multiplication of saturation solubility).

4.3. Results and Discussion

4.3.1. Theoretical consideration for the loading

The ideally loaded silica particles should contain the amorphous drug in the pores, and as little as possible on the particle surface. Based on this, the pore volume is the determining factor for the achievable maximum theoretical loading. For example, in case of the particles with 25 nm pores size (Syloid® XDP 3050), the maximum theoretical loading would be about

65% (w/w), calculated considering the crystalline density of the model active avobenzone (Table 2). Of course, the pore size has also an influence on the practically achievable loading. This influence is rather complex. Larger pores are more easily accessible to the loading fluid, smaller pores exhibit stronger capillary forces according to the Kelvin equation. Too small pores can hinder the loading (e.g. <2 nm), in case the molecule is relatively large (high molecular weight) in relation to the pore. It is an effect comparable to molecular sieving [21]. The molecular dimension of avobenzone is about 1.0-1.6 nm, that means in case of the 3 nm silica used in this study, it is a pore to molecule ratio of 2-3. Pore volume and pore size determine the overall surface of the particle, available for monomolecular adsorption. In some cases, the first monolayer adsorbed is more difficult to desorb (stronger interaction forces) when the active should be released, leading to some percentage of active remaining in the particles [22]. In overall, the key factors are pore volume and pore size, which are interconnected by the parameter total surface. A pore volume of 1.8 mL/g with a pore width of 25 nm supposing a cylindrical pore relate to an inner surface of 288 m²/g. Taking a certain surface roughness into account this value correlates well with the provided BET surface of 320 m²/g in the supplier specification.

CHAPTER 4

Table 2: Pore volume and resulting maximum mass fraction in case of 100% pore filling and of 48.8% pore filling for the different silica. BET surface and mass fraction of loading in case of monolayer adsorption (calculated using the projection area of the molecule avobenzene, using ChemAxon [23]).

name	pore volume [mL/g]	mass fraction with 100% pore filling according avobenzene density [%]	mass fraction with 48.8% pore filling [%]	BET surface area [m ² /g]	mass fraction (monolayer) according projection area [%]
Syloid [®] XDP 3050	1.8	64.72	47.23	320	1.69 – 3.23
Syloid [®] 244 FP	1.6	63.32	45.73	380	2.00 – 3.96
Syloid [®] 72 FP	1.2	56.42	38.72	370	1.95 – 3.85
Davisil [®] LC60A	0.9	49.27	32.15	550	2.87 – 5.73
Syloid [®] AL-1 FP	0.4	30.15	17.40	740	3.83 – 7.71

To investigate these effects, silica particles were selected ranging in pore volume from 0.4 mL/g to 1.8 mL/g and having pore sizes from 3 nm to 25 nm (Table 1). Logically the total surface is reciprocally proportional to the pore size, i.e. it ranges from 740 m²/g (3 nm) to 320 m²/g (25 nm). The surface areas cited are the measured BET surfaces, specified by the supplier. The calculated theoretical surface values are also listed in a separate column of Table 1.

When selecting the silica particles, preferentially particles were taken which are regulatorily accepted as pharmaceutical excipient (all apart from Davisil[®] LC60A). Due to toxicological considerations no aluminum silicates were used, because of the increasing discussion about aluminum toxicity in dermal products (e.g. deodorants [24]). Another important factor for selection was the particle size. The dermal products should not create any sandy feeling when applied onto the skin, that means the particle size should be maximum around 50 µm, as this

size cannot be sensed by the skin [13]. The size is also important for the physical stability of dermal products. The smaller the size, the less pronounced is sedimentation. Particles with decreasing particle size from about 50-65 μm to 3 μm were used in the study. However, reducing the sizes only slows down sedimentation velocity, but cannot avoid sedimentation in viscous systems. To solve the problem, viscoelastic dermal formulations were developed avoiding sedimentation completely even with silica particles of 50-65 μm (Syloid® XDP 3050) [25].

4.3.2. Avobenzone smartPearls loaded by the immersion evaporation method

In the immersion evaporation method, the unloaded silica particles are dispersed in the solution of active. The solvent is evaporated, the saturation solubility exceeded and the active precipitates. From theoretical considerations, precipitation should occur preferentially on the surface of the particle, because the rough surface acts as crystallization accelerator. There is little probability of crystals forming in the solvent phase. Because the pore surface represents more than 99% of the total particle surface, the active will preferentially localize in the pores, but some also on the surface. Thus, to achieve a complete loading of 100% of the pores is rather difficult without having some amount localizing on the surface. In contrast to the pores (e.g. 10 nm), this surface layer has no special restriction in thickness. Thus, exceeding a critical threshold of thickness, crystallization occurs. To minimize the risk of such crystallization, in this study a theoretical loading of about 50 % of the pore volume was aimed. This correlate to varying mass fractions of the active (Table 3).

CHAPTER 4

Table 3: Calculated loading (mass fraction) according to the used weight fractions (silica and avobenzonone solution) in the loading process, and the mass fraction determined by HPLC after loading for each silica.

name	mass fraction according used weight fractions [%]	mass fraction (HPLC)	
		mean [%]	SD [%]
25 nm	48.0	29.9	1.2
17 nm	41.9	28.2	4.1
10 nm	35.1	21.5	3.5
6 nm	28.9	16.6	4.2
3 nm	17.5	8.3	2.0

To assess the critical limit of loading (= occurrence of first crystallization), the silica particles were loaded, and the physical state of avobenzonone determined by DSC and X-ray diffraction. Avobenzonone has a melting peak of 81 °C, clearly detectable by DSC (Figure 1, upper curve). The empty silica particles are amorphous, no peak is detectable, exemplarily shown for the 6 nm silica. Mixing avobenzonone with 6 nm silica (physical mixture), an avobenzonone peak is detectable. In contrast, all thermograms – apart from the 25 nm – show no detectable peaks. The avobenzonone peak in the 25 nm silica particles is shifted to a lower temperature due to a melting point depression. This can be attributed to partial crystallization in confined spaces of a molecule pore ratio between 12 and 20 [26]. In summary from the DSC data, all particles apart from the 25 nm ones seem to be able to be loaded with about 50% (v/v) related to their respective pore volume. The loaded pore volume percentage is identical for all particles, but of course results in different mass percentages.

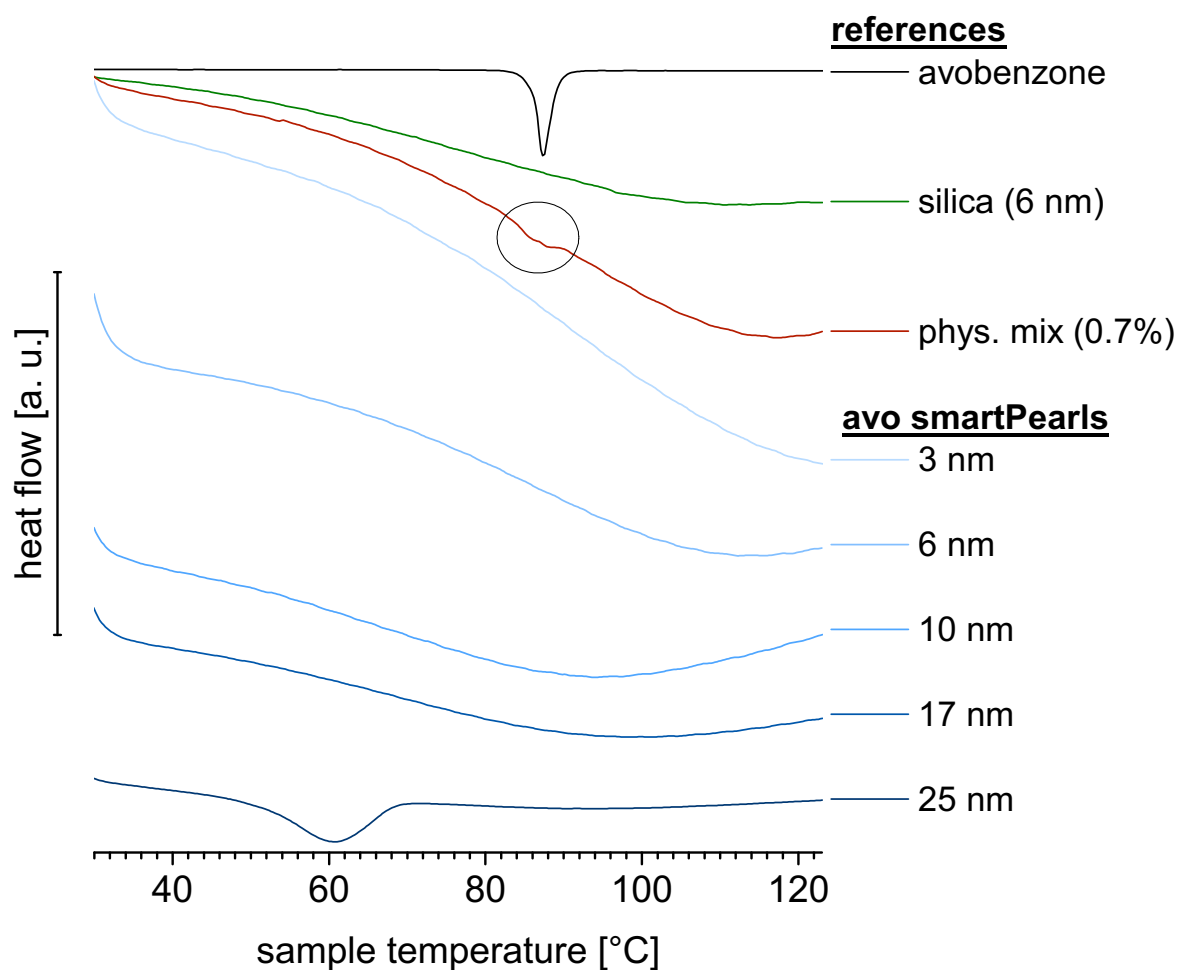


Figure 1: From upper to lower: Thermograms of avobenzene, silica particles (6 nm), 0.7% physical mixture and avobenzene smartPearls with 3, 6, 10, 17 and 25 nm pores, with avobenzene content according to Table 3.

To verify the amorphous state, X-ray diffraction (XRD) of the particles, being identified as amorphous by DSC, was performed. The X-ray diffractograms show a nice crystalline pattern for avobenzene, an amorphous halo for the empty silica particles and a small detectable peak in the physical mixture (Figure 2, upper 3 curves). In contrast to the DSC data, also crystallinity was detectable in both the 3 nm and the 17 nm particles. The XRD data were collected 4 weeks after particle loading. Performing again DSC with the 3 nm and 17 nm particles also revealed crystallinity (Figure 3; 3 and 17 nm DSC curves).

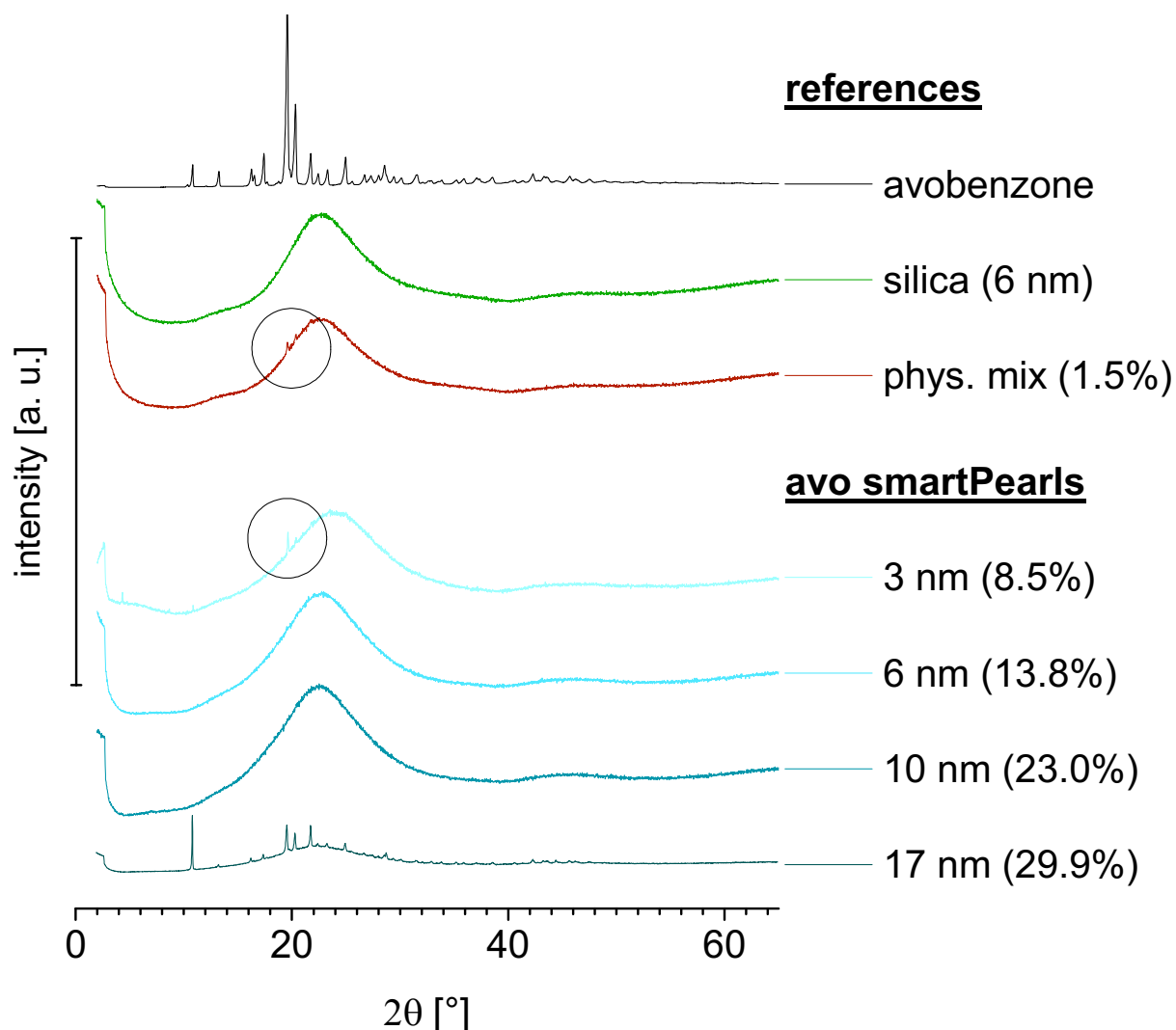


Figure 2: From top to bottom: XRD diffraction pattern of avobenzene, silica particles (6 nm), physical mixture (1.5%) and avobenzene (avo) smartPearls with 3, 6, 10, 17 nm pores (loading according to Table 3) 4 weeks after production.

A theoretical loading of 48.8% was tried to be achieved. This corresponds to avobenzene mass fractions between 17% and 48% depending on the silicas pore volume determined by weight (Table 3). In parallel, avobenzene was extracted for HPLC analysis. The percentages by HPLC were all below the calculated loading percentages (e.g. 25 nm particles: 29.9 % obtained by HPLC compared to 48% calculated based on the mass fractions used). This is a clear indication, that some avobenzene is bound firmly to the silica surface, a phenomenon described previously [22; 27]. The incomplete release needs to be considered when developing dermal formulations.

4.3.3. Loaded avobenzone smartPearls – 1 year long-term stability

All loaded particles were analyzed again by DSC and XRD during storage (Figure 3 and Figure 4). Directly after loading, only the 25 nm particles showed crystallinity by DSC. After 4 weeks of storage – the 3 nm and 17 nm particles also showed crystallinity (in agreement with 4 weeks XRD data). After 1 year of storage, the 6 nm and 10 nm particles showed still no peaks, i.e. according to DSC the avobenzone is still amorphous (Figure 3), of course within the detection limit of the method (0.7% avobenzone).

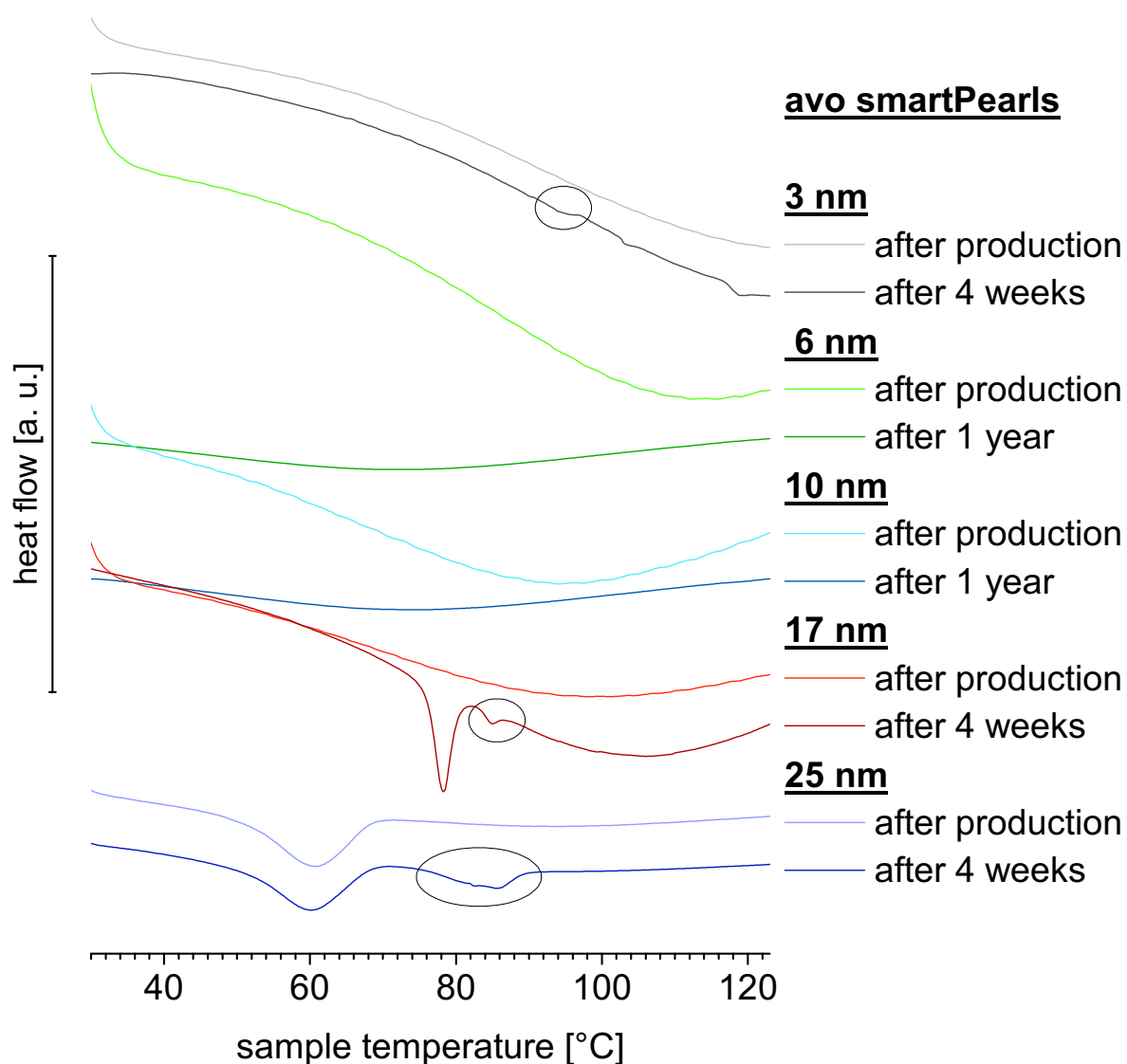


Figure 3: DSC thermograms of 3 nm (black), 6 nm (green), 10 nm (blue), 17 nm (red) and 25 nm (violet) smartPearls after production and after 4 weeks or one year storage (upper and lower curve, resp.).

Interestingly, also after 4 weeks, there was a change in the DSC diagram of the 25 nm particles. A second peak occurred at 81 °C, approx. the melting point of crystalline avobenzone. The first

peak detected directly after production showed only the peak associated to avobenzonone melting point depression compared to 81 °C. A possible explanation is that the two peaks originate from avobenzonone differently located. Potential different locations are at the particle surface and inside the pores. Thus, delayed crystallization is assumed within very large pores or at the surface of the particles. It should be kept in mind, that the specified pore diameter is an average, the pores show polydispersity with distinctly larger pores than the 25 nm. In these pores' crystallization should preferentially happen.

In parallel, the 6 nm and 10 nm particles were also analyzed by XRD. Figure 4 shows the diagrams after 4 weeks in comparison to after 1 year. No change occurred, the avobenzonone is physically stable in the amorphous state. Of course, one needs to consider the detection limit. Thus, physical mixtures were prepared with decreasing amounts of avobenzonone. By DSC an admixture of 0.7% avobenzonone was still detectable (Figure 1, 3rd curve from top), by XRD the detection limit was 1.5% (Figure 2, 3rd curve from top).

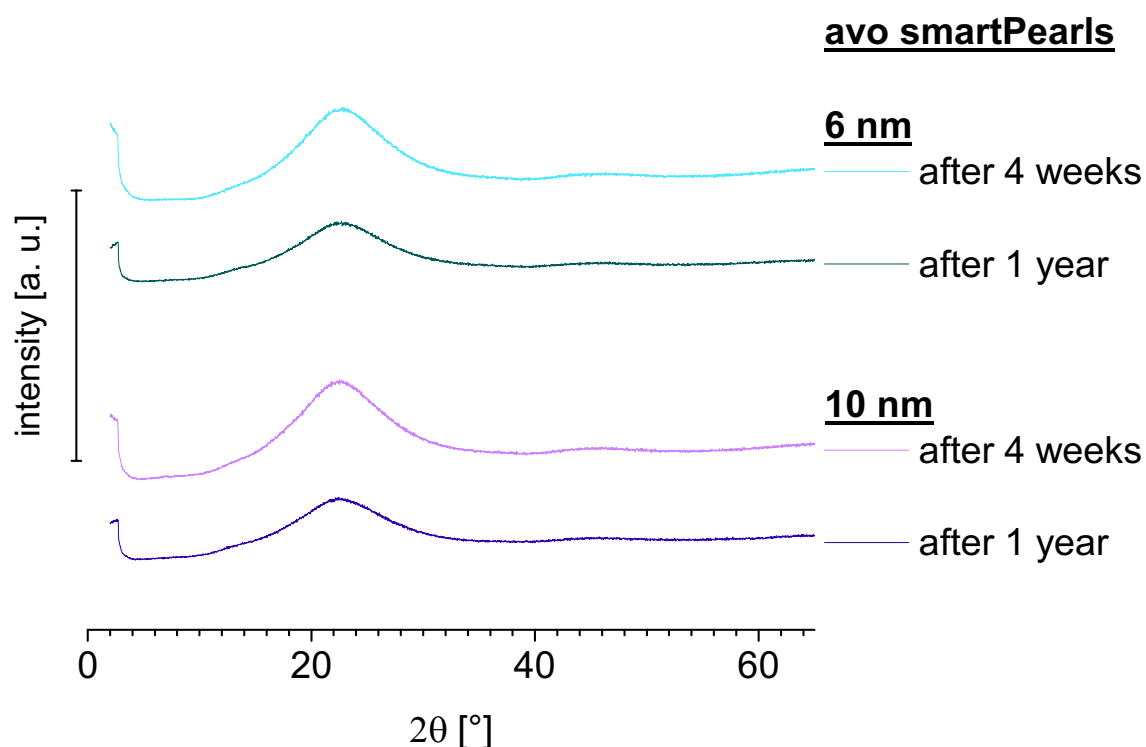


Figure 4: XRD diffraction pattern of physically stable avobenzonone smartPearls: with 6 nm (blue) and 10 nm (violet) pores after 4 weeks and 1 year storage.

4.3.4. Characterization of avobenzene smartPearls by microscopy

The physically stable particles (6 nm, 10 nm) were analyzed by light microscopy and scanning electron microscopy (SEM) to get an impression of their appearance, especially looking at potential changes after loading. Exemplarily the images of the 6 nm particles are shown. The results were identical for the 10 nm ones.

Light microscopy shows dark avobenzene particles in the range of about 50 to 150 μm . They are crystalline. The unloaded silica particles appear translucent. They are polydisperse with sizes from about 10 to 20 μm , the supplier specification of mean size is 12 μm (determined by laser diffraction). After loading, the silica particles slightly darkened, which was attributed to the avobenzene (Figure 5, upper).

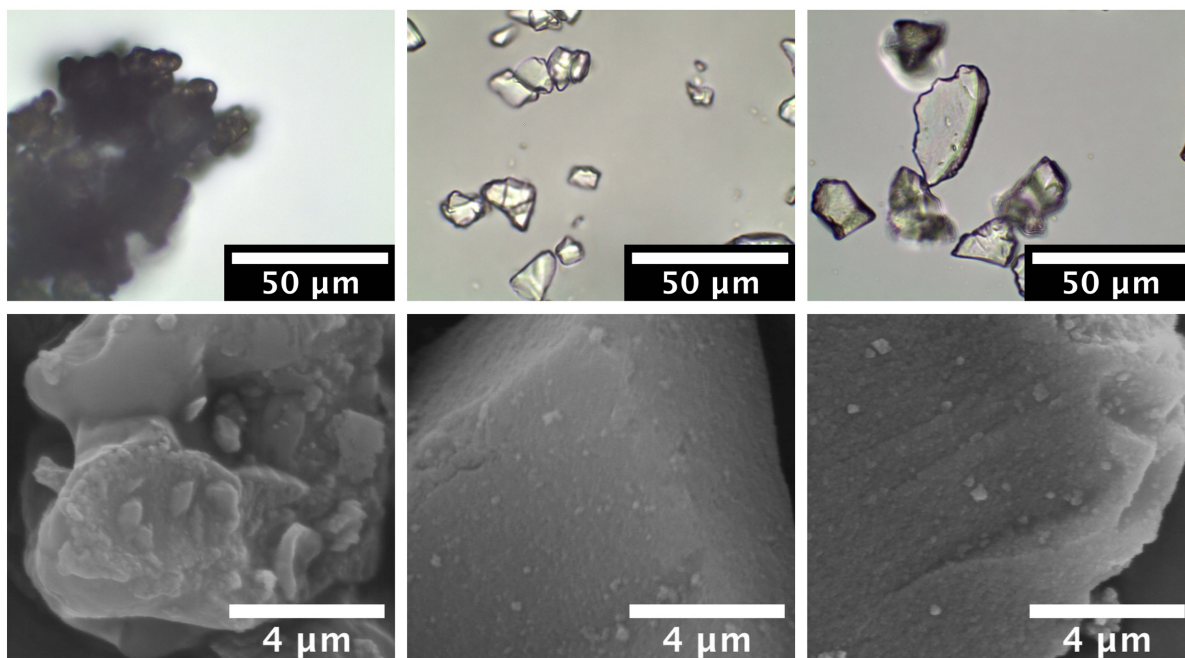


Figure 5: Upper: light microscopy images of avobenzene (left), 6 nm silica (middle) and respective avobenzene loaded silica (right), 1,000-fold magnified. Lower: corresponding SEM images 10,000-fold magnified.

The SEM images show large avobenzene particles, but also small crystals of about 1-2 μm adhering to the surface of the large avobenzene crystals. The unloaded silica show a smooth surface, with a few imperfections. After loading, the surface appearance did not significantly change, supporting that the dominant fraction of avobenzene is localized rather in the pores.

4.3.5. Nitrogen ad- and desorption studies

Nitrogen ad- and desorption is a commonly used method for determination of BET surface, pore volume and pore size [28-30]. This method was used to measure the change in BET surface, pore width and pore volume of the investigated silica by the loading with avobenzene. Data are shown for the physically stable 6 nm and 10 nm particles. The isotherms should give more insight into the loading mechanism of the avobenzene. Figure 6 shows the isotherms (upper) and the respective calculated pore volume and pore diameter (lower).

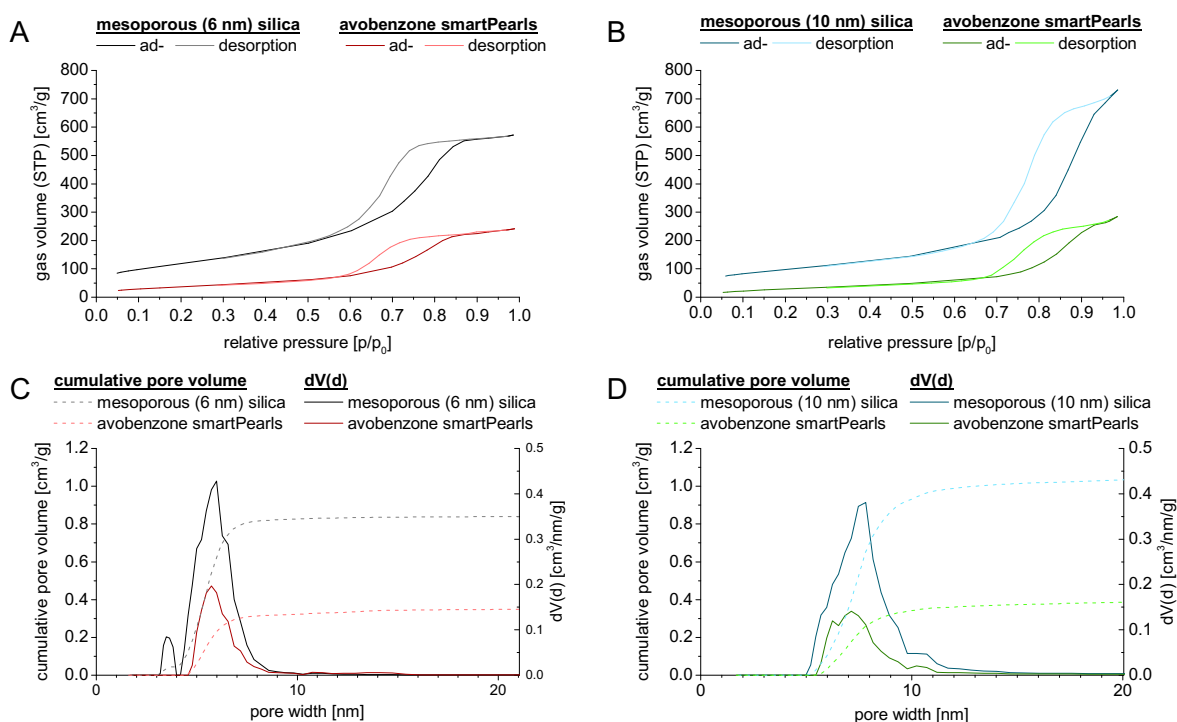


Figure 6: Top: Nitrogen ad- and desorption isotherms plotted for standard temperature and pressure (STP) of silica and their respective avobenzene loaded smartPearls with 6 nm (A) and 10 nm (B) pores. Bottom: Cumulative pore volume (straight lines) and pore volume distribution $dV(d)$ (dashed lines) over the pore width for silica and smartPearls with 6 nm (C) and 10 nm (D) pores.

The ad- and desorption isotherms show a H1 hysteresis [31]. This indicates that no bottle neck pores are present. After loading, the adsorbed nitrogen volume decreased clearly, but the hysteresis type of the isotherms remained. That means there is no change in the pore form, being the same for both, unloaded and loaded silica. Also, a pore blocking can be excluded (Figure 6, upper).

Figure 6 (lower left) shows that the mean pore width of 6 nm silica particles decreased very slightly from 5.69 nm to 5.44 nm after loading with avobenzene. The same was observed for

the 10 nm particles (decrease from 7.80 nm to 7.12 nm) (Figure 6, lower right). This very slight decrease supports that deposition of the avobenzone did not take place mainly by multilayer adsorption on the pore surface but by simple filling of the pores. The only very slight reduction in pore width indicates a thin layer (mono or bimolecular) of avobenzone on the surface. Hempel et al. assume this surface adsorption to be the main stabilizing effect for the amorphous phase [32]. In this study, mainly pore filling occurred, thus the space restriction/confinement by the small pore diameter is the mechanism for amorphous phase stabilization [26; 33].

By the loading, the pore volume decreased from 1.06 mL to 0.40 mL (10 nm silica) and from 0.84 to 0.35 mL (6 nm silica) (Figure 6, lower). Theoretically the volume should decrease by about 50 %, the measured decrease was about 58.3 % and 62.3%. A potential explanation is the different (lower) density of the amorphous phase compared to crystalline avobenzone.

From the isotherms, the BET surface was calculated. After loading, the BET surface decreased to 68% and 66% for the 10 and 6 nm silica, respectively. The surfaces decreased from 355 to 113 m²/g and from 412 to 139 m²/g, respectively. Such a pronounced surface reduction can only be explained by bottom to top pore filling; thus, the data support the proposed loading mechanism.

4.3.6. Determination of saturation solubility

The increase of the saturation solubility C_s is the interesting feature of the amorphous state in the porous silica particles. To reflect better the application situation in a dermal formulation, the loaded particles were incorporated into a carrageenan gel. Carrageenan was used because it creates a viscoelastic system avoiding the sedimentation of the particles [25].

Compared to the raw drug powder, C_s increased by about a factor of 4 for all different silica particles (Figure 7). This indicates that pore volumes, diameters and surface play no role – determining for the solubility is only the amorphous state. Several studies focus not on the saturation solubility but on the influence of the pore diameter on the release properties/dissolution velocity [34; 35]. With increasing pore size (~10 nm) the influence of the pore diameter gets less [34]. In comparison, Rikkonen et al. reports a strong dependency of the release on the loading level and no significant correlation with the carrier properties [36]. However, the focus of this study is on dermal application and the carrier is

already incorporated into a dermal formulation. The active is thus already in the supersaturated state within the formulation, when it will be applied to the skin. The release of the active out of the silica has only the function to replace dissolved molecules in the formulation which are penetrated into the skin. The release velocity is no determining factor for skin penetration (skin diffusion is limiting factor). Studies showed that the formed supersaturated state remains in the dermal formulation.

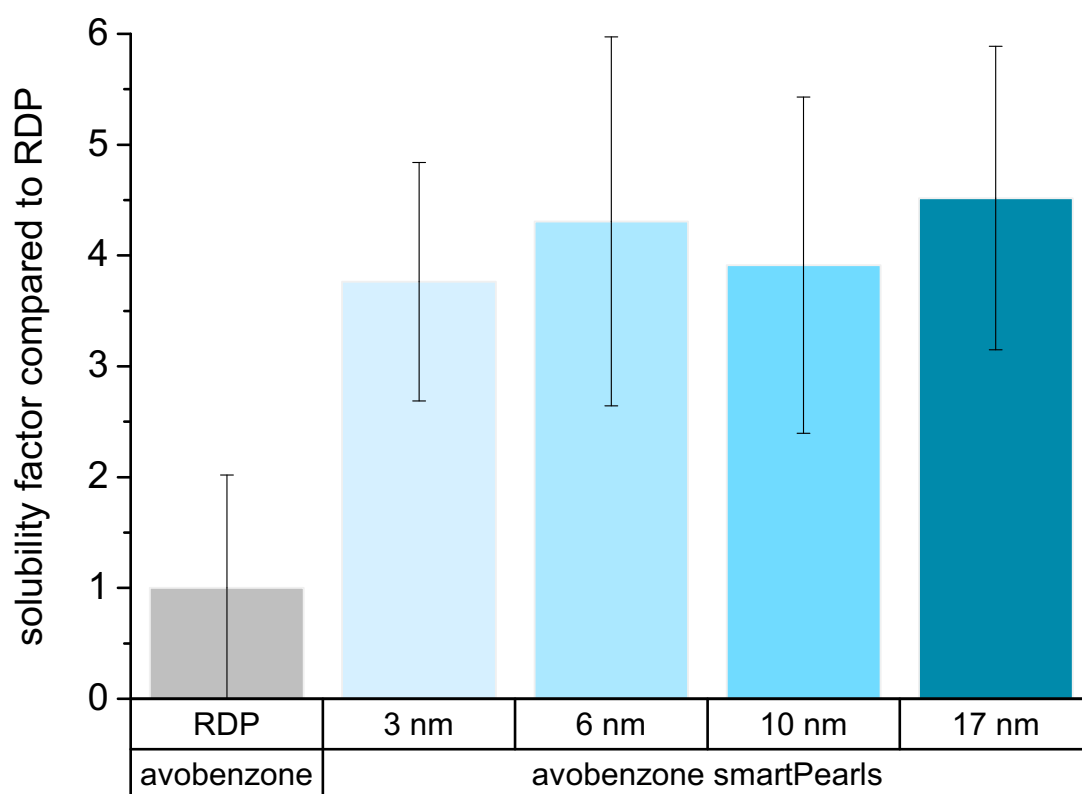


Figure 7: Mean saturation solubility of avobenzone RDP (raw drug powder), 3, 6, 10, and 17 nm pored avobenzone smartPearls.

Highly interesting is, that also the silica particles with a minor crystalline fraction (3 nm and 17 nm) had similar increase in solubility, that means, even particles with some crystalline fraction present can be used without problems in dermal formulation. Occurrence of a crystalline fraction during the shelf life is not limiting dermal products.

4.3.7. Mechanistic considerations – loading process

In the loading procedure, unloaded porous silica are dispersed in a saturated solution of the active, in this case avobenzene. In the subsequent step, a supersaturated solution is created by evaporation of solvent. The precipitation occurring can be better understood on the basis of the Ostwald-Miers diagram, and the Ostwald-Miers range [37; 38].

The Ostwald-Miers concentration range is the range in which supersaturation occurs during cooling of a solution, without the occurrence of spontaneous nucleation. To a given temperature T_s of a solution, a certain saturation solubility C_s is related. A solution with the concentration C_x is cooled. When it reaches T_s , C_x is equal to the saturation solubility C_s . In a close range below T_s (Ostwald-Miers range), the solution remains in a supersaturated state. Precipitation and following crystallization occur only, when it is initiated, e.g. by seed crystals or rough surfaces, which promote precipitation (in the case of the silica by their rough surface). In the Ostwald-Miers range, the concentration of the solute C_x is above the saturation solubility in the temperature range T_{s-crit} . Further cooling below the critical temperature T_{crit} leads to such a high energy state of the solution that spontaneous nucleation occurs. The precipitation starts (Figure 8, left). Further cooling of the solution leads to continuous precipitation, the concentration of the solute reduces and follows curve B (Figure 8, left).

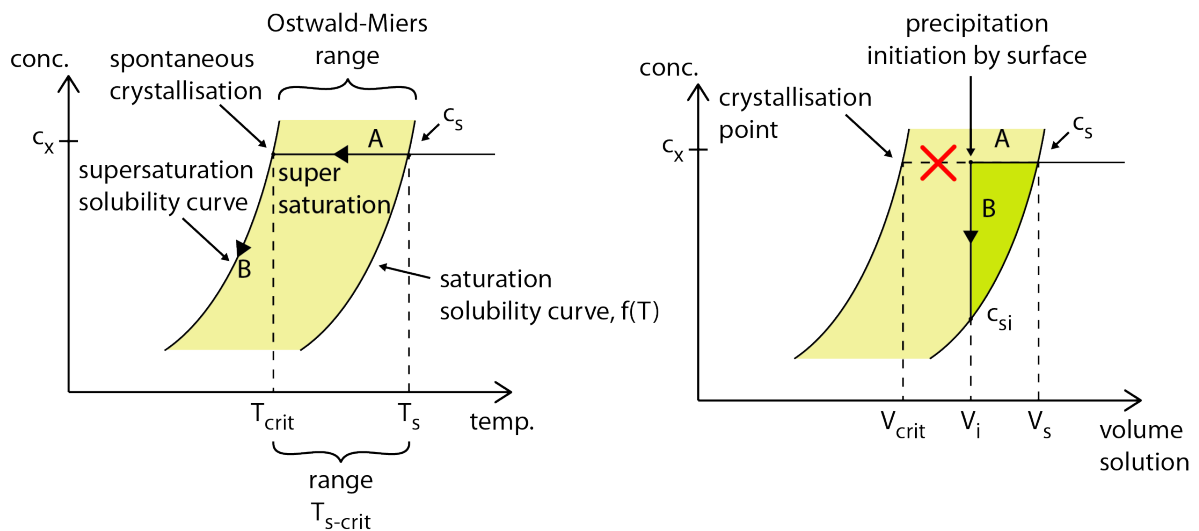


Figure 8: Left: Supersaturation and precipitation according to Ostwald-Miers depending on temperature. Right: Precipitation on silica surface induced by solvent evaporation (explanation cf. text).

Instead of cooling a solution, a supersaturation can be generated by evaporation of the solvent as it happens in the loading process of the silica. The volume decrease corresponds to the temperature decrease. Without the presence of silica particles, the active would remain in solution in the volume range V_{s-crit} . However, because the rough surface of the silica is present, precipitation is initiated (Figure 8, right) within the Ostwald-Miers range, at the volume V_i . Due to precipitation, the concentration of the solute reduces until the C_s and the volume V_i is reached ($= C_{si}$) (Figure 8, right, line B). Further removal of solvent leads to repetition of this process, continuing precipitation on the surface.

Precipitation takes place on the surfaces, the surface of the pores represents the largest surface area, thus on the mass balance preferentially precipitation occurs inside the pores. With continuing evaporation, the precipitation continues until the solvent has completely been evaporated.

Assuming a 50 μm particle (diameter) with a pore volume of 1.8 mL, and a pore diameter of 25 nm, the surface area of the particle (outer surface) assuming a sphere is 0.12 m^2/g (bulk density of 0.42 g/mL and silica density 2.2 g/mL). The total surface area of the particles (outer + inner pore surface) is 320 m^2/g , thus the outer surface is less than 1% of the total surface. Most of the active precipitated inside the pores is not able to form crystals, thus only the active precipitated at the outer surface or in large pores (as discussed for 25 nm silica) is able to form crystals if the active layer reaches a certain thickness.

During the precipitation, formation of separate crystals in the solvent phase has to be avoided. Spontaneous nucleation and separate formation of crystals can only occur, when very fast removal of the solvent is performed, and the supersaturation curve in the Ostwald-Miers diagram is reached. Based on these theoretical considerations, the evaporation should not be too fast, precipitation should be initiated by the silica surface in the Ostwald-Miers range.

4.3.8. Mechanistic considerations – pore volume & occurrence of crystalline fraction

The silica with the 3 nm pores showed already a crystalline fraction shortly after loading. This could be explained by the size restriction of the 3 nm pores for molecules with a diameter of 1.0-1.6 nm. The diameter from avobenzene was derived by the minimum and maximum projection radius (calculated by ChemAxon). Due to the hindered access into the pores an

increasing number of molecules localizes on the particle surface with continuous solvent evaporation in the immersion evaporation method (Figure 9, upper left and middle). When a critical threshold of surface layer thickness is exceeded, crystallization on the surface occurs (Figure 9, upper right). The pore volume is no critical point, because the anticipated loading was below the respective pore volume of all investigated silica particles.

For the particles with larger pore size, a crystalline fraction was observed directly after loading (25 nm), or after 1 month of storage (17 nm). In contrast to the small 3 nm pores, the molecules have easy access to these pores. With increasing removal of solvent, more and more molecules localize in the pores. In contrast to the small pores there is very little adsorption (seen as mass fraction) onto the particle surface (pore surface is 99% of total particle surface) (Figure 9, lower left and middle). In case of a large mean pore size (25 nm), due to the polydispersity of the pore sizes, very large pores are also present. There is no efficient size restriction, the molecules of the unordered amorphous state can re-orientate and form crystals. In case of slightly less pore size (17 nm), there is a certain hindrance of the smaller pores, delaying the process of re-ordering. It takes more time, and a minor crystalline fraction can be observed after 4 weeks of storage (Figure 9, lower right).

Ideal for a stable amorphous state are the particles with medium pore size of about 6 nm to 10 nm. They allow sufficient access for the model molecule to the pores (pores to molecule size ratio >2). In addition, the pore diameter is sufficiently small for effective space restriction (pores to molecule size ratio <12 [26]) hindering molecular ordering leading to crystallization.

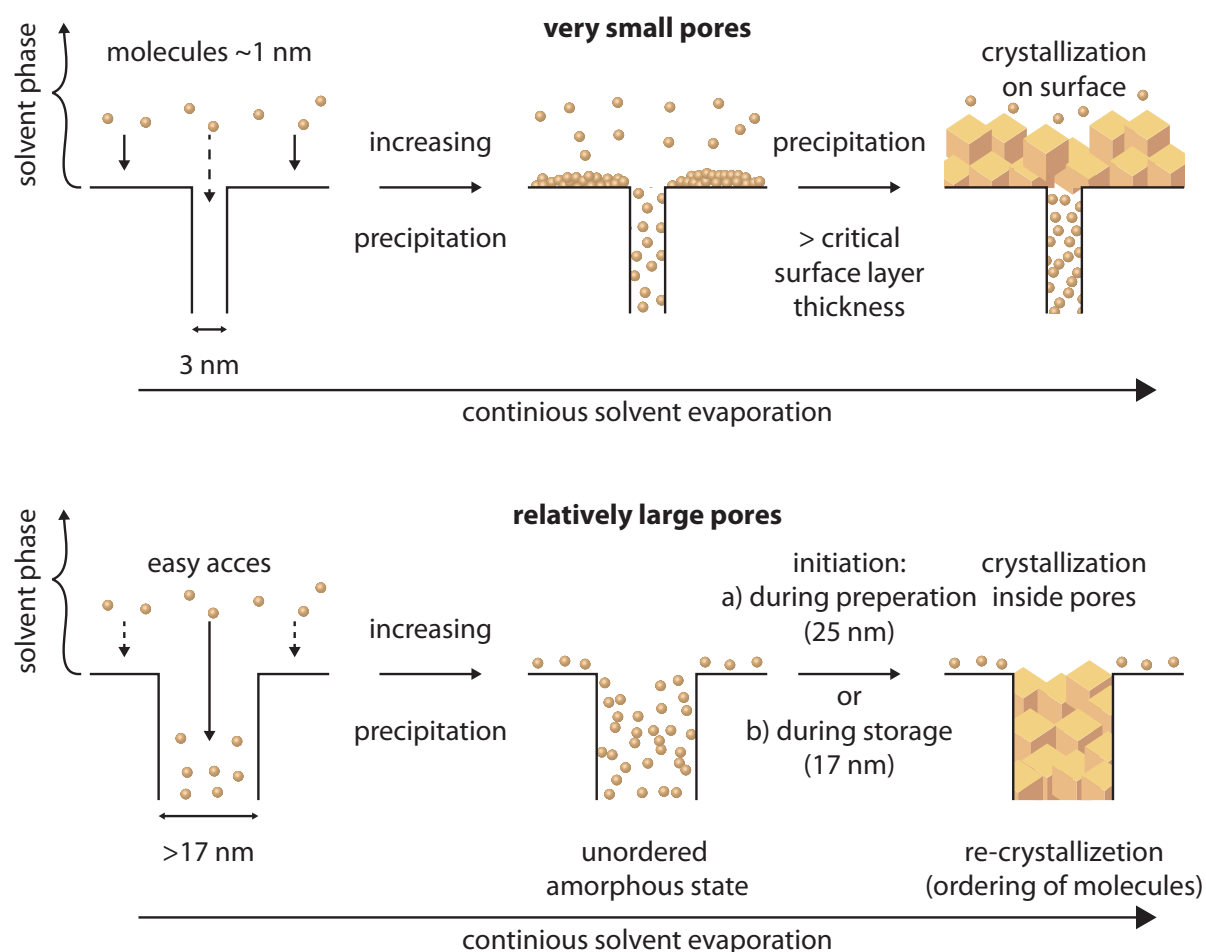


Figure 9: Mechanisms of molecule deposition during the immersion evaporation process on silica particles with small pores (upper) and relatively large pores (lower). During solvent evaporation, the molecules deposit differently inside the pores (hindered vs. easy pore access) and on the surface (pronounced deposition vs. slight deposition) for the silica with small and large sized pores, respectively. Detailed explanation cf. text, section 4.3.8.

4.4. Conclusion

Different silica particles varying in mesopore size, pore volume and surface were investigated. To be industrially feasible for products, a loading of about 50% pore volume is desirable which should be long-term stable. In summary, very small pores of 3 nm at the lower edge are not suitable. They hinder the location of molecules in the pores, and a crystalline fraction occurs. Larger pores of 17 nm and 25 nm lead also to crystallization, due to the polydispersity in the pore size. The very large pores being present promote crystallization. Thus, pore sizes of 6 nm to 10 nm proved to be ideal (Davisil® LC60A, Syloid® 72 FP), providing long-term stability over 1 year.

Based on nitrogen isotherms, the basic mechanism of loading was primarily filling pores from bottom to top. Adsorption onto the pore surface takes also place, as proven by the HPLC data. No 100% recovery of the loaded avobenzone was possible due to firm binding of molecules to the pore surface (being 99% of total surface of the particles). Thus, when developing products, excess of drug needs to be used to compensate the non-releasable fraction.

Highly interesting is, that formation of a small crystalline fraction did not affect the solubility increase generated by the amorphous form. Partial crystallinity does not impair the quality of the dermal formulation/product. Finally, important is that the loading was performed with a method which can be used in industrial production [17]. Combining the loading method with the use of the identified optimized silica particles enables commercial products.

Reference

- [1] Hancock, B.C.; Parks, M.; 2000. What is the True Solubility Advantage for Amorphous Pharmaceuticals? *Pharmaceutical Research* 17(4), 397-404.
<https://doi.org/10.1023/A:1007516718048>
- [2] Flynn, G.L.; Yalkowsky, S.H.; Roseman, T.J.; 1974. Mass transport Phenomena and Models: Theoretical Concepts. *Journal of Pharmaceutical Sciences* 63(4), 479-510.
<https://doi.org/10.1002/jps.2600630403>
- [3] Scheuplein, R.J.; Blank, I.H.; 1971. Permeability of the Skin. *Physiological Reviews* 51(4), 702-747. <https://doi.org/10.1152/physrev.1971.51.4.702>
- [4] Zhou, D.; Zhang, G.G.Z.; Law, D.; Grant, D.J.W.; Schmitt, E.A.; 2002. Physical stability of amorphous pharmaceuticals: Importance of configurational thermodynamic quantities and molecular mobility. *Journal of Pharmaceutical Sciences* 91(8), 1863-1872. <https://doi.org/10.1002/jps.10169>
- [5] Laitinen, R.; Löbmann, K.; Strachan, C.J.; Grohgan, H.; Rades, T.; 2013. Emerging trends in the stabilization of amorphous drugs. *International Journal of Pharmaceutics* 453(1), 65-79. <https://doi.org/10.1016/j.ijpharm.2012.04.066>
- [6] Wei, Q.; Keck, C.M.; Müller, R.H.; 2015. CapsMorph® technology for oral delivery— theory, preparation and characterization. *International Journal of Pharmaceutics* 482(1), 11-20. <https://doi.org/10.1016/j.ijpharm.2014.10.068>

- [7] Nolte, M.; Mayer, J.; Ferreiro, M.G.; Assogba-Zandt, A.; Fehring, V.; Kröhne, L.; Voigt, A.; Dunmann, C., inventors; 2009. Stabilization of amorphous drugs using sponge-like carrier matrices. International Publication Number WO 2009/153346 A2, patent application PCT/EP2009/057688, June 19.
- [8] Rengarajan, G.T.; Enke, D.; Steinhart, M.; Beiner, M.; 2008. Stabilization of the amorphous state of pharmaceuticals in nanopores. *Journal of Materials Chemistry* 18(22), 2537-2539. <https://doi.org/10.1039/B804266G>
- [9] Müller, R.H.; Wei, Q.; Keck, C.M.; 2013. CapsMorph: >4 Years long-term stability of industrially feasible amorphous drug formulations, #833, Int. Symp. Control. Rel. Bioact. Mater. 40, Honolulu/Hawaii, 21.-24. July.
- [10] Maleki, A.; Kettiger, H.; Schoubben, A.; Rosenholm, J.M.; Ambrogi, V.; Hamidi, M.; 2017. Mesoporous silica materials: From physico-chemical properties to enhanced dissolution of poorly water-soluble drugs. *Journal of Controlled Release* 262, 329-347. <https://doi.org/10.1016/j.jconrel.2017.07.047>
- [11] Bremmell, K.E.; Prestidge, C.A.; 2019. Enhancing oral bioavailability of poorly soluble drugs with mesoporous silica based systems: opportunities and challenges. *Drug Development and Industrial Pharmacy* 45(3), 349-358. <https://doi.org/10.1080/03639045.2018.1542709>
- [12] Juère, E.; Florek, J.; Bouchoucha, M.; Jambhrunkar, S.; Wong, K.Y.; Popat, A.; Kleitz, F.; 2017. In Vitro Dissolution, Cellular Membrane Permeability, and Anti-Inflammatory Response of Resveratrol-Encapsulated Mesoporous Silica Nanoparticles. *Molecular Pharmaceutics* 14(12), 4431-4441. <https://doi.org/10.1021/acs.molpharmaceut.7b00529>
- [13] Monsuur, F.H.; Hoefer, H.H.; Keck, C.M., inventors; Grace GmbH & Co. KG, Pharmasol GmbH, assignee; 2014. Active-loaded particulate materials for topical administration. International Publication Number WO 2016/041992 A1, patent application PCT/EP2015/071138, Sep 15.
- [14] Keck, C.M.; Monsuur, F.; Höfer, H.H.; Jin, N.; Staufenbiel, S.; Müller, R.H.; 2014. smartPearls - new dermal injection-like delivery system without use of a needle, p. 10, Menopause, Andropause, Anti-aging, Vienna, 10-13 December.

- [15] Jin, N.; 2017. Nanocrystals & loaded porous silica for increased dermal bioavailability [doctoral thesis]. [Germany]: Freie Universität Berlin. urn:nbn:de:kobv:188-fudissthesis000000105191-3
- [16] Bouledjoudja, A.; Masmoudi, Y.; Van Speybroeck, M.; Schueller, L.; Badens, E.; 2016. Impregnation of Fenofibrate on mesoporous silica using supercritical carbon dioxide. *International Journal of Pharmaceutics* 499(1), 1-9. <https://doi.org/10.1016/j.ijpharm.2015.12.049>
- [17] Hespeler, D.; Kaltenbach, J.; Müller, R.H.; 2019. Nanoporous dermal smartPearls – Identification of optimal silica types & scale-able production process as pre-requisites for marketed products. *Beilstein Journal of Nanotechnology*. submitted [Manuscript ID: 16769373]
- [18] Šoltys, M.; Kovačik, P.; Dammer, O.; Beránek, J.; Štěpánek, F.; 2019. Effect of solvent selection on drug loading and amorphisation in mesoporous silica particles. *International Journal of Pharmaceutics* 555, 19-27. <https://doi.org/10.1016/j.ijpharm.2018.10.075>
- [19] Juère, E.; Kleitz, F.; 2018. On the nanopore confinement of therapeutic drugs into mesoporous silica materials and its implications. *Microporous and Mesoporous Materials* 270, 109-119. <https://doi.org/10.1016/j.micromeso.2018.04.031>
- [20] Thommes, M.; Kaneko, K.; Neimark, A.V.; Olivier, J.P.; Rodriguez-Reinoso, F.; Rouquerol, J.; Sing, K.S.W.; 2015. Physisorption of gases, with special reference to the evaluation of surface area and pore size distribution (IUPAC Technical Report). *Pure and Applied Chemistry* 87(9-10), 1051-1069. <https://doi.org/10.1515/pac-2014-1117>
- [21] Bavnhøj, C.G.; Knopp, M.M.; Madsen, C.M.; Löbmann, K.; 2019. The role interplay between mesoporous silica pore volume and surface area and their effect on drug loading capacity. *International Journal of Pharmaceutics: X* 1, 100008. <https://doi.org/10.1016/j.ijpx.2019.100008>
- [22] Wei, Q.; Keck, C.M.; Müller, R.H.; 2017. Preparation and tableting of long-term stable amorphous rutin using porous silica. *European Journal of Pharmaceutics and Biopharmaceutics* 113(Supplement C), 97-107. <https://doi.org/10.1016/j.ejpb.2016.11.009>
- [23] ChemAxon - Software Solutions and Services for Chemistry & Biology, 2018, <https://chemaxon.com/products/chemicalize> [accessed: 2018 December 13]

- [24] Bundesamt für Risikobewertung, 2014. Aluminiumhaltige Antitranspirantien tragen zur Aufnahme von Aluminium bei. position statement No. 007/2014, Feb 26. <https://www.bfr.bund.de/cm/343/aluminiumhaltige-antitranspirantien-tragen-zur-aufnahme-von-aluminium-bei.pdf> [accessed: 2019 June 27]
- [25] Hespeler, D.; Knoth, D.; Keck, C.M.; Müller, R.H.; Pyo, S.M.; 2019. smartPearls® for dermal bioavailability enhancement – Long-term stabilization of suspensions by viscoelasticity. *International Journal of Pharmaceutics* 562, 293-302. <https://doi.org/10.1016/j.ijpharm.2019.03.016>
- [26] Sliwinska-Bartkowiak, M.; Dudziak, G.; Gras, R.; Sikorski, R.; Radhakrishnan, R.; Gubbins, K.E.; 2001. Freezing behavior in porous glasses and MCM-41. *Colloids and Surfaces A: Physicochemical and Engineering Aspects* 187–188, 523-529. [http://dx.doi.org/10.1016/S0927-7757\(01\)00637-9](http://dx.doi.org/10.1016/S0927-7757(01)00637-9)
- [27] McCarthy, C.A.; Ahern, R.J.; Devine, K.J.; Crean, A.M.; 2018. Role of Drug Adsorption onto the Silica Surface in Drug Release from Mesoporous Silica Systems. *Molecular Pharmaceutics* 15(1), 141-149. <https://doi.org/10.1021/acs.molpharmaceut.7b00778>
- [28] Brunauer, S.; Emmett, P.H.; Teller, E.; 1938. Adsorption of gases in multimolecular layers. *Journal of the American Chemical Society* 60(2), 309-319. <https://doi.org/10.1021/ja01269a023>
- [29] Ojeda, M.L.; Esparza, J.M.; Campero, A.; Cordero, S.; Kornhauser, I.; Rojas, F.; 2003. On comparing BJH and NLDFT pore-size distributions determined from N₂ sorption on SBA-15 substrata. *Physical Chemistry Chemical Physics* 5(9), 1859-1866. <https://doi.org/10.1039/B300821E>
- [30] Ravikovitch, P.I.; Haller, G.L.; Neimark, A.V.; 1998. Density functional theory model for calculating pore size distributions: pore structure of nanoporous catalysts. *Advances in Colloid and Interface Science* 76, 203-226. [https://doi.org/10.1016/S0001-8686\(98\)00047-5](https://doi.org/10.1016/S0001-8686(98)00047-5)
- [31] Sing, K.S.W.; Williams, R.T.; 2004. Physisorption Hysteresis Loops and the Characterization of Nanoporous Materials. *Adsorption Science & Technology* 22(10), 773-782. <https://doi.org/10.1260/0263617053499032>

- [32] Hempel, N.-J.; Brede, K.; Olesen, N.E.; Genina, N.; Knopp, M.M.; Löbmann, K.; 2018. A fast and reliable DSC-based method to determine the monomolecular loading capacity of drugs with good glass-forming ability in mesoporous silica. *International Journal of Pharmaceutics* 544(1), 153-157.
<https://doi.org/10.1016/j.ijpharm.2018.04.035>
- [33] Godec, A.; Maver, U.; Bele, M.; Planinšek, O.; Srčič, S.; Gaberšček, M.; Jamnik, J.; 2007. Vitrification from solution in restricted space: Formation and stabilization of amorphous nifedipine in a nanoporous silica xerogel carrier. *International Journal of Pharmaceutics* 343(1), 131-140. <https://doi.org/10.1016/j.ijpharm.2007.05.022>
- [34] Yazdi, I.K.; Ziemys, A.; Evangelopoulos, M.; Martinez, J.O.; Kojic, M.; Tasciotti, E.; 2015. Physicochemical properties affect the synthesis, controlled delivery, degradation and pharmacokinetics of inorganic nanoporous materials. *Nanomedicine: Nanotechnology, Biology, and Medicine* 10(19), 3057-3075.
<https://doi.org/10.2217/nnm.15.133>
- [35] Ukmar, T.; Maver, U.; Planinšek, O.; Kaučič, V.; Gaberšček, M.; Godec, A.; 2011. Understanding controlled drug release from mesoporous silicates: Theory and experiment. *Journal of Controlled Release* 155(3), 409-417.
<https://doi.org/10.1016/j.jconrel.2011.06.038>
- [36] Riikonen, J.; Xu, W.; Lehto, V.-P.; 2018. Mesoporous systems for poorly soluble drugs – recent trends. *International Journal of Pharmaceutics* 536(1), 178-186.
<https://doi.org/10.1016/j.ijpharm.2017.11.054>
- [37] Voorhees, P.W.; 1985. The theory of Ostwald ripening. *Journal of Statistical Physics* 38(1), 231-252. <https://doi.org/10.1007/BF01017860>
- [38] Spencer, L.J.; 1944. Biographical notice of Sir Henry A. Miers (1858-1942). *Mineralogical Magazine and Journal of the Mineralogical Society* 27(185), 17-28.
<https://doi.org/10.1180/minmag.1944.027.185.01>

5. Nanoporous dermal smartPearls – Identification of optimal silica types & scale-able production process as pre-requisites for marketed products⁴

Abstract

Dermal smartPearls are a dermal delivery system for poorly soluble active agents, consisting of nanoporous silica particles loaded with a physically long-term stable amorphous active agent in its mesopores (2-50 nm). The amorphous state increases dermal bioavailability. For use in marketed products, optimal silica types were identified from commercially available, regulatorily accepted silica. In addition, a scale-able production process was used. Loading of the particles was performed applying the immersion-evaporation method. The antioxidant rutin was used as model active agent, ethanol as unproblematic solvent. Various silica particles (Syloid®, Davisil®) differing in particle size (7-50 µm), pore diameter (3-25 nm) and pore volume (0.4-1.75 mL/g) were investigated regarding their ease of processing. Evaporation from the silica-ethanol suspensions was performed in a rotary evaporator. Best flowable powders were obtained with larger sized silica. The maximum amorphous loadings achieved were between 10% and 25% (w/w), depending on the silica type. A mechanism of loading is proposed. Most suitable regarding processing was the large sized silica Syloid® XDP 3050 with 50 µm particle size and largest pore diameter of 25 nm and 18% (w/w) maximum loading. Based on a 10% (w/w) loading and the amorphous solubility of the active agent, for 100 kg dermal formulation about 500 g loaded particles are required. This corresponds to production of 5 kg loaded smartPearls for a formulation batch size of a ton. Production of 5 kg (= about 25 L solvent removal) can industrially be realized in a commercial 50 L rotary evaporator.

⁴ This chapter has been submitted for publication as:

Hespeler, D.; El Nomeiri, S.; Kaltenbach, J.; Müller, R.H.; 2019. Nanoporous dermal smartPearls – Identification of optimal silica types & scale-able production process as pre-requisites for marketed products. *Beilstein Journal of Nanotechnology*, submitted [Manuscript ID: 16769373].

5.1. Introduction

Many interesting active agents in pharma and cosmetics are poorly soluble. Active agents poorly soluble in water, but soluble in lipophilic media can easily be formulated as creams or gels (e.g. the popular coenzyme Q10). The problems start when the active agents are poorly soluble simultaneously in aqueous and lipophilic/organic media. Classical examples are antioxidants (e.g. rutin, hesperidin, etc.), presently highly en vogue in cosmetics for anti-pollution products (the “molecular barrier” against ROS (reactive oxygen species), IR radiation and blue light from computers) [1; 2]. For the delivery of such molecules efficient delivery systems are the only solution, because applying simple suspensions to the skin normally does not provide a sufficient dermal bioavailability.

Classic delivery systems such as liposomes [3] or solid lipid nanoparticles (SLN) [4; 5] do not work, because the active agents do not dissolve in the lipidic phase of these systems. A simple but very effective approach is to increase the saturation solubility of these active agents. This leads to an increased concentration gradient between formulation and skin $C_s - C_{s_{skin}}$, and thus to an increased diffusional flux into the skin. Moreover, using e.g. complexes with polymers or cyclodextrins can be of limited effect, because of insufficient release of the molecules from such complexes (too high binding constants) [6; 7]. Additionally, many molecules are not able to form such complexes. A highly effective way is the dermal administration of nanocrystals (trade name smartCrystals®) [8-10]. They are on the market in commercial dermal cosmetic products since 2007 (e.g. hesperidin, la prairie Switzerland) [11; 12]. They can be considered as the present “gold standard”.

The trick with nanocrystal is that transfer of the material from the μm -dimension into the nano-dimension changes distinctly physicochemical properties, e.g. the saturation solubility distinctly increases [13]. In general, amorphous materials have an even higher C_s than nanocrystalline materials [14]. Thus, it would be most effective to use active agents in the amorphous state.

However, the amorphous state is physically unstable. Because of the high free energy the amorphous phase tends to re-crystallize [15], especially in presence of liquids [16]. This hindered the broad use of amorphous active agents in dermal formulations. The company Capsulation (Berlin) incorporated active agents in the amorphous state inside the pores of

silica particles with mesopores (2-50 nm) [17], technology CapsMorph for oral administration [18]. By this, the amorphous state could be stabilized over years [19]. Porous silica particles are commercially available e.g. from Grace, Merck Millipore and Formac [20]. They are nanoporous materials, because their pore diameter is in the nanometer dimension (>1 nm and below 1,000 nm) [21]. The silica used had so called "mesopores", i.e. nanopores in the range 2-50 nm. In 2006 this delivery technology was transferred from the oral to the dermal administration route [22], technology called smartPearls [23]. The name was changed to smartPearls to clearly differentiate them from silica used for oral administration.

SmartCrystals are in products on the cosmetic market, because industrial large scale production is possible and there is an industrial supplier (Dr. Rimpler GmbH, Germany) for manufacturers of cosmetics. SmartCrystals are crystals in the nanometer dimension, typically 200-400 nm, which can be produced on large scale by bead milling or high pressure homogenization. Skin penetration studies showed that the smartPearls were superior to the nanocrystals [8; 24; 25]. However, the market introduction in final cosmetic products is blocked due to the lack of an industrial supplier of active agent-loaded smartPearls. To establish an industrial supply, an industrially feasible production method is required.

Silica particles can be loaded e.g. by co-milling [26; 27], but a large part of the active agents stays outside the pores. Loading can be performed by supercritical carbon dioxide [28], but it is expensive. Loading is possible by the impregnation-evaporation method [29], but this is less suitable in large scale. In this study, the immersion-evaporation method [30] was applied and systematically investigated to define large scale production parameters for an industry friendly one step production process. Rutin was used as model active agent, because it has high application potential in cosmetic products, but is also of use in dermal pharmaceutical products [31]. A mechanism of loading in this industrial process is proposed. In addition, concentrations of smartPearls in final dermal products are suggested based on achieved loadings and on solubility data. This could be a guideline for manufacturers of dermal products. Different silica types were investigated (particle size, pore diameter, pore volume) to identify the particles which are most easily processable.

5.2. Materials and Methods

5.2.1. Materials

Rutin with a purity of 95% was purchased from Denk Ingredients (Munich, Germany). Various mesoporous silica particles (Table 1) with pores of 3 nm (Syloid® AL-1 FP), 6 nm (Davisil® LC 60 Å 12 µm), 10 nm (Syloid® 72 FP), 17 nm (Syloid® 244 FP), and 25 nm (Syloid® XDP 3050) were kindly provided by Grace GmbH & Co. KG (Worms, Germany). Ethanol, isopropanol, butanol, acetone, ethyl acetate, acetonitrile, and dimethyl sulfoxide (DMSO) in gradient grade were purchased from VWR (Darmstadt, Germany), and purified water was used produced by a Milli-Q system from Merck Millipore (Darmstadt, Germany).

Table 1: Silica particles used and their properties according the certificate of analysis (manufacturer: company W. R. Grace & Co., USA).

product code	pore diameter	specific surface area	pore volume	particle size
	[nm]	[m ² /g]	[mL/g]	[µm]
Syloid® XDP 3050	25	300	1.8	50
Syloid® 244 FP	17	380	1.6	3
Syloid® 72 FP	10	370	1.2	5
Davisil® SP53D	6	550	0.9	12
Syloid® AL-1 FP	3	740	0.4	7

5.2.2. Methods

Solubility investigations

To assess maximum solubility of rutin, rutin suspensions were prepared with different solvents (dimethyl sulfoxide (DMSO), ethanol, isopropanol, butanol, acetone, ethyl acetate, acetonitrile, and water) (n=1). The suspensions with 20% (w/w) rutin were shaken overnight at room temperature, centrifuged, filtrated and the rutin concentration in the filtrate was analyzed after dilution in ethanol (factor 100-1000) by UV spectrophotometry (UV-1700 PharmaSpec, Shimadzu, China), at 360 nm. Evaluation was conducted by the provided

“UVprobe” software (version 2.21). Concentration was calculated based on calibration curves determined in ethanol.

Loading of particles

Prior to loading, the silica particles were dried in an oven at 120°C for at least 2 hours. The saturated rutin solution was produced by preparing a 2% (w/w) rutin suspension in ethanol (96 vol.%), heating it under agitation to 60 °C for 1 hour and subsequent filtration. After cooling, it was checked that no rutin crystals were precipitated. Rutin content was determined prior using the rutin solution for loading. For loading, 3 g silica particles were dispersed in a respective volume of rutin ethanol solution. The volume used depended on how much rutin should be loaded into the silica particles (increasing amounts of solution with increased % of loading). The suspension was stirred for 5 min to achieve a fine dispersion of the particles. Then the suspension was placed into a rotary evaporator (Büchi, Germany). Solvent evaporation took place at 40°C±2 °C and 150±10 mbar, until a film was formed on the wall of the evaporation flask. Evaporation time depended on the amount of solvents used (i.e. increased with increase of loading percentage). For removal/minimization of solvent residues, a secondary drying phase at 40°C +/- 2°C and 20 mbar was performed for 30 min. All fractions presented are weight fractions unless otherwise stated. Each loading for each type of silica was performed once.

Differential scanning calorimetry (DSC) for crystallinity investigation

The physical state of silica particles, rutin raw active agent powder and rutin smartPearls was investigated by differential scanning calorimetry (DSC 1, Mettler Toledo GmbH, Germany) and calculated by the provided STARE software (version 12.10b). Exact amounts between 1-5 mg rutin loaded silica based on the respective mass of rutin (aimed 0.5-1 mg) were weighted in a punctured 40 µl aluminum pan and sealed (n=1). Measurements were performed at a heating rate of 20 K/min between 25 and 300 °C under 80 mL/min nitrogen purge.

Determination of amorphicity by X-ray diffraction (XRD)

To determine the amorphous state and possible residual crystal fractions of rutin in smartPearls X-ray diffraction was performed using a Bruker D8 (Bruker, USA) (n=1). A scan rate of 0.02° (2=2-60°) was applied and the goniometer equipped with a Cu-anode (K α =0.15406 nm) run with a voltage of 40 kV and current of 35 mA.

Light microscopy (LM) and scanning electron microscopy (SEM)

Light microscope imaging was performed using a Motic Microscope BA210 (Motic Deutschland GmbH, Germany) with a Moticom camera and the Software Motic Images Plus at 100, 400, and 1,000-fold magnification. Scanning electron microscopy (SEM) was performed at 10,000-fold magnification using a Zeiss DSM950 (Carl Zeiss AG, Germany). Samples were sputter-coated with gold-palladium in an argon atmosphere with 15-20 kV at 0.05 mbar for four minutes.

Determination of recovery rate

For photometric analysis, a precisely weighted amount of rutin loaded silica particles around 25 mg was dispersed in 5 mL DMSO. DMSO was used because of the high rutin solubility in this solvent. After 10 minutes shaking and 10 minutes ultrasonication the suspension was centrifuged at 10,000 rpm for 10 minutes and an aliquot of the supernatant was diluted in ethanol by a factor 100. Absorption determination was performed at 360 nm wavelength by a PharmaSpec UV-1700 (Shimadzu, China). Peaks were evaluated using the PharmSpec software "UVprobe" (version 2.21).

HPLC measurement of the same samples were performed using a Kontron 400 System (Kontron Instruments GmbH, Germany) equipped with a 20 µl loop and an Eurospere 100 C18 (5 µm 250x4 mm) column at 25 °C. Determination was performed at 360 nm with 20:80 acetonitrile: acetate buffer (pH 4.8, 0.1 mol/L) as mobile phase and a flow rate of 1.25 mL/min. Peaks were evaluated with the provided Software KromaSystem 2000 (version 1.82).

Solubility determination of rutin dissolved from smartPearls

Solubility of rutin raw active agent powder and rutin smartPearls were determined for one hour in 0.15 molar NaCl solution using *in situ* UV/VIS measurement (Sirius inForm®, UK) with a fiber optic and a path length of 5 mm. Therefore, the 0.15 molar NaCl solution was placed in a beaker. The aqueous phase was tempered to 25 °C. After calibration of the pH electrode and UV/VIS optic the sample was added manually and immediately after that the UV/VIS fiber optic for measurement. Spectra were corrected using the software providing the Tyndall Rayleigh correction function. Different concentrations of raw active agent powder and rutin smartPearls were investigated limited by a maximum overall absorption up to 2.5. pH was determined over the whole measurement period.

5.3. Results and Discussion

5.3.1. Considerations for selection of the production method/variables

The production method should yield a high loading of the pores and complete transformation of the active agent into the amorphous state; thus, co-grinding was excluded. Also excluded was supercritical CO₂ due to production cost reasons, complexity of the process and costs of a production unit. The method should be desirably a one-step method. This excludes the impregnation-evaporation process, because in many cases one impregnation is not sufficient to reach the anticipated loading. Multiple steps are normally required. Thus, the immersion-evaporation process was selected.

Evaporation times of the solvent removal step ranged from 75 min to 180 min depending on the solvent volume. After the second drying step, the obtained free flowing dry powder was removed. In case of film forming on the glass wall, the film was removed from the wall using a spatula. Potential aggregates were de-aggregated by stirring the powder, potential aggregates were easily to disperse (Figure 1).

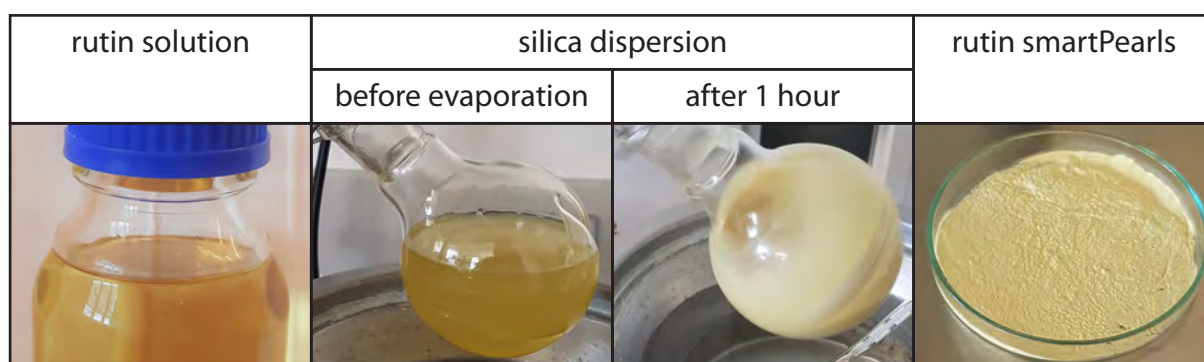


Figure 1: From left to right: rutin-ethanol solution, silica dispersed in rutin solution attached to the rotary evaporator, after the first hour solvent evaporation and obtained loaded silica powder SP53D (right).

The principle was to suspend the particles in an amount of solvent containing the total amount of active agent to be loaded into the pores of the particles. During the evaporation process, the concentration of the active agent increases, precipitation takes place continuing until complete removal of the solvent. It was hoped that precipitation should take place preferentially in the pores because of the largest available surface area. Minor precipitation on the outer side of the particles in a thin layer represents no problem, as long as the active agent on the surface stays amorphous. It is obvious that in addition to the inner surface in the pores, localization on the surface of silica particles takes place. To be avoided is the formation

of crystals of active agent outside the particles. This was checked by light microscopy and scanning electron microscopy.

To study the suitability of the process, silica particles differing in particle size, in pore diameter and pore volume were selected (Table 1). The investigation should also give evidence, which particle type is optimal regarding achieved maximum loading, and being most easy to process.

5.3.2. Solubility of rutin in solvents

A compromise had to be made between solubility for rutin as high as possible and the tolerability of the solvent by the skin. Further, processing parameters such as evaporation temperature were crucial. DMSO was used in previous studies with the impregnation evaporation method [24] because it has high solubility and thus reduces the number of loading steps. Disadvantage was the long time period for solvent removal at high temperatures (>80°C) which can cause degradation of active agent. In addition, it is tedious to remove DMSO efficiently by rotary evaporation. Despite DMSO can be contained in products applied to the skin, it is less skin friendly. Efficient removal of critical solvents below the ppm specification is also a cost factor in the production process. Thus, a different, better tolerable solvent was desirable.

Table 2 shows the obtained solubility of rutin in the various tested solvents. Rutin has highest solubility in DMSO (17%), as expected, but it was decided to select ethanol as compromise. With a maximum of 2%, rutin solubility is substantial lower than in DMSO but distinctly higher than e.g. in acetone (0.8%) and the other organic solvents. The rutin ethanol solution showed a clear, yellowish appearance.

Table 2: Solubility at room temperature of rutin in various solvents (weight/weight %) and macroscopic appearance.

solvent	solubility [% (w/w)]	appearance
DMSO	17.05	brown
ethanol	2.09	clear, bright-yellow
n-butanol	2.07	clear, bright-yellow
isopropanol	1.85	clear, bright-yellow
acetone	0.83	pale yellow
ethyl acetate	0.42	mildly cloudy
acetonitrile	0.22	mildly cloudy
water	0.03	cloudy, slight yellow

5.3.3. Loading Process of silica particles, powder appearance

Different silica from Table 1 were loaded with rutin by dispersing them in saturated rutin ethanol solution, evaporating the solvent in a rotary evaporator, until dry powders were obtained. Nitrogen ad-/desorption studies were performed showing little decrease in pore diameter, but reduction of the pore volume supporting the bottom to up filling of the pores [32; 33]. Depending on the particle size and the pore diameters, the powders showed different macroscopic appearance. The silica AL-1 FP tended more towards aggregate formation, they possess particle size of 7 μm and smallest pore diameter (3 nm). 244 FP and 72 FP showed slight agglomeration (particle size 3 and 5 μm , resp; pore diameter 10 and 17 nm). SP53D with medium size of 12 μm showed almost no agglomeration, at higher loading of 28% and 30% a film formed on the wall of the evaporator glass, respectively. The XDP 3050 particles with largest size of 50 μm (pores 25 nm) showed neither agglomeration nor film formation. Figure 2 shows the macroscopic appearance.

	AL-1 FP	72 FP	244 FP	SP53D	XDP
particle size [μm]	7	5	3	12	50
pore size [nm]	3	10	17	6	25
pore volume [ml/g]	0.4	1.2	1.6	0.9	1.8




Figure 2: Macroscopic appearance of loaded silica powders, from left to right with decreasing agglomeration tendency (explanations cf. text).

It can be summarized, that silica particles get more adhesive with decreasing size, easily explainable by powder technology. The surface and contact area increase, thus promoting particle-particle interaction. Additionally, with increasing pore diameter decreased the agglomeration tendency. The particles with clear agglomeration tendency (AL-1 FP) have smallest pore size of 3 nm, and additionally smallest pore volume. It is assumed that the pore parameters play only a significant role in agglomeration tendency in case pore volume is completely filled with active agent or pores are too small, that means an overloading takes place and precipitating active agent acts as a kind of glue between silica particles. This was assumed for the AL-1 FP samples since rutin with a molar weight of 610.5 g/mol and a minimum projection area of 9.2 nm² was assumed to be oversized to diffuse efficiently into the pores prior precipitation. Thus, such small pores promote agglomeration outside of the pores. Based on the behavior observed, silica particles with larger size, pores and pore volume are easier to process on large scale.

5.3.4. Determination of amorphous content by DSC and X-ray

Amorphicity determination of the loading was performed in parallel by DSC and X-ray diffraction. An amount of 5% rutin in the physical mixture with amorphous unloaded silica was detectable by DSC. Analysis of physical mixtures of silica with crystalline rutin powder showed

that an amount of only 3% crystalline rutin was clearly detectable by X-ray, 1.5% were hardly detectable (X-ray diffractogram not shown).

Figure 3 shows the DSC thermograms for maximum loaded silica SP53D, loaded with different solvents, compared to unloaded silica, rutin and their physical mixture. In the physical mixture, 5% rutin were clearly detectable. No rutin peak was detectable for loadings up to 25% with ethanol, 28% with butanol and 35% with DMSO. Crystalline rutin was clearly detectable for 28% loading with ethanol (detectable in temperature range of 175-190°C). From this was concluded that the limit of loading in the amorphous state was achieved at 25% with ethanol as solvent. As reported from Jin N. et al. loadings of 32% are achievable with DMSO and the impregnation evaporation method [24]. Same loading or even higher can be reached by the immersion evaporation method, thus they are at least even efficient. However, the immersion evaporation method is scalable and thus of more practical relevance. Since DMSO is a hardly processable solvent and more expensive than ethanol, loading of 25% is favored, reached with the use of ethanol.

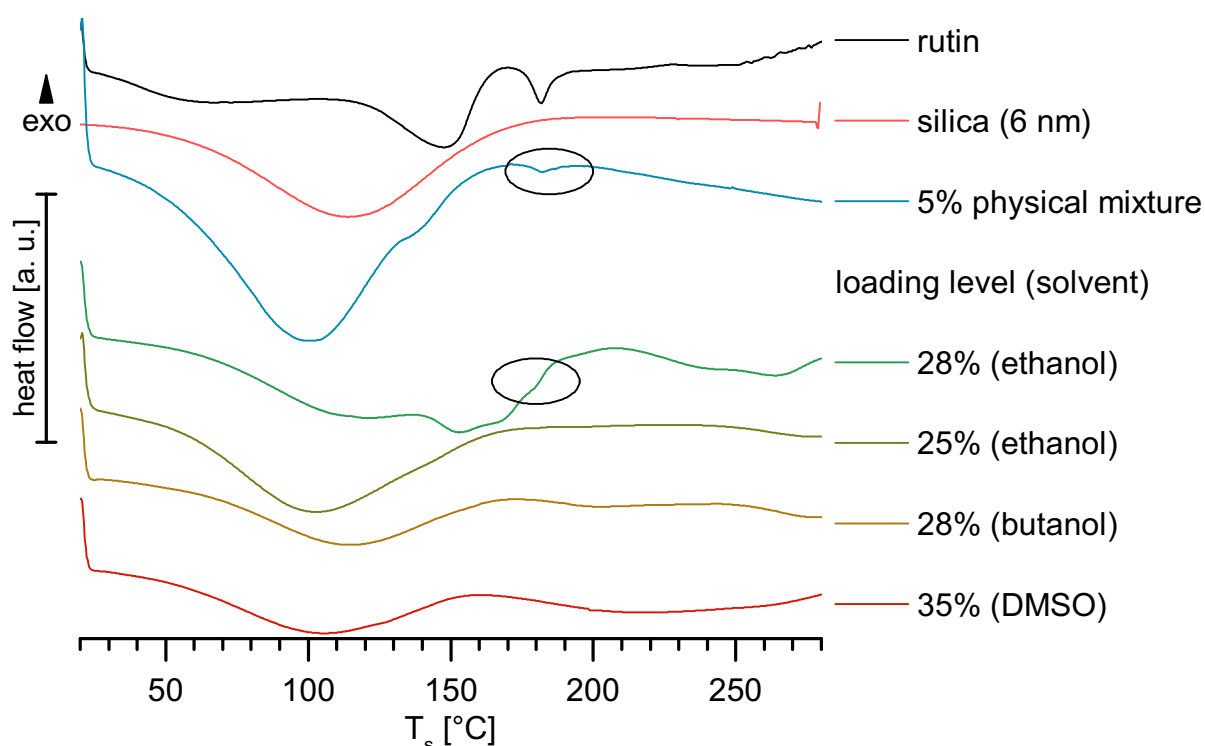


Figure 3: DSC thermograms of crystalline rutin, amorphous unloaded silica, physical mixture (5% rutin) in comparison to SP53D loaded with ethanol (28% and 25%), butanol (28%) and DMSO (35%).

Figure 4 shows X-ray diffraction patterns of rutin in comparison to unloaded amorphous silica, crystalline rutin and their physical mixture. The respective X-ray diffraction patterns of rutin

loaded SP53D silica and ethanol (25% loading), butanol (28% loading) and DMSO (35% loading) as solvent revealed the amorphicity of these samples. A rutin peak was detectable in the physical mixture with 3% rutin. Peaks were only detectable for SP53D loaded with 28% rutin and ethanol as solvent, being in agreement with the DSC data. Even the high loading up to 35% (loaded with DMSO) was stable amorphous. As mentioned, the industrial feasibility is more important than a maximum achievable loading. To be on the safe side, 20% loadings produced with ethanol were used for determination of the saturation solubility and is recommended as maximum for commercial use.

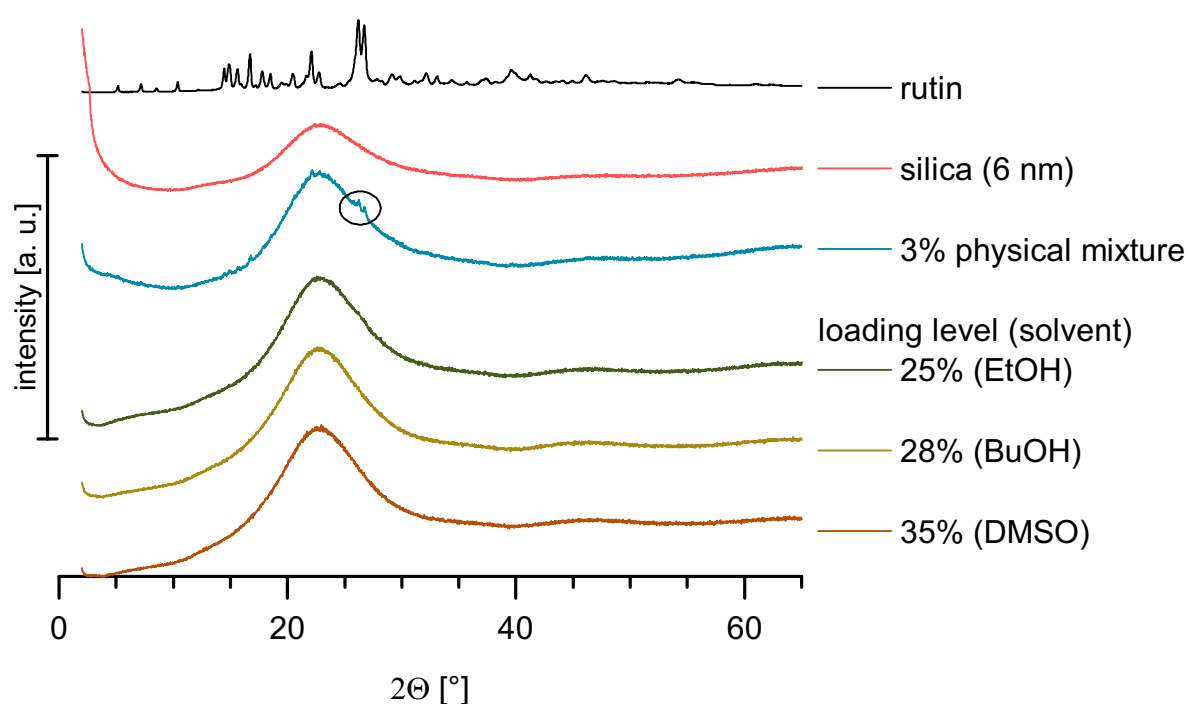


Figure 4: X-ray diffractograms of rutin, unloaded silica (SP53D), physical mixture (3% rutin) in comparison to the maximum loading with silica SP53D loaded with different solvents (ethanol, butanol, DMSO).

Figure 5 shows a comparison between all investigated silica, DSC curves (left) and X-ray diffraction patterns (right), the curves are plotted with the highest achievable amorphous loading for each silica type, showing no peaks. Only for 72FP, the curve with no peaks (20% loading), and the curve with peaks are plotted (system overloaded, 25%). For AL-1 FP, the silica with smallest pore size (3 nm) only overloaded curves are shown (12% and 15%). The comparison between DSC and X-ray shows, that X-ray was more sensitive. In all overloaded systems detected by peaks in X-ray, no peaks could be seen in DSC. Thus, applying both

methods in parallel was sensible. In conclusion, silica with very small pore size of 3 nm are less suited. The loading of the other silica was generally between 15% and 25%.

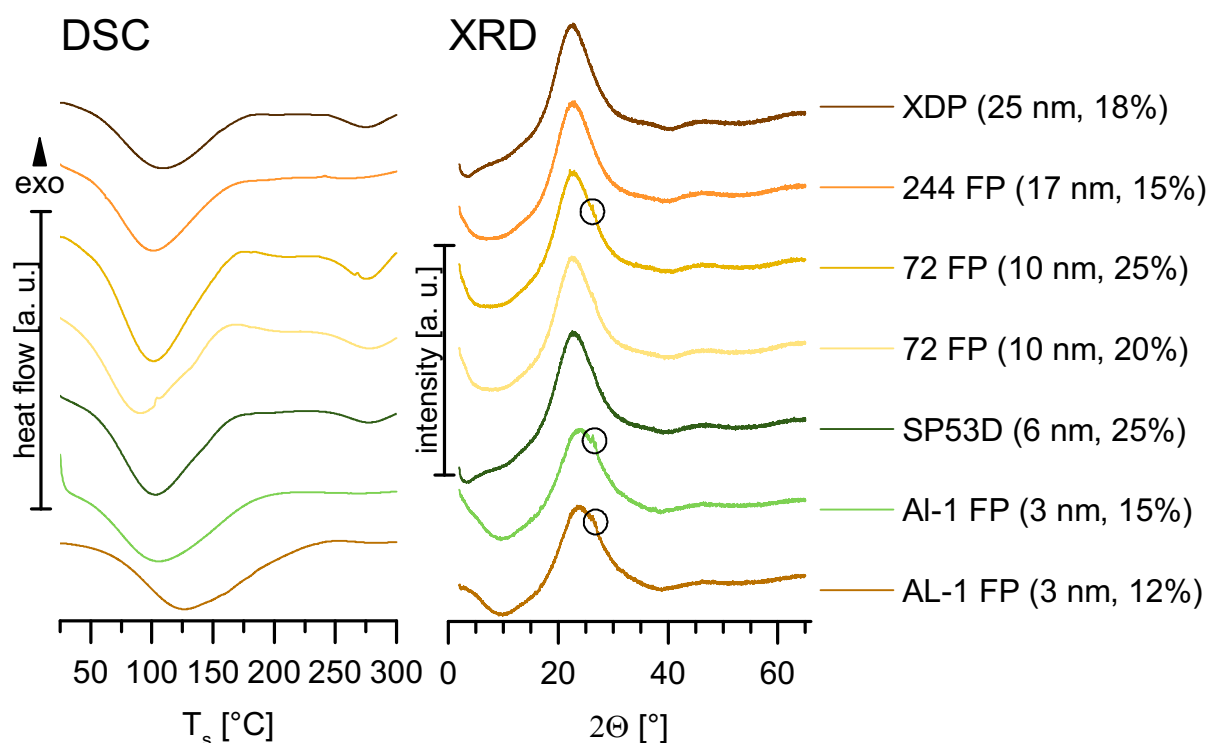


Figure 5: DSC thermograms (left) and X-ray diffractograms (right) for selected investigated silica, all loaded with ethanol as solvent for rutin, showing curves with highest amorphous loading (no peaks). For 72 FP (10 nm pores) also the curves obtained with the overloaded system (25%) are shown, for AL-1 FP only overloaded curves are presented (pore size 3 nm, 12% and 15% loading).

5.3.5. Light microscopy and scanning electron microscopy (SEM)

Light microscopy is readily accessible and fast to perform; thus, it was also used to follow the process of increasing loading. In case rutin crystals appear besides the silica particles, they should be easily detectable. Also, it was expected to see changes on the surface of the silica, i.e. deposition of rutin. Figure 6 (upper) shows exemplarily the XDP 3050 particles. Unloaded the silica appear clearly translucent (upper left), loading rutin into the pores leads to darkening of the particles (upper middle). Apparent is, that some particles are still relatively translucent, other particles are slight to medium dark, also very dark particles can be seen. That means not all particles are loaded to the same degree, there is a loading distribution between the particles from slightly to heavily loaded. This is important for understanding the process. When adding more rutin solution, the heavily loaded particles will first show a crystalline

fraction (rutin crystallizing on the surface). The overloaded system with 20% rutin (upper right) shows a majority of dark particles.

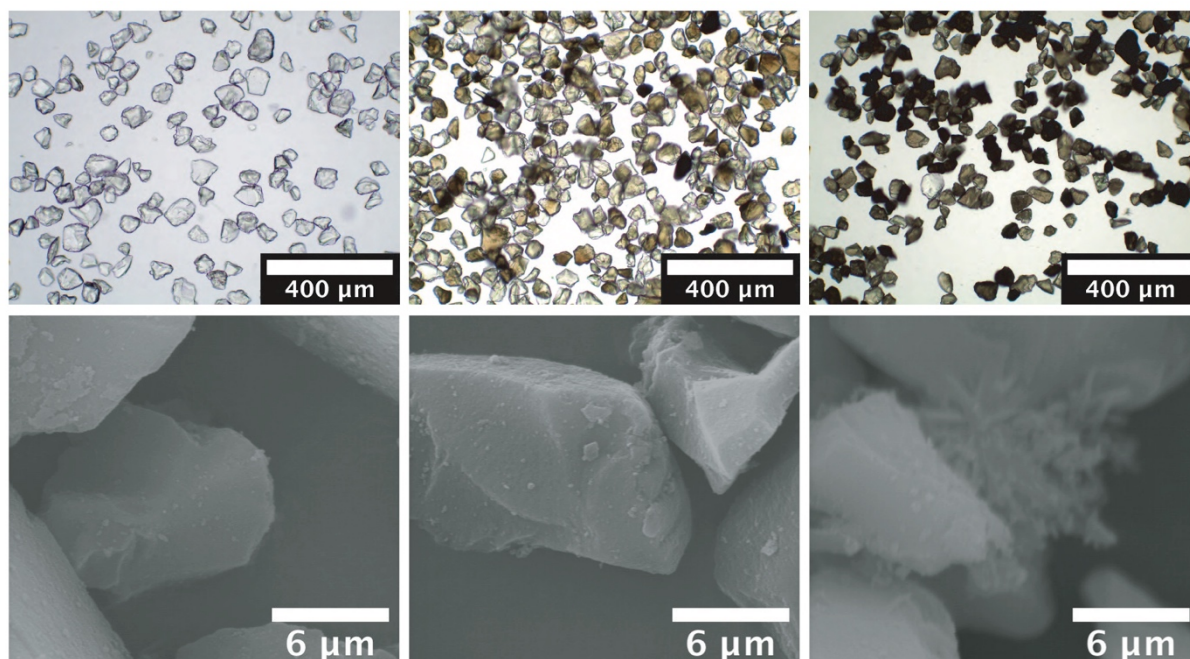


Figure 6: Upper: light microscopy images of silica XDP 3050 unloaded (left), loaded with maximum amorphous fraction of 18% (middle) and overloaded silica (20% rutin, right). Lower: corresponding SEM images (from left to right).

In Figure 6 (lower), the SEM images of unloaded silica shows a smooth surface, almost free of adhering fine particulate material (lower left). The maximum loaded particles (lower middle) show some fine particulate material on the surface. From light microscopy it is known, that there is a distribution in the degree of particle loading. Thus, the problem in SEM analysis is to distinguish to which particles the microscope is focusing on. In light microscopy one gets the overview with one glance. In the sample XDP 3050 with overloaded silica (20% loading), particles can be found with pronounced fine particulate material on the surface of some 50 μm silica particles.

In conclusion, light microscopy is a suitable complementary tool for following the loading process, SEM gives some more visual insight of basic academic understanding, but is not essential for monitoring an industrial production process.

Based on these analyses, a mechanism of loading is proposed (Figure 7), example is a silica with 1.8 mL pore volume per gram. At the beginning before loading, all pores are empty – represented by the bar at 0 mL/g filled (Figure 7, upper, left bar). As seen from the light

microscopy images – after the loading process, obviously some particles remain unfilled (light particles), some are medium filled, some are heavily filled (very dark particles). This is represented in Figure 7, middle. Penetration of solvent is different into different particles, leading to particles remaining not filled (low bar at 0 mL/g filling) or particles little or medium filled (bars at 0-0.4 and 0.4-0.8 mL/g, resp.) There are also particles with higher pore volume filling (0.8-1.2 and 1.2-1.8 mL/g). There are also particles with completely filled pores (filled volume 1.8 mL), which have additionally rutin on the surface, that means the rutin volume per gram particles is >1.8 mL (Figure 7, middle, right bar). This surface amount is amorphous, since no crystallinity is detected.

In case too much rutin solution is used, and evaporation continues, rutin continues to precipitate on the surface of completely loaded particles. By rutin deposition in thin layers on the surface, the rutin stays amorphous, with increasing layer thickness above a critical threshold crystallization occurs, being detectable by DSC/X-ray (Figure 7, lower, right bar). For the performance of the particles on the skin one could discuss, if even overloaded systems can be used, because the vast majority of the particles contains pure amorphous active agent.

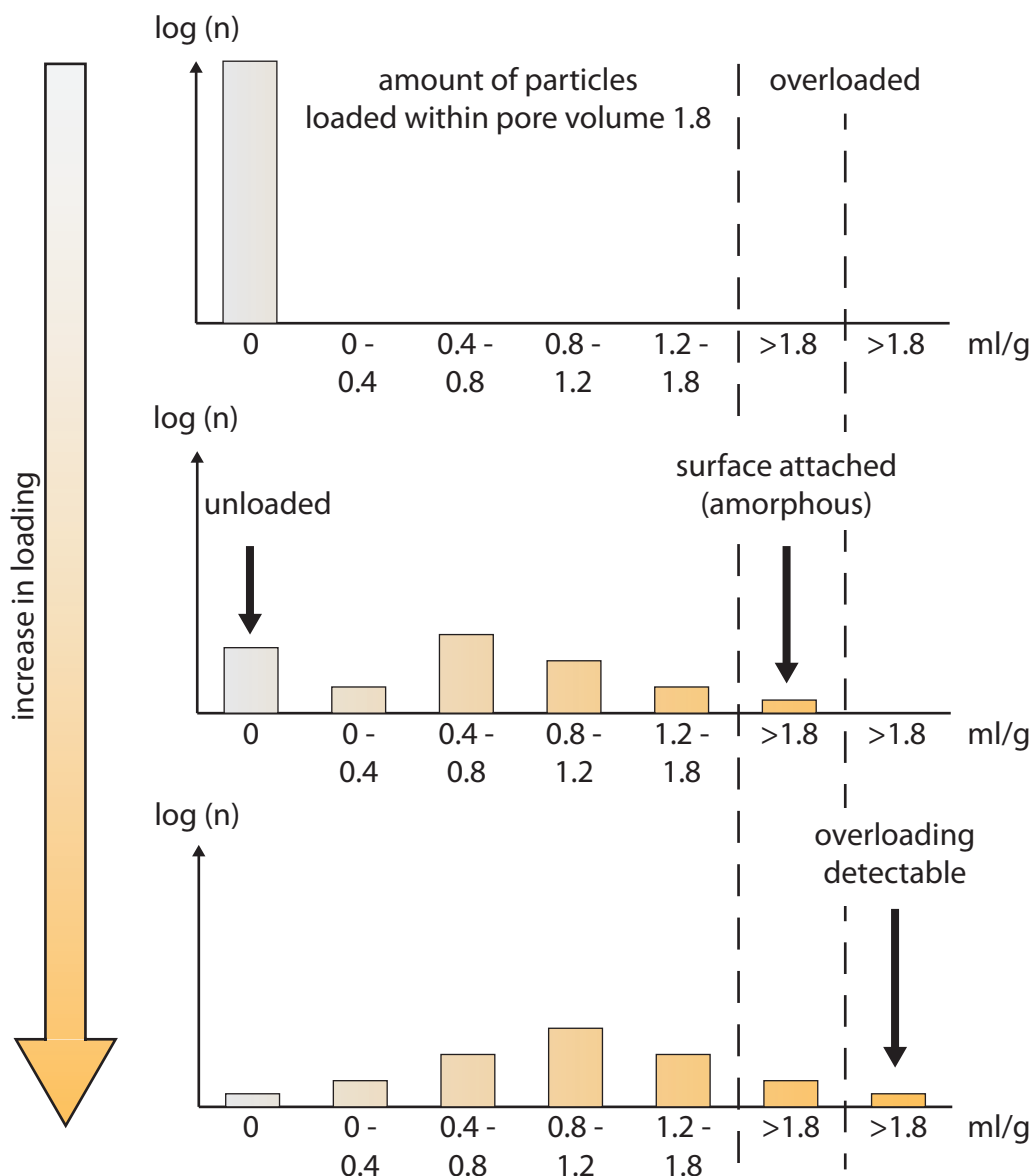


Figure 7: Mechanism model of loading of the silica particles, distribution of differently filled particles as function of increasing loading. The fractions of particle with “different loading levels” are plotted (0, 0-0.4, 0.4-0.8 mL/g etc.). Upper: in unloaded state all particles are in the 0 fraction. Middle: maximum loading with no detectable crystallinity, particles are filled to a different extend, possibly including a minor number being overloaded (>1.8 mL/g, but no detectable peaks in X-ray). Lower: Particles are overloaded, the population contains a particle fraction in which detectable crystallization occurred (details cf. text).

5.3.6. Loading efficiency – recovery rate

It was investigated if the nominal content of rutin in the different particle types could be recovered. The rutin was extracted with solvent, and the content determined by spectrophotometry and HPLC. The coefficient of determination was 0.9943 for HPLC and 0.9921 for UV spectrophotometric measurements. Figure 8 shows the amount recovered for

the two silica SP53D and 72 FP, with increasing loading from 20% to 30%. Silica SP53D and 72 FP are shown because of the high loadings (>20%) and suitability for amorphous rutin stabilization.

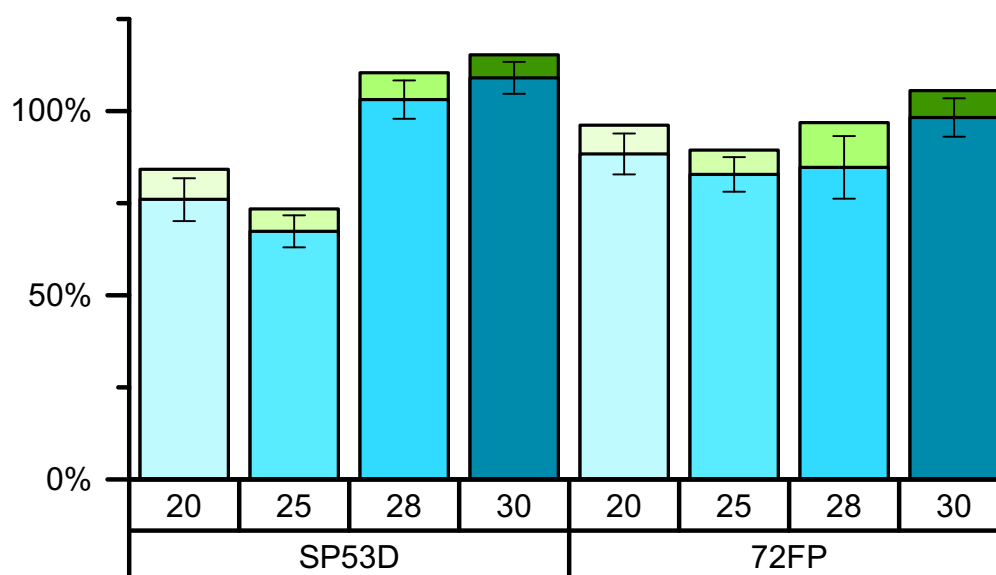


Figure 8: Recovered fraction of rutin after extraction of silica SP53D (left) and 72 FP (right) with increasing loading of 20%, 25%, 28% and 30% measured with HPLC (blue) and spectrophotometry (green). Standard derivation is shown for mean of all measurements (HPLC n=2, UV n=1).

At lower loadings (20%, 25%) a minor fraction could not be recovered. It is reported in the literature, that due to the large surface area, a delayed release takes place, some active agent is quite firmly bound to the surface area and is thus not released [34]. Thus, absolute retrieved amount increases in percentage with increasing loading. Additionally, remarkable was the higher recovery rates for samples with a certain crystallinity. This could explain the higher recovery rate at higher loadings of 28-30%. Silica with smaller pores (3 nm, AL-1 FP) showed at low maximum loading (12%) and a recovery rate of about 35% only. Analysis of the recovery rate was also performed by HPLC, the data are all slightly below the spectrophotometric results but are in agreement as shown in Figure 8.

Different results from the UV spectrophotometry and the HPLC analysis can be explained by the extraction times applied for HPLC and UV spectrophotometry samples. In general, a higher

recovery rate was found in spectrophotometry analysis due to a 2 hours prolonged extraction time (about 30 minutes for HPLC analysis versus 2 hours). The incomplete release from small pores and the influence of time has relevance for the *in vivo* situation. Often dermal formulations are applied for 10-12 hours (morning application onto the face, face wash in the evening). To have a release as complete as possible, larger pores are thus favorable for dermal products. Apart from the consequence for dermal delivery, the data show that for better comparison of data, the extraction procedures need to be exactly identical.

5.3.7. Solubility determination of rutin dissolved from smartPearls

The saturation solubility reported from Mauludin et al. for rutin nanocrystals and rutin as raw material is about 130 $\mu\text{g}/\text{mL}$ [35]. The solubility of the raw active agent powder is thereby attributed to a minimal content of nanosized rutin particles in the raw material used. Measuring the solubility of the rutin raw powder with the setup used in this study yielded saturation solubilities from 30 to 70 $\mu\text{g}/\text{mL}$ at pH 5.5 ± 0.5 (Figure 9 lower curves). Temperature was thereby constant at 25 °C. Apart from content of nanosized material, the general high values reported in literature can be attributed to a higher pH (6.8) and temperature (37°C) than used in this study (pH 5.5 for skin products and 25°C). Additionally, the *in situ* measurement with baseline correction and the used 0.15 molar NaCl solution had an influence on the difference to the values reported in literature. The theory that a minimal content of nanosized rutin particles are present in the raw material is supported by the fact, that the measured C_s increased from 30 to 70 $\mu\text{g}/\text{mL}$ with increasing amount of rutin powder added to the solvent (from 0.28 mg/mL to 2.03 mg/mL), i.e. adding increasing amounts of nanosized rutin, which dissolved and lead to this increase in measured solubility.

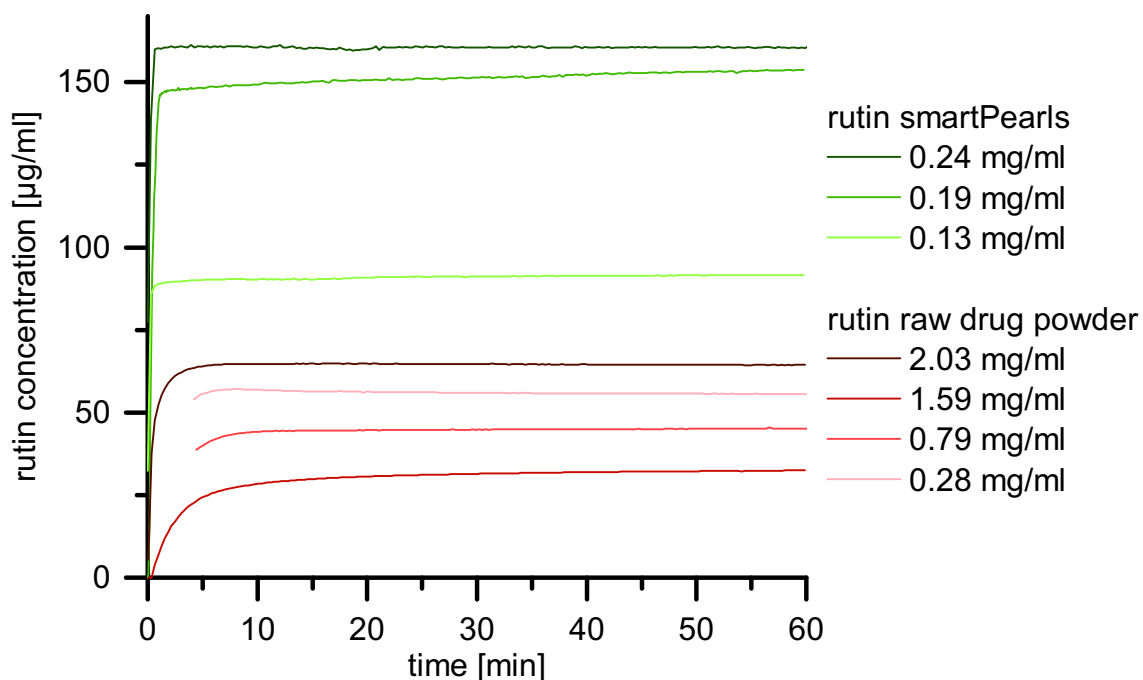


Figure 9: *In situ* determined saturation solubility of rutin raw active agent powder (lower curves, red) and amorphous rutin loaded in smartPearls (upper curves, green) with various rutin concentrations.

In contrast to the rutin powder, in this study an increased C_s of about 160 $\mu\text{g}/\text{mL}$ was obtained with amorphous rutin dissolved from smartPearls, that means about factor 2 higher than the respective raw active agent powder. This higher C_s leads to an increased concentration gradient between dermal formulation and skin, thus to an increased flux into the skin.

The dissolution kinetics of rutin from the smartPearls is much faster than from the raw rutin. With smartPearls, the plateau of solubility is practically reached after 1 minute, for the raw rutin it takes 5-10 min. However, for the dermal formulation the kinetics is not relevant, only the saturation solubility C_s . The smartPearls are added in the preparation of the dermal formulation, and a saturated state will occur in the formulation. It does not matter if this takes 1 or 10 min. When applied to the skin, it can be predicted, that the rate limiting step is the slow diffusion of dissolved rutin into the skin. There will be no difference if the diffused rutin molecules are replaced in the dermal formulation by faster or slower dissolution.

In vitro skin penetration studies showed an even higher increase in penetration comparing a gel with smartPearls to a gel with rutin powder (pig skin penetration test, tape stripping [24]). Especially in the deeper skin layers, an increase by a factor of about 4 was observed.

5.3.8. Concentration of smartPearls in final market products

When adding smartPearls to the water phase of a dermal product, a part of the rutin in the pores will dissolve, forming a supersaturated solution. A part has to remain undissolved in the pores, to provide a rutin depot. When dissolved rutin in the water phase has penetrated into the skin, it should be replaced by new rutin molecules dissolving from the pores. By this a constant supersaturated state will be maintained. Based on this, the rutin concentration required for a dermal product can be calculated.

The measured saturation solubility of rutin from smartPearls is 150 µg/mL, i.e. 0.15 mg/mL. This will be the amount which dissolves when adding the smartPearls to the formulation. In addition, one needs a rutin depot in the pores. Thus, it is recommended to use about minimum two times the amount dissolved. In cases of highly penetrating active agents, the required depot amount might even be higher. Based on this, a minimum of about 0.5 mg/mL final product is required. Assuming a low loading of the pearls of 10% (w/w), a total of 5 mg loaded smartPearls need to be added per mL (g) product (i.e. 5 g/1 kg product).

5.3.9. Definition of production parameters for large scale

Based on this, producing a batch of 100 kg requires 500 g smartPearls, with assumed only 10% loading this corresponds to 50 g rutin powder. In the production process, this 50 g rutin have to be dissolved in ethanol. Based on an ethanol solubility of 2%, 2.5 kg ethanol are required. In this rutin solution, 450 g unloaded silica particles are dispersed. For evaporation, a rotary evaporator with about 2.5 L solvent evaporation capacity is required, i.e. a rotary evaporator with a volume of about 20 L.

Large rotary evaporators are available up to volumes of 200 L (e.g. from GlasKeller AG, Basel, Switzerland). That means in one loading process 5 kg smartPearls sufficient for 1000 kg final product could be produced. This makes the smartPearls industrially feasible.

5.4. Conclusions

For best monitoring of the loading process a combination of DSC, X-ray and light microscopy is most suitable. In this study, X-ray was proved more sensitive than DSC.

Particles were obtained showing a maximum amorphous loading of 25% loaded with ethanol. With DMSO a loading of up to 35% was reachable. Thereby DMSO is hard to remove because of its high boiling point. However, ethanol is preferable because of its better tolerability, price and better technical processability.

To ensure complete amorphization a loading of 20% rutin is recommended. Re-crystallization was detected first at loadings of 28%, thus 20% is far below. Saturation solubilities increased by factor 2 with just one tenth amount of amorphous rutin compared to raw active agent powder.

Light microscopy contributed to the understanding of the loading process. It nicely revealed that filling the pores follows a distribution of filling degree (unloaded to highly loaded). Only a part of the particles reaches complete loading, these are the particles which might show first crystalline fractions.

Regarding ease of process-ability: Small particles such as AL-1 FP (7 μm) – as predictable - tend to more adhesiveness, and in combination with the small pore size of 3 nm maximum loading is low (< 12 %). Favorable for loading are larger particles with larger pores and pore volume, most favorable is Syloid® XDP 3050.

Due to the solubility properties, the amount of 5 kg loaded smartPearls for a ton of final product is relatively low, and – with the established basic process – should be able to be producible in commercially available industrial 50 L evaporators (i.e. is scale-able. To imitate exactly the situation in the large scale studied on small scale, just temperature and vacuum need to be set this way, that the same amount of solvent evaporates per time unit (i.e. copying the situation in the Ostwald-Miers range).

References

- [1] Krutmann, J.; Liu, W.; Li, L.; Pan, X.; Crawford, M.; Sore, G.; Seite, S.; 2014. Pollution and skin: From epidemiological and mechanistic studies to clinical implications. *Journal of Dermatological Science* 76(3), 163-168. <https://doi.org/10.1016/j.jdermsci.2014.08.008>
- [2] Jin, S.-P.; Li, Z.; Choi, E.K.; Lee, S.; Kim, Y.K.; Seo, E.Y.; Chung, J.H.; Cho, S.; 2018. Urban particulate matter in air pollution penetrates into the barrier-disrupted skin and produces ROS-dependent cutaneous inflammatory response in vivo. *Journal of Dermatological Science* 91(2), 175-183. <https://doi.org/10.1016/j.jdermsci.2018.04.015>
- [3] Sharma, D.; Ali, A.A.E.; Trivedi, L.R.; 2018. An Updated Review on: Liposomes as drug delivery system. *PharmaTutor* 6(2), 50-62. <https://doi.org/10.29161/PT.v6.i2.2018.50>
- [4] Müller, R.H.; Shegokar, R.; Keck, C.M.; 2011. 20 years of lipid nanoparticles (SLN & NLC): present state of development & industrial applications. *Current Drug Discovery Technologies* 8(3), 207-227. <https://doi.org/10.2174/157016311796799062>
- [5] Joseph, S.; Bunjes, H.; 2013. Solid Lipid Nanoparticles for Drug Delivery, in: Douroumis, D.; Fahr, A. (Eds.), *Drug Delivery Strategies for Poorly Water-Soluble Drugs*. John Wiley & Sons Ltd, 103-149. <https://doi.org/10.1002/9781118444726.ch4>
- [6] Loftsson, T.; Brewster, M.E.; 2013. Drug Solubilization and Stabilization by Cyclodextrin Drug Carriers, *Drug Delivery Strategies for Poorly Water-Soluble Drugs*. John Wiley & Sons Ltd, 67-101. <https://doi.org/10.1002/9781118444726.ch3>
- [7] Jambhekar, S.S.; Breen, P.; 2016. Cyclodextrins in pharmaceutical formulations II: solubilization, binding constant, and complexation efficiency. *Drug Discovery Today* 21(2), 363-368. <https://doi.org/10.1016/j.drudis.2015.11.016>
- [8] Petersen, R., inventors; PharmaSol GmbH, assignee; 2007. Nanocrystals for use in topical cosmetic formulations and method of production thereof. European Union patent EP 2 099 420 B8 B8, Nov 19.
- [9] Petersen, R., inventors; Abbvie Deutschland GmbH & Co KG, assignee; 2007. Nanocrystals for use in topical cosmetic formulations and method of production thereof. United States patent US 9,114,077 B2, Nov 19.

- [10] Müller, R.H.; Keck, C.M.; 2012. Twenty years of drug nanocrystals: where are we, and where do we go? *European Journal of Pharmaceutics and Biopharmaceutics* 80(1), 1-3. <https://doi.org/10.1016/j.ejpb.2011.09.012>
- [11] Romero, G.B.; Chen, R.; Keck, C.M.; Müller, R.H.; 2015. Industrial concentrates of dermal hesperidin smartCrystals® – production, characterization & long-term stability. *International Journal of Pharmaceutics* 482(1), 54-60. <https://doi.org/10.1016/j.ijpharm.2014.11.039>
- [12] Müller, R.H.; Hespeler, D.; Keck, C.M.; 2018. More beautiful than Cleopatra SmartCrystals® – the smart principle to deliver the beauty secrets of Cleopatra more efficiently into the skin. *Eurocosmetics* 26(11/12), 20-23.
- [13] Müller, R.H.; Shegokar, R.; Gohla, S.; Keck, C.M.; 2011. Nanocrystals: production, cellular drug delivery, current and future products, in: Prokop, A. (Ed.), *Intracellular Delivery*. Springer, 411-432. https://doi.org/10.1007/978-94-007-1248-5_15
- [14] Hancock, B.C.; Parks, M.; 2000. What is the True Solubility Advantage for Amorphous Pharmaceuticals? *Pharmaceutical Research* 17(4), 397-404. <https://doi.org/10.1023/A:1007516718048>
- [15] Qian, K.K.; Bogner, R.H.; 2012. Application of Mesoporous Silicon Dioxide and Silicate in Oral Amorphous Drug Delivery Systems. *Journal of Pharmaceutical Sciences* 101(2), 444-463. <https://doi.org/10.1002/jps.22779>
- [16] Murdande, S.B.; Pikal, M.J.; Shanker, R.M.; Bogner, R.H.; 2011. Aqueous solubility of crystalline and amorphous drugs: Challenges in measurement. *Pharmaceutical Development and Technology* 16(3), 187-200. <https://doi.org/10.3109/10837451003774377>
- [17] Cremer, K.; Kröhne, L.; Mayer, J., inventors; Capsulation Nanoscience AG, assignee; 2003. Schnellfreisetztende, feste Darreichungsform zur oralen Applikation schwerlöslicher Wirkstoffe. International Publication Number WO002004030648A1, Sep 24.
- [18] Grabo, M.; Dunmann, C.; Müller, R.H.; Keck, C.M.; 2011. CapsMorph technology for generation of amorphous oral formulations, W4131, Annual Meeting of the American Association of Pharmaceutical Scientists (AAPS), Washington D.C., 23.-27. October.

- [19] Wei, Q.; Keck, C.M.; Müller, R.H.; 2015. CapsMorph® technology for oral delivery— theory, preparation and characterization. *International Journal of Pharmaceutics* 482(1), 11-20. <https://doi.org/10.1016/j.ijpharm.2014.10.068>
- [20] Choudhari, Y.; Hoefler, H.; Libanati, C.; Monsuur, F.; McCarthy, W.; 2014. Mesoporous silica drug delivery systems, in: Shah, N.; Sandhu, H.; Choi, D.; Chokshi, H.; Malick, A. (Eds.), *Amorphous Solid Dispersions*. Springer, New York, 665-693. https://doi.org/10.1007/978-1-4939-1598-9_23
- [21] Fan, H.; Van Swol, F.; Lu, Y.; Brinker, C.J.; 2001. Multiphased assembly of nanoporous silica particles. *Journal of Non-Crystalline Solids* 285(1), 71-78. [https://doi.org/10.1016/S0022-3093\(01\)00434-3](https://doi.org/10.1016/S0022-3093(01)00434-3)
- [22] Monsuur, F.H.; Hoefler, H.H.; Keck, C.M., inventors; Grace GmbH & Co. KG, Pharmasol GmbH, assignee; 2014. Active-loaded particulate materials for topical administration. International Publication Number WO 2016/041992 A1, patent application PCT/EP2015/071138, Sep 15.
- [23] Müller, R.H.; Hespeler, D.; Jin, N.; Pyo, S.M.; 2019. smartPearls – Novel physically stable amorphous delivery system for poorly soluble dermal actives. *International Journal of Pharmaceutics* 555, 314-321. <https://doi.org/10.1016/j.ijpharm.2018.11.018>
- [24] Jin, N.; 2017. Nanocrystals & loaded porous silica for increased dermal bioavailability [doctoral thesis]. [Germany]: Freie Universität Berlin. urn:nbn:de:kobv:188-fudissthesis000000105191-3
- [25] Jermain, S.V.; Brough, C.; Williams, R.O.; 2018. Amorphous solid dispersions and nanocrystal technologies for poorly water-soluble drug delivery – An update. *International Journal of Pharmaceutics* 535(1), 379-392. <https://doi.org/10.1016/j.ijpharm.2017.10.051>
- [26] Stein, J.; Fuchs, T.; Mattern, C.; 2010. Advanced Milling and Containment Technologies for Superfine Active Pharmaceutical Ingredients. *Chemical Engineering & Technology* 33(9), 1464-1470. <https://doi.org/10.1002/ceat.200900590>
- [27] Watanabe, T.; Wakiyama, N.; Usui, F.; Ikeda, M.; Isobe, T.; Senna, M.; 2001. Stability of amorphous indomethacin compounded with silica. *International Journal of Pharmaceutics* 226(1), 81-91. [https://doi.org/10.1016/S0378-5173\(01\)00776-1](https://doi.org/10.1016/S0378-5173(01)00776-1)

-
- [28] Smirnova, I.; Mamic, J.; Arlt, W.; 2003. Adsorption of Drugs on Silica Aerogels. *Langmuir* 19(20), 8521-8525. <https://doi.org/10.1021/la0345587>
- [29] Ahern, R.J.; Hanrahan, J.P.; Tobin, J.M.; Ryan, K.B.; Crean, A.M.; 2013. Comparison of fenofibrate–mesoporous silica drug-loading processes for enhanced drug delivery. *European Journal of Pharmaceutical Sciences* 50(3), 400-409. <https://doi.org/10.1016/j.ejps.2013.08.026>
- [30] Hespeler, D.; Kaltenbach, J.; Pyo, S.M.; 2019. Glabridin smartPearls – Silica selection, production, amorphous stability and enhanced solubility. *International Journal of Pharmaceutics* 561, 228-235. <https://doi.org/10.1016/j.ijpharm.2019.02.028>
- [31] Narayana, K.R.; Reddy, M.S.; Chaluvadi, M.R.; Krishna, D.R.; 2001. Bioflavonoids classification, pharmacological, biochemical effects and therapeutic potential. *Indian Journal of Pharmacology* 33(1), 2-16.
- [32] El Nomeiri, S.; 2019. Entwicklung und Charakterisierung von amorphen Rutin-Carriern zur dermalen Applikation [master thesis]. [Germany]: Beuth University of Applied Science Berlin.
- [33] Hespeler, D.; Pyo, S.M.; Müller, R.H.; 2019. Dermal smartPearls – Optimized silica particles for commercial products & mechanistic considerations. *International Journal of Pharmaceutics*, *submitted [Manuscript ID: IJP-S-19-01888]*.
- [34] Wei, Q.; Keck, C.M.; Müller, R.H.; 2017. Preparation and tableting of long-term stable amorphous rutin using porous silica. *European Journal of Pharmaceutics and Biopharmaceutics* 113(Supplement C), 97-107. <https://doi.org/10.1016/j.ejpb.2016.11.009>
- [35] Mauludin, R.; Müller, R.H.; Keck, C.M.; 2009. Kinetic solubility and dissolution velocity of rutin nanocrystals. *European Journal of Pharmaceutical Sciences* 36(4–5), 502-510. <http://dx.doi.org/10.1016/j.ejps.2008.12.002>

6. Glabridin smartPearls – Silica selection, production, amorphous stability and enhanced solubility⁵

Abstract

Glabridin, a compound in the root extract of *Glycyrrhiza glabra*, has been identified as an effective tyrosinase inhibitor. Applied on skin, melanin synthesis is inhibited, making glabridin an interesting candidate for skin whitening or for the treatment of age spots. However, main obstacle for its practical use is its low dermal bioavailability, caused by its poor water solubility (1-20 mg/L). In this work smartPearls technology was used to increase the glabridin's water solubility. smartPearls consist of silica particles with mesopores in which actives can be loaded. By this, actives are stabilized in amorphous state and simultaneously finely distributed in nm-range. Both amorphization and nanoization are well known approaches to increase saturation solubilities. In smartPearls these approaches are combined. In the first step, glabridin smartPearls formulation was developed, screening systematically the suitability of 4 different silica varying in their pore sizes (3, 6, 10, 17 nm). Also, most suited filling level of glabridin was determined (25, 50, 80% referred to total pore volume of respective silica). Silica loading was performed by the immersion-evaporation method, resulting in pores filled with glabridin from bottom to top. By light microscopy, differential scanning calorimetry and X-ray diffraction the sample with 6 nm pore size and filling levels of 25% and 50% have been verified to be completely amorphous. Highest physical storage stability of 7 months up to now was obtained for the 25% filled sample. In the next step, concept of increased saturation solubility for smartPearls was proven. Dissolution profiles were recorded *in situ* for glabridin smartPearls and compared to glabridin raw drug powder. Both saturation solubility and dissolution velocity were remarkably improved. The water solubility for example increased by a factor of more than 4. This makes glabridin smartPearls promising for creating skin products with improved dermal bioavailability.

⁵ This chapter has been published as:

Hespeler, D.; Kaltenbach, J.; Pyo, S.M.; 2019. Glabridin smartPearls – Silica selection, production, amorphous stability and enhanced solubility. *International Journal of Pharmaceutics* 561, 228-235.
<https://doi.org/10.1016/j.ijpharm.2019.02.028>

6.1. Introduction

Glabridin is a chemical compound that is found in the root extract of *Glycyrrhiza glabra*. Since its characterization in 1976 increasing number of publications reports its various biological effects, e.g. anti-oxidative, anti-inflammatory, neuroprotective and skin whitening effects [1]. Therefore, Glabridin can be of interest not only as pharmaceutical active but also as cosmetic agent [2].

Especially as skin whitener glabridin is of interest for the Asian cosmetic market, as bright skin is the ideal of Asian beauty. But also, for the European cosmetic market glabridin can be of interest for age spot treatment. Both tanned skin and age spots have in common that this area of skin is rich in melanin. Synthesis of the skin pigment melanin is triggered by UV light. It activates the enzyme tyrosinase, which converts tyrosine stepwise to melanin [3]. Glabridin, one main active component of the root extract, is an efficient inhibitor of tyrosinase. Yokota et al. [4] reported, that skin pigmentation induced by UVB radiation on the backs of the brownish guinea is significantly reduced (34% inhibition over control) when glabridin is topically applied as a 0.5% solution in ethanol/propylene glycol/water (6.5/2.5/1.0).

However, only a small number of glabridin containing products exists on the cosmetic market. One reason limiting its use can be its low water solubility (1.5 mg/L, estimated by EPISuite [5] or 20 mg/L by ChemAxon [6]). Skin penetration is a passive diffusional process. The amount of penetrating active is therefore directly proportional to the concentration gradient between formulation and skin. Hence, the low solubility results in low bioavailability. A simple increase of glabridin amount for compensation is practically not realizable due to the high glabridin prize of 20 USD per gram [7]. This explains the numerous publications dealing with the penetration enhancement of glabridin. One commonly reported approach is the increase of glabridin's lipophilicity by esterifying or etherifying one or both hydroxyl groups of glabridin [8-10]. However, the whitening effects is coupled to these hydroxyl groups, and masking either one or both leads to distinctly reduced efficacy [4]. Hence, chemical modification is not a meaningful method [11]. Increasing the penetration can be also implement by physical modifications improving the water solubility. One well-known solubility increasing approach is the reduction of the crystal size to the nano-dimension [12]. These so-called nanocrystals of glabridin were already invented by PharmaSol GmbH, Berlin and are commercially available.

A recently invented physical transformation is the formation of glabridin smartPearls [13]. smartPearls consists of regulatory accepted mesoporous silica particles (up to 50 μm) with pore widths between 2 and 50 nm. In these pores, actives can be loaded and long-term preserved in amorphous state for up to 7 years [14]. Since amorphous state is thermodynamically unstable and tend to re-crystallize within few days or months, 7 years is remarkable. Hence, loaded active in smartPearls combines two principles of solubility increase [15].

- 1) dispersion of active in nm-range comparable to nanocrystals, and
- 2) stabilized amorphous state of active.

This combination of two saturation solubility increasing principles may explains why smartPearls are reported to be even superior to the current “gold standard” nanocrystals, only working with one principle. In comparative studies with poorly soluble anti-oxidants, e.g. hesperidin, smartPearls possessed a 5-times higher saturation solubility than nanocrystals [16]. Similar observations were made for their penetration in an *ex vivo* investigation on porcine ears by the tape stripping method. The penetrated amount of azithromycin from smartPearls was up to 30-times higher in the deeper layers of the stratum corneum (represented by tapes 20-30) than for nanocrystals [16]. Therefore, smartPearls appear promising in improving the penetration of poorly soluble glabridin into skin – even better than the nanocrystals currently available on the market.

Therefore, aim of this study was to develop a physically and chemically long-term stable glabridin smartPearls formulation. This formulation should enable market formulations with improved skin penetration by simultaneously decreased costs. Therefore, 4 different silica with different physical properties, e.g. pore widths (3, 6, 10 and 17 nm), were selected. Each of the silica was then loaded in 3 different filling levels (25, 50 and 80% of total pore volume) to examine if the filling level has an influence on amorphization and its preservation. All loadings were performed by the immersion-evaporation method [17], and its suitability for loading the chemically sensitive glabridin in mesoporous silica was verified by HPLC analysis. Also, the question was answered, how the glabridin is located in the pores, since localization will influence its release. Finally, for proving the concept of increased solubility by smartPearls, the saturation solubility of stable glabridin smartPearls formulation was measured and compared to the saturation solubility of glabridin raw drug powder.

6.2. Materials and Methods

6.2.1. Materials

Glabridin with a high purity of 98% was purchased from Actives International (Allendale, USA). Various mesoporous silica particles were kindly provided from Grace GmbH & Co. KG (Worms, Germany), and are listed in Table 1 with their respective physical properties. Ethanol in HPLC grade was purchased from VWR (Darmstadt, Germany), and purified water was used produced by a Milli-Q system from Merck Millipore (Darmstadt, Germany).

Table 1: Overview of mesoporous silica used in this study with respective physical properties [18]

trade name	pore width [nm]	pore volume [mL/g]	BET surface [m ² /g]	particle size [μm]
Syloid® AL-1 FP	3	0.4	740	7
Davisil® LC60A	6	0.9	550	12
Syloid® 72 FP	10	1.2	370	5
Syloid® 244 FP	17	1.6	380	3

6.2.2. Methods

Density determination by helium pycnometer

In this study, the production of smartPearls with glabridin loadings of 25, 50 and 80% (related to the total pore volume of respective silica) were aimed. Since the loading is related to the volume, but mass is needed for weighing glabridin and silica, densities of both were determined in advance using a helium pycnometer AccuPyc II 1340 (Micromeritics Instrument Corp., Norcross, USA). In a 1 cm³ sample cell 0.25 g of either glabridin or silica were weighted and purged 20 times with helium. One sample was measured for 5-times and the resulting average was used for subsequent calculation.

Production of glabridin smartPearls

For loading by immersion-evaporation method, the active first had to be brought in solution. For glabridin smartPearls, which will be used on skin, ethanol was selected as solvent and 10% (w/w) glabridin solutions were prepared. Then, 2 g of silica was weighted into a 250 mL

round-bottom flask and required amount of this solution to obtain desired loadings of 25, 50 or 80% was added (Table 2). By rotating the flask using a rotary evaporator (Büchi Labortechnik GmbH, Germany) without applying heat or pressure, glabridin solution was thoroughly mixed with silica. As next step, ethanol was removed stepwise, first at $40\pm 2^\circ\text{C}$ and 150 ± 5 mbar, then below 50 mbar. To obtain completely dry and free flowing glabridin smartPearls, additional drying step was implemented using a desiccator under vacuum (<20 mbar) for 12 hours.

Table 2: Overview of 10% ethanolic glabridin solution needed for loading 2 g silica at pore volume loadings of 25%, 50% and 80%.

silica	pore volume [mL/g]	10% ethanolic glabridin solution [g] added to 2 g silica to obtain following PV loadings:		
		25% PV	50% PV	80% PV
Syloid® AL-1 FP	0.4	not produced	5.20	6.24
Davisil® LC60A	0.9	5.85	11.71	18.72
Syloid® 72 FP	1.2	7.80	15.60	24.96
Syloid® 244 FP	1.6	10.40	20.80	33.28

Characterization of glabridin smartPearls

High performance liquid chromatography (HPLC)

The glabridin content in loaded smartPearls were investigated directly after production and after 6 months storage at room temperature. 50 mg glabridin smartPearls were dispersed in 10 mL ethanol. To dissolve glabridin completely from smartPearls, the dispersion was extensively shaken and sonicated for 10 minutes. By centrifugation silica fraction was separated. The so obtained glabridin solution was diluted for measurement by a factor of 125. Measurement was performed using a Kontron 400 System (Kontron Instruments GmbH, Germany) equipped with a 20 µl sample loop and an Eurosphere 100 C18 (5 µm 250x4 mm) column. The mobile phase consisted of a 57:43 mixture of 2% acetic acid and acetonitrile, respectively. Flow rate was set to 1.2 mL/min, column oven to 30°C and detector wavelength to 282 nm. The peak evaluation was carried out by the supplied software KromaSystem 2000. Retention time of glabridin was 12 minutes. By applied measurement settings, the limit of

detection was determined to be 0.24 µg/mL and the limit of quantification 0.72 µg/mL with a slope of 0.2947 and a standard deviation of 0.0213.

Light microscopy (LM)

Under light microscope both shape and size of smartPearls were investigated before loading, directly after loading and after storage at room temperature for 1 week, and 1, 3 and 6 months. Therefore, the Motic BA210 LED was used at 100, 400 and 1000-fold magnification and photos were taken by Moticom 3.0 MP (both from Motic Deutschland GmbH, Germany).

Differential scanning calorimetry (DSC)

The physical state of silica particles, glabridin raw drug powder and glabridin smartPearls was examined by differential scanning calorimetry (DSC 1, Mettler Toledo GmbH, Germany). In a punctured 40 µl aluminum pan exact amount between 1-10 mg were weighted, based on the respective mass of glabridin. Measurements were then performed at a heating rate of 20 K/min between 20 and 280°C.

X-ray diffraction (XRD)

In addition, X-ray diffraction were performed using a Bruker D8 (Bruker, USA) to determine the amorphous state and possible residual crystal fractions of glabridin in smartPearls. Measurements were carried out after production and 7 months of storage at room temperature. A scan rate of 0.02° (2=2-60°) was applied and the goniometer equipped with a Cu-anode ($K\alpha=0.15406$ nm) run with a voltage of 40 kV and current of 35 mA.

Nitrogen ad- and desorption

After outgassing samples for 24 hours at 30°C, nitrogen isotherms were recorded with 20 measurement points of adsorption and 24 points of desorption using a NOVA Quantachrome 4000e (Quantachrome GmbH & Co. KG, Germany). The so obtained isotherms were evaluated with supplied NOVAwin 11.0 software. Surface areas were determined after the Brunauer-Emmett-Teller (BET) method [19], and pore widths and pore volumes after the density functional theory (DFT) [20].

Determination of saturation solubility

The saturation solubility was assessed for best glabridin smartPearls formulation and raw drug powder using a Sirius inform (Sirius Analytical Instruments Ltd., Forest Row, UK). This device allows in situ UV/VIS measurements of the samples. All tests were performed for 30 minutes

aqueous NaCl solution (0.15 N) at 25 °C. Non-sink conditions were selected with glabridin amounts 10 times higher than the saturation solubility of glabridin from literature. Tyndall-Rayleigh scattering occurring due to unsolved particles were corrected by aligning the spectrum between 400 and 500 nm [21].

6.3. Results and Discussion

6.3.1. Pre-considerations and explanations

Selection of silica for smartPearls production

Theory behind amorphous preservation in mesoporous particles is the so-called “space restriction principle”. For re-crystallization certain space is needed by the active which the pores do not provide. Selecting the correct pore size will therefore be decisive for preservation. According to Sliwinska et al. [22], the ratio of silica pore width to active molecule size must be smaller than 12 for an efficient preservation of amorphous state. For ratios being between 12 and 20, amorphous state can be obtained and may preserved. And ratios greater than 20 considerably tend to re-crystallize. According molar volume of glabridin ($257.9 \pm 3 \text{ cm}^3$), a spherical diameter of 0.94 nm was assumed. Hence, for the desired ratio of either <12 or <20, pore widths of <11.6 or <19.4 are needed. Therefore, 3 silica providing the required ratio <12 were selected (pore width of 3, 6 and 10 nm) for this study. In addition, one silica being between the ratio of 12-20 were chosen (pore width of 17 nm) may allowing the production of stable smartPearls with considerably higher glabridin content.

Sample name

Glabridin smartPearls samples produced in this study varied in used silica and loaded amount of glabridin. Hence, samples were named after these two characteristics following the pattern: “Pore size of silica in nm – loading in volume percentage”. Sample 6-25% for example is produced by filling 25% of total pore volume of Davisil® LC60A with glabridin.

Calculation of glabridin mass fraction

3 different pore volume loadings of 25%, 50% and 80% were selected to gain a better understanding of the pore stabilization mechanism. However, for loading process, respective glabridin to silica mass ratios were needed for correct weighing. Also, the glabridin fraction is crucial for dosing glabridin smartPearls in final formula, e.g. creams or gels. To calculate the

glabridin mass fraction in each sample, the densities of silica and glabridin were determined in advance to be 2.14 g/mL and 1.32 g/mL, respectively. The resulting mass fractions for each sample are listed in Table 3. After calculation, sample 3-25% was withdrawn, as this pore volume loading would have led to a glabridin mass fraction <20% being insufficient for practical use.

Table 3: List of glabridin mass fraction for all prepared samples in this study. To clarify the difference to the mass fraction %, the pore volume % was named as PV in the list.

silica	pore width [nm]	pore volume [mL/g]	glabridin content in mass fraction [% (w/w)] calculated for desired 3 pore volume loadings:		
			25% PV	50% PV	80% PV
Syloid® AL-1 FP	3	0.4	-/-	20.9	29.7
Davisil® LC60A	6	0.9	22.9	37.3	48.7
Syloid® 72 FP	10	1.2	28.4	44.2	55.9
Syloid® 244 FP	17	1.6	34.6	51.4	62.8

6.3.2. Characterization of glabridin smartPearls

Preselection by light microscopy

To get a quick first impression of freshly produced glabridin smartPearls, light microscopy (LM) is ideally suited. It allows to preselect samples for further investigations being more time consuming and costly, e.g. nitrogen ad- and desorption or DSC. If the majority of glabridin is firmly loaded in the pores, no change can be observed in their appearance. An example for firmly loaded glabridin is given in Figure 1. On the left, LM image of unloaded silica with 6 nm pore width is shown at 1000-fold magnification. On the right, same silica with pore volume loading of 50% is shown. No visible changes occurred. In contrast, overloaded samples show newly formed smaller crystals in addition to the silica. As example, 3-80% glabridin smartPearls are shown in Figure 1 right. Compared to the unloaded silica, formation of new crystals is visible. Hence, these samples can be dropped out. Even though LM can be used for preselection, no change in appearance is no guarantee for firm inclusion. These samples need further investigation by e.g. XRD or DSC for reliable evidence.

After intensive evaluation of LM images, all samples with 3 nm pore width were excluded from further investigations. All other samples looked inconspicuous, even all silica samples with 17 nm pore width.

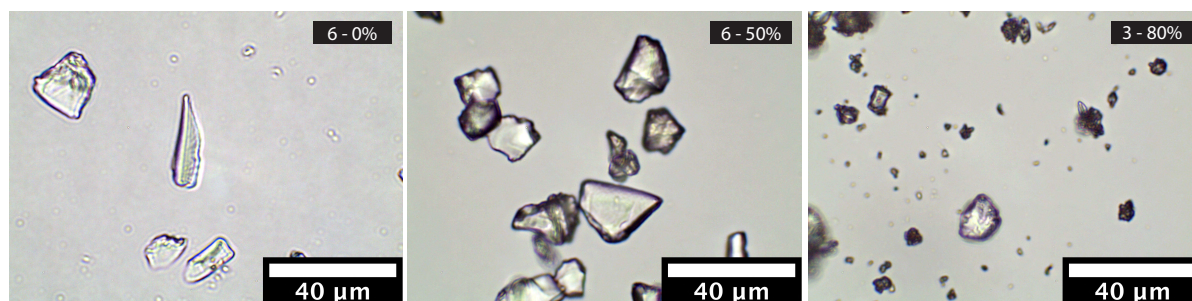


Figure 1: Light microscope images at 1000-fold magnification of unloaded samples 6-0% (left), and loaded samples 6-50% (middle, showing no visible changes) and 3-80% (right, showing additional crystals of unloaded glabridin).

Proof of absence of crystalline glabridin fractions by DSC

By DSC measurements, a more sensitive determination of crystalline fractions is possible [23]. The detection limit of glabridin was determined by measuring the physical mixture of glabridin raw drug powder with silica particles at various ratios to be 1% (Figure 2, lower graph).

The DSC thermogram of glabridin raw drug powder showed an onset temperature of 229 °C and a melting peak at 232 °C (Figure 2, middle graph). In contrast, the DSC thermogram of unloaded silica showed no melting peaks (Figure 2, upper graph). Only a broad peak around 100°C was detected representing adhered water on silica surface. This peak appeared also for loaded silica (Figure 3). As no shift of this water peak to lower temperatures occurred it can be concluded that no detectable amount of ethanol (boiling point ~80 °C) is left in the sample. Hence, the applied drying process is suited to remove the solved completely.

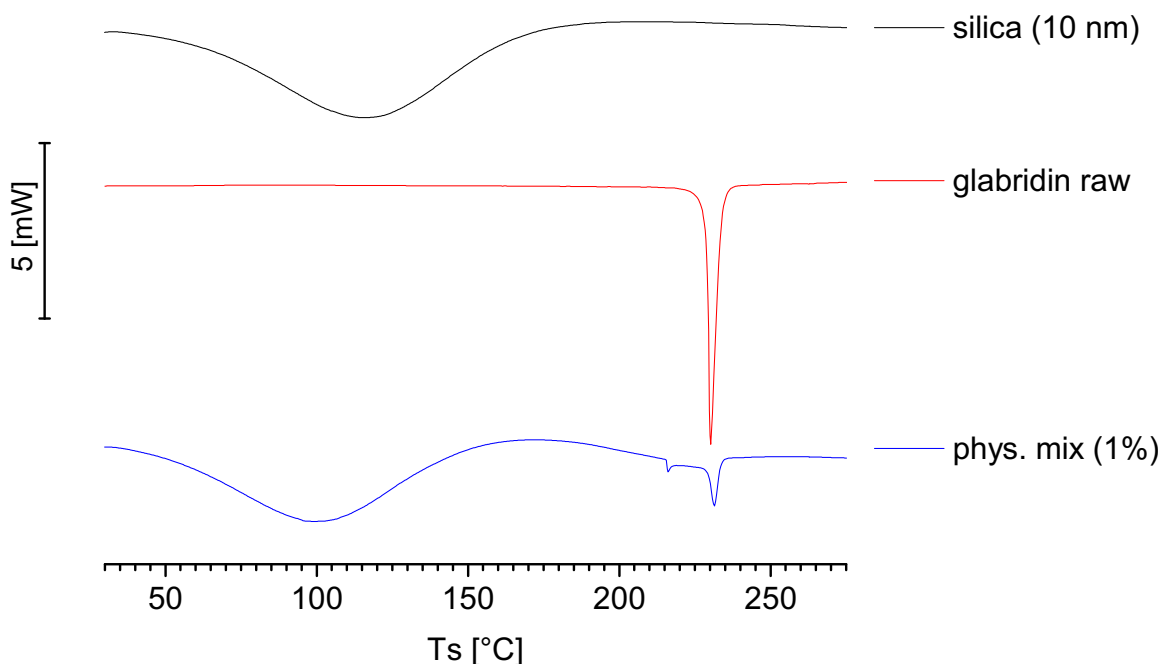


Figure 2: From upper to lower: DSC thermograms of silica particles with pore width of 10 nm, glabridin raw drug powder, and a physical mixture of 1% glabridin raw drug powder and 99% silica particles.

In addition to the expected glabridin melting peak at 232 °C an additional peak at 216 °C was observed for the physical mixture. Since this peak is absent in the thermogram of pure raw drug powder, even the very gentle blending of the silica with glabridin raw drug powder seems to cause a change in glabridin's crystallinity. Since no pressure nor temperature was applied to prepare this blend, the peak seems to be caused most likely by surface interactions. As the melting point is lower (216 °C) than the melting point of raw drug powder (232 °C), a thermodynamically more unstable form seems to be created. However, by present data no certain statement can be made what exactly is formed.

Conceivable is the transformation of glabridin into more thermodynamically unstable crystalline form. Also possible is a fractional transformation of crystalline glabridin into amorphous state. Then the peak would represent a glass transition peak with a small endothermic baseline shift and a relaxation peak. Whichever of the theories apply, this additional peak should not appear in an amorphously stabilized sample: If it is a melting peak of metastable crystalline glabridin the sample is partially crystalline, and if it represents a relaxation peak the amorphous glabridin is not sufficiently stabilized [24].

For the samples 6-25% and 6-50%, there are no further peaks in the range of 20-280 °C apart from the water peak at 100 °C (Figure 3). For sample 10-25%, however, the peak at 216 °C occurs identical to physical mixture. Therefore, this sample can be considered as overloaded, either with metastable crystalline glabridin or not sufficiently stabilized amorphous glabridin. For sample 17-25% both peaks are slightly shifted to lower temperatures probably because of partly reformed glabridin. Since a crystalline fraction demonstrably exists besides an amorphous fraction, this sample was excluded too. All other samples showed a clear melting peak of crystalline glabridin at 232 °C. Therefore, they were also excluded from further investigations.

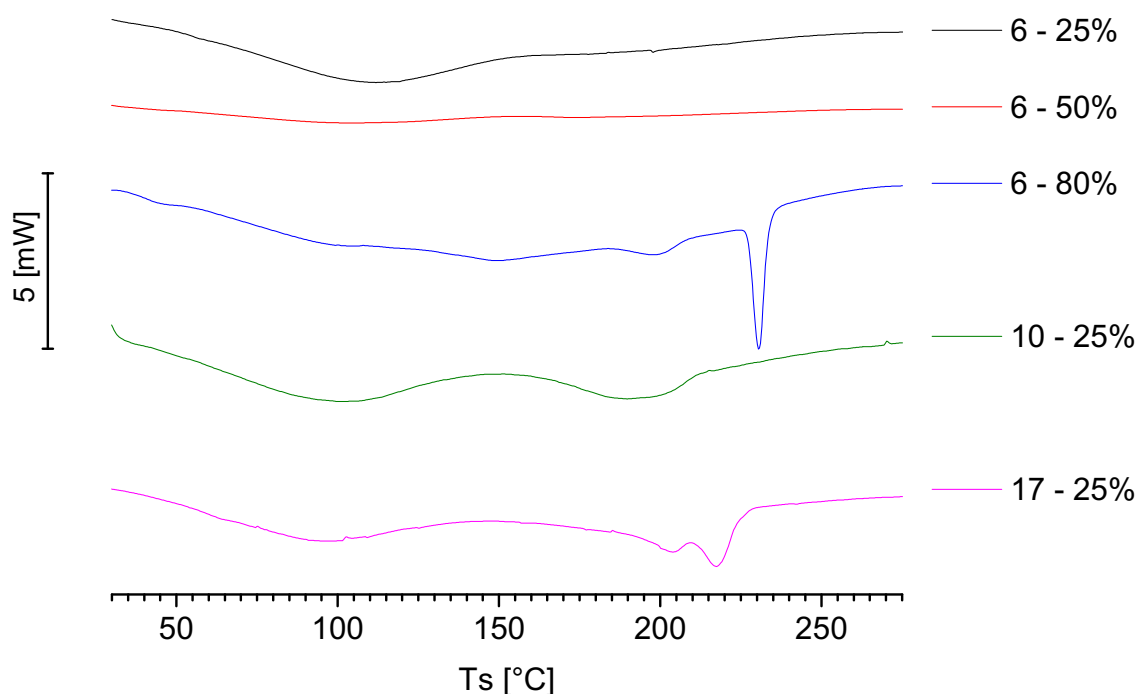


Figure 3: From upper to lower: DSC thermograms of the samples 6-25%, 6-50% and 10-25% showing no clear melting peak of glabridin at 232 °C, and 6-80% and 17-10% as examples for samples having a clear crystalline glabridin fraction visible by respective melting peak.

Proof of amorphous state of glabridin by XRD diffractograms

XRD is widely known as the standard method to characterize crystalline structures. Even if their sensitivity is below that of DSC measurements [17; 25], they allow a clear confirmation of amorphous phases by an amorphous halo. In contrast, DSC only proof the absence of a melting peak and thus crystallinity. Hence, the combination of DSC with XRD measurements seems reasonable.

The XRD measurements of promising samples (6-25%, 6-50%, 10-25%) were performed and the respective diffractograms are displayed in Figure 4.

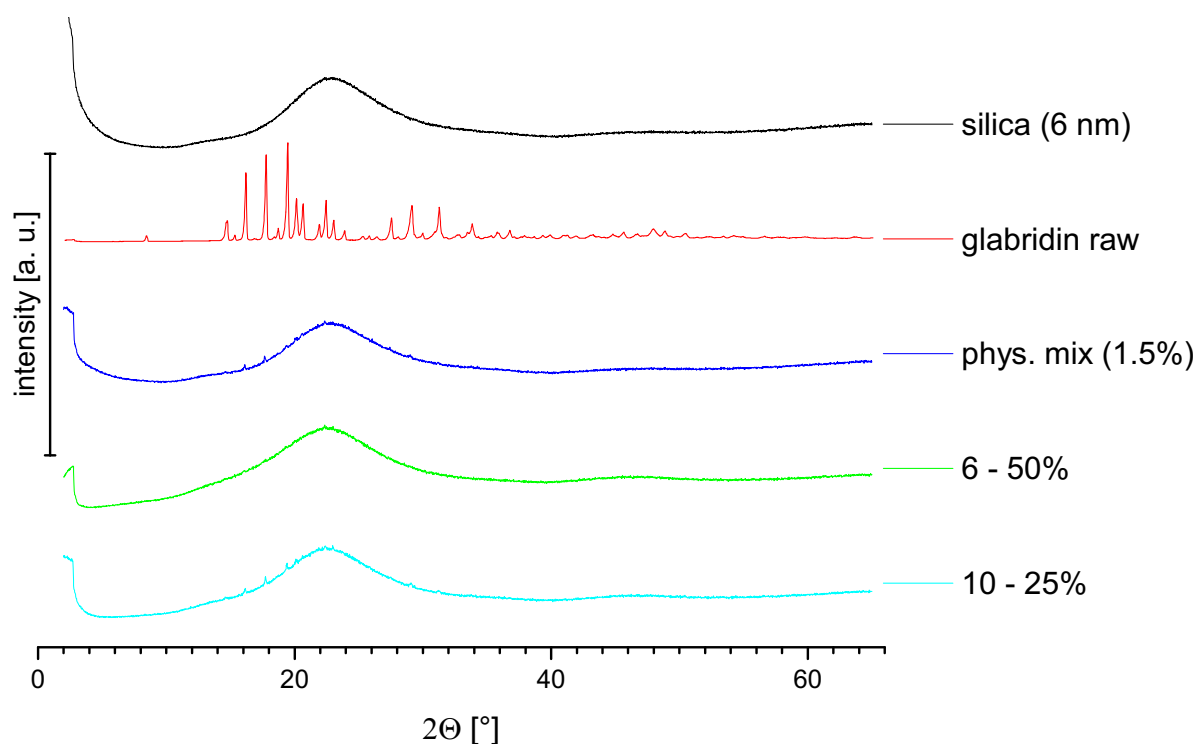


Figure 4: From upper to lower: XRD diffractograms of unloaded silica particles, glabridin raw drug powder, physical mixture at 1.5%, sample 6-50% and sample 10-25%.

XRD diffractograms confirmed substantially the DSC results. For the silica particles, a broad amorphous halo was detected, being in accordance with the absence of melting peak in DSC thermogram. Same applies to the glabridin raw drug powder. Highly crystalline state without an amorphous halo was detected. Also, for the XRD measurements various ratios of physical mixtures were prepared and measured. The detection limit for XRD was determined to be 1.5%. As already known, amorphous fraction can already be generated by preparing the physical mixtures. Therefore, the limit of detection (LOD) can possibly be slightly below 1.5%. XRD diffractograms for sample 10-25% showed small peaks between 16 and 20 2θ indicating the presence of small crystalline fractions about the LOD. But the sample 6-50% has been proven to be completely amorphous. Hence, a stable formulation with a high glabridin mass fraction of 37% can be produced.

Why did the above-mentioned rule “ratio <12” not applied?

Silica were selected beforehand following the rule of pore size to molecule size ratio <12. The only exception was made for one silica, providing a ratio <20, being still promising for amorphization. However, results revealed, that glabridin was only completely amorphized using the silica Davisil® LC60A with a pore width of 6 nm.

How can this observation be explained? For this study, only non-ordered silica were used. Compared to ordered silica [23], they have a wider pore size distribution [26]. Thus, the existence of pores exceeding the required ratio of <12 is possible and can be an explanation.

Ordered silica were not used in this study, even though they provide a narrower pore size distribution. On the one hand they are not available in pharmaceutical grade up to now. Also, ordered silica are around 10-times more expensive than non-ordered silica. In combination with the high price of glabridin, the chance of entering the market seemed to be clearly lowered.

To investigate if the assumption of broad pore width distribution is correct, further investigations were performed by nitrogen ad- and desorption.

Localization of glabridin in the pores

The nitrogen ad- and desorption technique is frequently used to measure the pore width as well as the volume and BET surface [19; 27]. Hence, this technique was used to measure the width of pore size distribution of used silica. The maximum pore size of the silica with declared mean pore size of 6 nm was 12 nm. This is still in the range of the required pore size to obtain molecule size ratio <12. In contrast, measurements of the silica Syloid® 72 FP with a declared pore size of 10 nm had a broad variation of 5-15 nm, exceeding indeed the needed ratio of <12. Thus, non-ordered silica with mean pore sizes should be selected with a sufficiently high safety margin to the maximum possible pore size.

This method further allows the localization of glabridin within the sample. If for example the surface area increases after loading, the glabridin is primarily outside the silica and therefore not located in the pores. Also, Wei Q. et al. [14] reported, that the deposition of actives in the pores influences their release profiles. To give an insight on the deposition of glabridin in the pores hence allows the prediction of its release profile. For the prediction of glabridin release, its deposition was investigated for all 6 nm pore width samples as well as unloaded silica and

glabridin raw drug powder, both as references. The obtained results are all displayed in Figure 5.

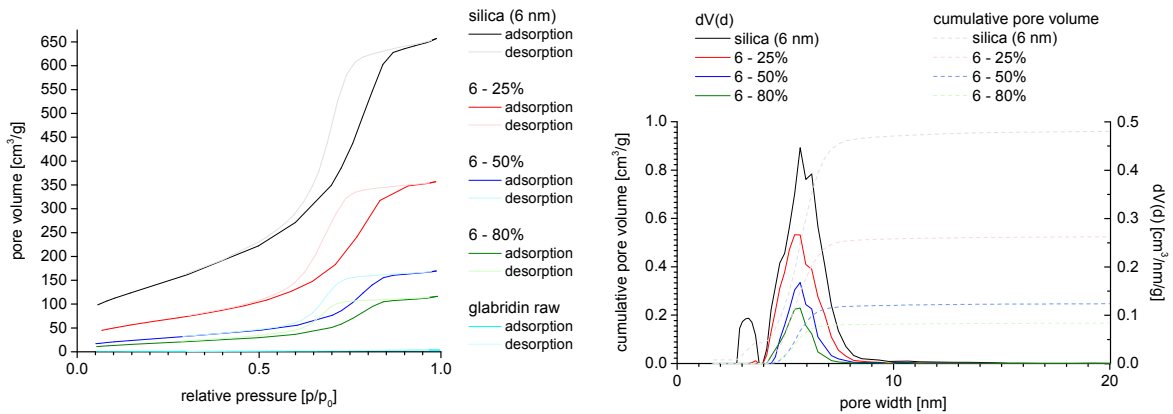


Figure 5: Left: Nitrogen ad- and desorption isotherms of unloaded silica, samples 6-25%, 6-50% and 6-80%, and glabridin raw drug powder. Right: Distribution of pore volume ($dV(d)$) and width determined after DFT method for respective isotherms.

Unloaded silica shows a characteristic hysteresis loop [28] in H1 form (Figure 6, blue curves). This indicates cylindrically shaped pores of unloaded silica (Figure 6, upper right) [29]. After loading, the hysteresis loop did not change its form (Figure 6, purple curves). Thus, the cylindrical shape remains after loading, suggesting a filling by covering the pore surface evenly or a bottom to top filling. Since the pore width did not decrease with increasing loading (Figure 5, right), the second suggestion can be confirmed.

Compared to a pore surface-covered loading, a slower release can be expected here [14]. However, the smartPearls are going to be used incorporated in vehicles. The release therefore is not that decisive as it was for Wei et al., focusing on oral administration.

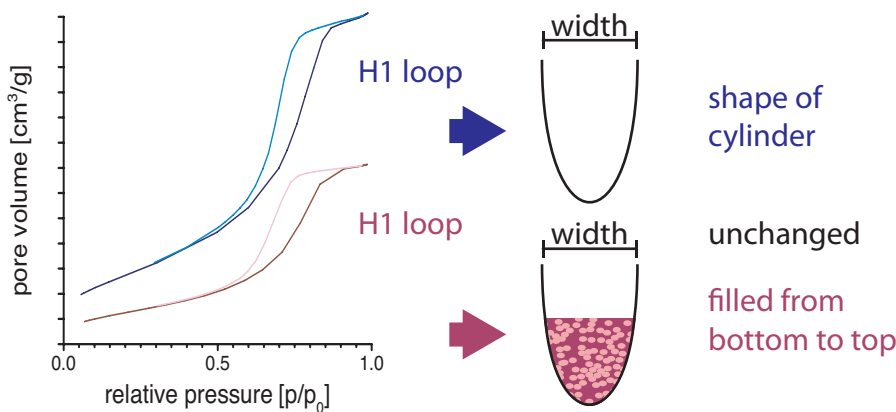


Figure 6: Shape of typical H1 loop, being representative for cylindrically shaped pores.

Why are none of the 80% loaded samples stable?

With increasing loading, the BET surface [25] clearly decreased. Sample 6-25% has a BET surface of 412 m²/g, sample 6-50% a BET surface of 234 m²/g, and sample 6-80% a BET surface of only 66 m²/g. Also, the pore volumes according the DFT method [20] decreased with increasing loading from 0.53 mL/g to 0.25 mL/g and 0.17 mL/g, respectively. This means, that more than 1/3 (37%) of the pore volume is filled for the 6-25% sample. Also, the sample 6-50% was more than expected 50% (almost 70%).

This discrepancy certainly occurs because the density of the glabridin raw drug powder was used for the calculation of the theoretical loading of the pore volume, being crystalline. No amorphous glabridin was available for density determination, nor reported in literature. The different values of theoretical and real loading % suggests a higher density for amorphous glabridin by a factor of 1.4-1.5. Means, the theoretical loading of 80% corresponds to a practical/real loading of >100%. Therefore, all samples with theoretical loadings of 80% must be overloaded also confirmed by all measurements.

6.3.3. Storage stability of glabridin smartPearls*Physical storage stability assessed by XRD*

The special feature of smartPearls is the preservation of thermodynamically unstable amorphous state. Therefore, the physical stability of glabridin smartPearls was of outstanding interest for this study. XRD and DSC measurements were hence repeated after 2 and 7 months of storage at room temperature. The obtained diffractograms for the samples 6-25% and 6-50% are shown in Figure 7.

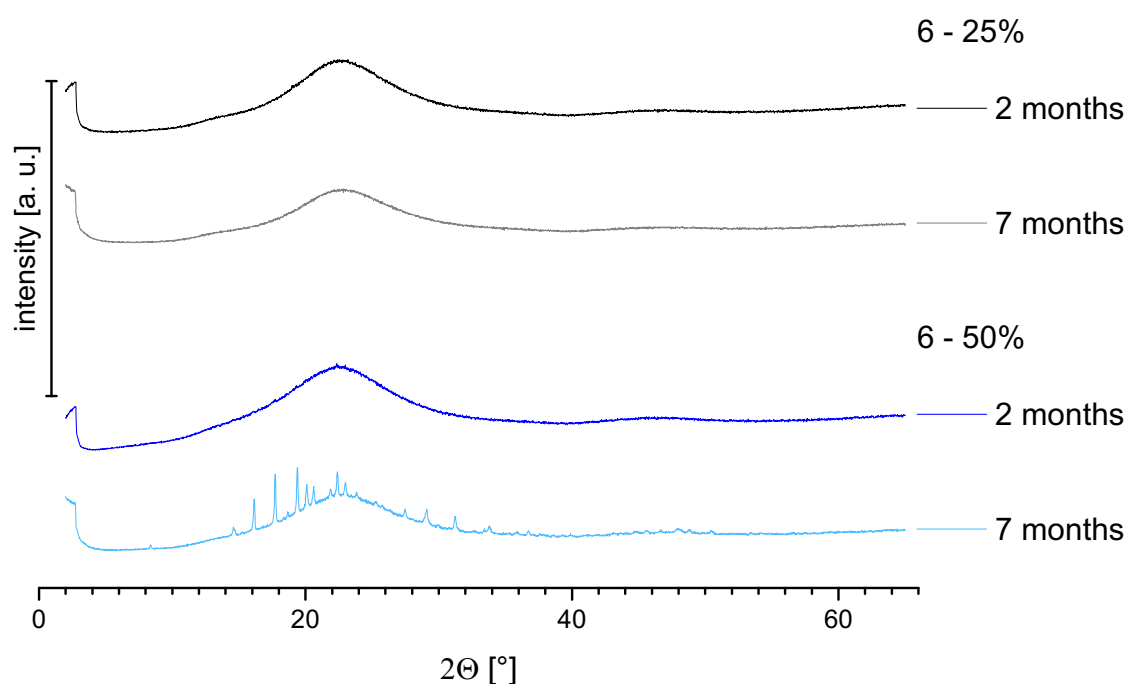


Figure 7: XRD diffractograms of 6-25% and 6-50% samples after 2 and 7 months of storage.

Sample 6-25% remained completely in amorphous state after 7 months. In contrast, sample 6-50% was only stable for 2 months as after 7 months (subsequent measurement point), recrystallization occurred. DSC thermograms underlined the XRD results. Hence, the loading of glabridin into the pores of the silica Davisil® LC60A enables the production and preservation of amorphous state until a theoretical pore volume loading of 25%. This corresponds to a glabridin mass fraction of 22.8% (w/w). Preservation of thermodynamically labile amorphous state is proved to be feasible by loading actives into suitable mesopores of silica particles.

Chemical stability of glabridin assessed by HPLC

In addition to the physical stability, the chemical stability of glabridin was investigated by HPLC directly after loading and after a storage time of 6 months – for the samples 6-25%, 6-50%, 6-80% as well as 10-25% and 10-50%.

Even though glabridin is known to be chemically sensitive in solutions and at higher temperatures, no degradation occurred during the loading process for all samples. Hence, the immersion-evaporation method used in this study presents a gentle method. This enables the loading of mesoporous particles with a broad spectrum of active.

After storing the samples for 6 months at room temperature without any special protection against oxygen or light, the mass fraction of glabridin for 6 nm pore samples slightly decreased by 2.4% in average. However, this reduction was statistically not significant and therefore negligible. Firm inclusion seemed to be connected to the chemical stability of loaded active. The 10 nm pore samples with greater tendencies for re-crystallization also showed the highest glabridin degradation of 4.7% among investigated samples, followed by sample 10-25% with 3.1% glabridin degradation.

For a general statement, that chemical stability can be increased by loading sensitive actives into mesopores, certainly not enough data were captured. However, this statement should be clarified in further studies.

To sum up, glabridin smartPearls produced with 6 nm pore sized silica filled to 25% of total volume were stable physically and chemically for at least 6 months. Hence, a market feasible glabridin smartPearls formulation was successfully developed.

6.3.4. Saturation solubility enhancement

To prove the concept of enhanced saturation solubility for smartPearls, dissolution profiles were determined for freshly produced 6-25% sample and glabridin raw drug powder. Advantage of the Sirius system was, that the scattered light from unsolved particles were corrected. Hence, no remove of these particles was needed to obtain the pure absorption value of dissolved glabridin.

Both profiles were generated over a period of 30 minutes. Within this time, no constant value was reached for both samples. Dissolution curve of smartPearls for example still slightly flattens (Figure 8, upper curve), where the curve of glabridin raw drug powder still slightly increases (Figure 8, lower curve). Thus, the “real” saturation solubility cannot be directly taken from the profiles and had to be calculated. Extrapolation according to the dissolution rate law of Noyes Whitney [30] were therefore applied, resulting in real saturation solubility of glabridin smartPearls of 6.8 $\mu\text{g}/\text{mL}$ (coefficient of determination of 0.9912), and of glabridin raw drug powder of 1.6 $\mu\text{g}/\text{mL}$ (coefficient of determination of 0.9977). Hence, the saturation solubility increased more than 4-fold. This demonstrates clearly that the concept of smartPearls – amorphous active dispersed in nm-range – works, and remarkably increases the saturation solubility.

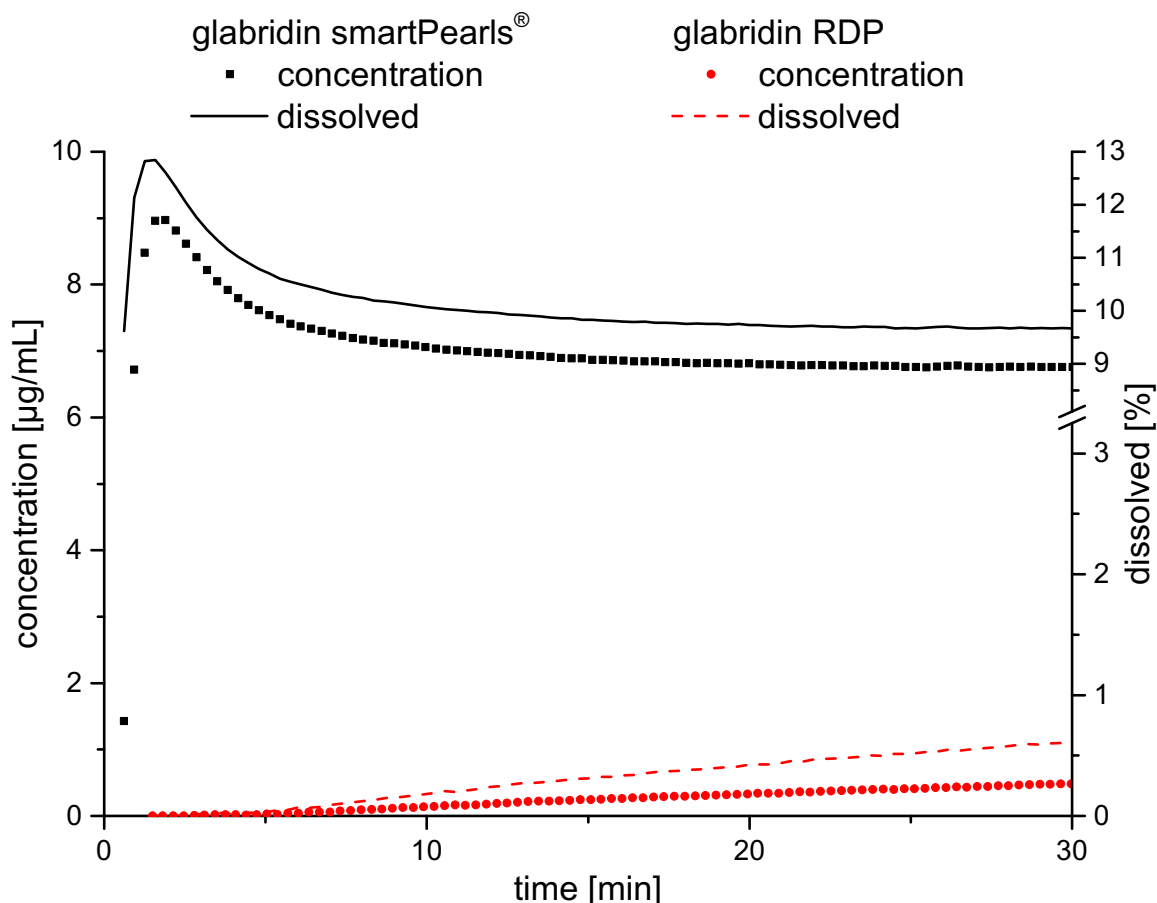


Figure 8: Dissolution profiles (left axis: absolute amount of dissolved glabridin ($\mu\text{g/mL}$) and right axis: relative amount of dissolved glabridin (m/m %)) over 30 minutes of glabridin smartPearls (black, sample 6-25%) and glabridin raw drug powder (red, RDP) obtained by *in situ* UV/VIS measurement.

Unexpectedly, the dissolution profile of glabridin smartPearls showed a maximum at $9 \mu\text{g/mL}$ after 2 minutes. Then, glabridin concentration decreased slightly over time till a plateau at around $7 \mu\text{g/mL}$ is reached after 15 minutes. The maximum of $9 \mu\text{g/mL}$ represents most likely the saturation solubility of pure amorphous glabridin in smartPearls, leading to an oversaturated system with high internal energy. The surface of the silica seems to serve as a crystallization germ on which glabridin partially precipitates and lowers the internal energy. This is in good agreement with the turbidity remaining constant over measurement time and therefore excluding the formation of individual crystals. The precipitation on silica surface is fast and seems limited to a certain amount as the decreasing portion of curve is only from 2-15 minutes. Thus, precipitation of glabridin on silica surface as small nm-sized crystals seems most plausible. As an amorphous part shall still be present in the silica, the real saturation solubility of $6.8 \mu\text{g/mL}$ seems to reflect a solubility equilibrium of the two existing forms. This

explains also why smartPearls are reported to be superior or at least as effective as nanocrystals.

Notable is the quick reach of the maximum saturation (already after 2 minutes) for the smartPearls. In contrast, the maximum saturation for glabridin raw drug powder was not reached still after 30 minutes. Hence, by smartPearls not only the saturation solubility is increased, but also the dissolution velocity. This is important, since the glabridin smartPearls will be added as final step into an already prepared cream, lotion, or another dermal base. Hence, already during the incorporation process the full potential of glabridin is unfold, and no time is lost for interim storage.

Both the increase in saturation solubility and dissolution velocity are highly favorable for the skin penetration. By the 4-fold increased saturation solubility, the concentration gradient between formulation and skin will be increased, leading to higher glabridin flux into skin. The higher dissolution rate is important to quickly replace the penetrated glabridin in the formulation. This will ensure that the concentration gradient being important for the flux is kept high for a long period. Hence glabridin penetration is improved by two increased parameters: saturation solubility and dissolution velocity.

6.4. Conclusions

Glabridin smartPearls were effectively produced by the immersion-evaporation method. By selected production parameters, pores were filled with glabridin from bottom to top. Most stable formulation was obtained by using Davisil® LC60A (6 nm pore width) with a theoretical pore volume filling of 25%. This corresponds to a high glabridin mass fraction of 23% (w/w) in final smartPearls formulation. Amorphous state of glabridin was preserved efficiently for 7 months up to now. Hence, space restriction to suppress re-crystallization can be achieved efficiently by mesoporous silica particles with appropriate pore width. The concept of saturation solubility enhancement by smartPearls was proved. A more than 4-times higher saturation solubility was achieved by smartPearls compared to raw drug powder. Also, the dissolution velocity was distinctly improved. All these features of glabridin smartPearls makes them promising for skin care products with improved glabridin efficacy by simultaneously reduced production costs.

References

- [1] Simmler, C.; Pauli, G.F.; Chen, S.-N.; 2013. Phytochemistry and Biological Properties of Glabridin. *Fitoterapia* 90, 160-184. <https://doi.org/10.1016/j.fitote.2013.07.003>
- [2] Belinky, P.A.; Aviram, M.; Fuhrman, B.; Rosenblat, M.; Vaya, J.; 1997. The antioxidative effects of the isoflavan glabridin on endogenous constituents of LDL during its oxidation. *Atherosclerosis* 137(1), 49-61. [https://doi.org/10.1016/S0021-9150\(97\)00251-7](https://doi.org/10.1016/S0021-9150(97)00251-7)
- [3] Abdel-Malek, Z.; Swope, V.; Smalara, D.; Babcock, G.; Dawes, S.; Nordlund, J.; 1994. Analysis of the UV-Induced Melanogenesis and Growth Arrest of Human Melanocytes. *Pigment Cell Research* 7(5), 326-332. <https://doi.org/10.1111/j.1600-0749.1994.tb00635.x>
- [4] Yokota, T.; Nishio, H.; Kubota, Y.; Mizoguchi, M.; 1998. The Inhibitory Effect of Glabridin from Licorice Extracts on Melanogenesis and Inflammation. *Pigment Cell Research* 11(6), 355-361. <https://doi.org/10.1111/j.1600-0749.1998.tb00494.x>
- [5] Glabridin | C₂₀H₂₀O₄ | ChemSpider, 2018, https://www.chemspider.com/Chemical-Structure.110560.html?rid=f93ad795-ee98-40ba-ad57-73b50a48f8f8&page_num=0 [accessed: 2018 December 13]
- [6] ChemAxon - Software Solutions and Services for Chemistry & Biology, 2018, <https://chemaxon.com/products/chemicalize> [accessed: 2018 December 13]
- [7] Actives International | ViaPure® Licorice, 2018, <https://activesinternational.com/ai/viapure-licorice> [accessed: 2018 December 13]
- [8] Jirawattanapong, W.; Saifah, E.; Patarapanich, C.; 2009. Synthesis of glabridin derivatives as tyrosinase inhibitors. *Archives of Pharmacal Research* 32(5), 647-654. <https://doi.org/10.1007/s12272-009-1501-x>
- [9] Murakami, T.; Miyoshi, S.; Kishida, N.; Doi, K., inventors; Maruzen Pharmaceut Co Ltd, assignee; 2004. Glabridin glycoside and production method therefore, and skin care preparation for external use containing glabridin glycoside. Japan patent JP 2004-277309 A, October 7.

- [10] Schoenrock, U.; Untiedt, S.; Kux, U.; Inoue, K., inventors; Beiersdorf AG, assignee; 1996. Verfahren zur Herstellung von Mono- und/oder Diglucosiden des Glabridins und deren Verwendung als antiirritativer Wirkstoff in kosmetischen und topischen dermatologischen Zubereitungen Germany patent application DE 19615576 A1, April 19.
- [11] Chen, J.; Yu, X.; Huang, Y.; 2016. Inhibitory mechanisms of glabridin on tyrosinase. *Spectrochimica Acta Part A: Molecular and Biomolecular Spectroscopy* 168, 111-117. <https://doi.org/10.1016/j.saa.2016.06.008>
- [12] Keck, C.M.; Müller, R.H.; 2010. smartCrystals-Review of the Second Generation of Drug Nanocrystals, in: Torchilin, V.; Amiji, M.M. (Eds.), *Handbook of Materials for Nanomedicine*. Pan Stanford Publishing Pte. Ltd., New York, 555-580.
- [13] Hespeler, D.; Kaltenbach, J.; Müller, R.H.; Pyo, S.M.; 2018. smartPearls® – stable amorphous glabridin for dermal application, T1330-09-068, AAPS – Annual Meeting: PharmSci 360 Washington DC, 4.-7. November.
- [14] Wei, Q.; Keck, C.M.; Müller, R.H.; 2017. Preparation and tableting of long-term stable amorphous rutin using porous silica. *European Journal of Pharmaceutics and Biopharmaceutics* 113(Supplement C), 97-107. <https://doi.org/10.1016/j.ejpb.2016.11.009>
- [15] Müller, R.H.; Hespeler, D.; Jin, N.; Pyo, S.M.; 2019. smartPearls – Novel physically stable amorphous delivery system for poorly soluble dermal actives. *International Journal of Pharmaceutics* 555, 314-321. <https://doi.org/10.1016/j.ijpharm.2018.11.018>
- [16] Jin, N.; 2017. Nanocrystals & loaded porous silica for increased dermal bioavailability [doctoral thesis]. [Germany]: Freie Universität Berlin. urn:nbn:de:kobv:188-fudissthesis000000105191-3
- [17] Yan, H.-m.; Sun, E.; Cui, L.; Jia, X.-b.; Jin, X.; 2015. Improvement in oral bioavailability and dissolution of tanshinone IIA by preparation of solid dispersions with porous silica. *Journal of Pharmacy and Pharmacology* 67(9), 1207-1214. <https://doi.org/10.1111/jphp.12423>
- [18] W. R. Grace & Co.-Conn., 2016. Grace Product Data Sheets. <https://grace.com/en-us/Pages/Products.aspx> [accessed: 2016 November 4]

- [19] Brunauer, S.; Emmett, P.H.; Teller, E.; 1938. Adsorption of gases in multimolecular layers. *Journal of the American Chemical Society* 60(2), 309-319.
<https://doi.org/10.1021/ja01269a023>
- [20] Thommes, M.; Kaneko, K.; Neimark, A.V.; Olivier, J.P.; Rodriguez-Reinoso, F.; Rouquerol, J.; Sing, K.S.W.; 2015. Physisorption of gases, with special reference to the evaluation of surface area and pore size distribution (IUPAC Technical Report). *Pure and Applied Chemistry* 87(9-10), 1051-1069. <https://doi.org/10.1515/pac-2014-1117>
- [21] Colombo, M.; Staufenbiel, S.; Rühl, E.; Bodmeier, R.; 2017. In situ determination of the saturation solubility of nanocrystals of poorly soluble drugs for dermal application. *International Journal of Pharmaceutics* 521(1), 156-166.
<http://dx.doi.org/10.1016/j.ijpharm.2017.02.030>
- [22] Sliwinska-Bartkowiak, M.; Dudziak, G.; Gras, R.; Sikorski, R.; Radhakrishnan, R.; Gubbins, K.E.; 2001. Freezing behavior in porous glasses and MCM-41. *Colloids and Surfaces A: Physicochemical and Engineering Aspects* 187–188, 523-529.
[http://dx.doi.org/10.1016/S0927-7757\(01\)00637-9](http://dx.doi.org/10.1016/S0927-7757(01)00637-9)
- [23] Xu, W.; Riikonen, J.; Lehto, V.-P.; 2013. Mesoporous systems for poorly soluble drugs. *International Journal of Pharmaceutics* 453(1), 181-197.
<https://doi.org/10.1016/j.ijpharm.2012.09.008>
- [24] Hempel, N.-J.; Brede, K.; Olesen, N.E.; Genina, N.; Knopp, M.M.; Löbmann, K.; 2018. A fast and reliable DSC-based method to determine the monomolecular loading capacity of drugs with good glass-forming ability in mesoporous silica. *International Journal of Pharmaceutics* 544(1), 153-157.
<https://doi.org/10.1016/j.ijpharm.2018.04.035>
- [25] Saffari, M.; Ebrahimi, A.; Langrish, T.; 2016. A novel formulation for solubility and content uniformity enhancement of poorly water-soluble drugs using highly-porous mannitol. *European Journal of Pharmaceutical Sciences* 83, 52-61.
<https://doi.org/10.1016/j.ejps.2015.12.016>
- [26] Choudhari, Y.; Hoefler, H.; Libanati, C.; Monsuur, F.; McCarthy, W.; 2014. Mesoporous silica drug delivery systems, in: Shah, N.; Sandhu, H.; Choi, D.; Chokshi, H.; Malick, A. (Eds.), *Amorphous Solid Dispersions*. Springer, New York, 665-693.
https://doi.org/10.1007/978-1-4939-1598-9_23

- [27] Ravikovitch, P.I.; Haller, G.L.; Neimark, A.V.; 1998. Density functional theory model for calculating pore size distributions: pore structure of nanoporous catalysts. *Advances in Colloid and Interface Science* 76, 203-226.
[https://doi.org/10.1016/S0001-8686\(98\)00047-5](https://doi.org/10.1016/S0001-8686(98)00047-5)
- [28] Ojeda, M.L.; Esparza, J.M.; Campero, A.; Cordero, S.; Kornhauser, I.; Rojas, F.; 2003. On comparing BJH and NLDFT pore-size distributions determined from N₂ sorption on SBA-15 substrata. *Physical Chemistry Chemical Physics* 5(9), 1859-1866.
<https://doi.org/10.1039/B300821E>
- [29] Wagenhöfer, J.; 2013. Mikro-und mesoporöse Silicate als Wirkstoffspeichersysteme [doctoral thesis]. Julius-Maximilians-Universität Würzburg. urn:nbn:de:bvb:20-opus-103848
- [30] Noyes, A.A.; Whitney, W.R.; 1897. The rate of solution of solid substances in their own solutions. *Journal of the American Chemical Society* 19(12), 930-934.
<https://doi.org/10.1515/zpch-1897-2341>

Summary

The **first aim** of this thesis was to summarize the existing knowledge in an overview, a “white paper” providing the scientific background (**chapter 2**). Covered are the historical development, intellectual property aspects (relevant for industrial products), mechanistic considerations and marketing aspects. Most important, the smartPearls technology was compared with the existing gold standard “nanocrystals” showing even better or at least similar penetration performance. smartPearls have the advantage of not being “nano”, which meets the increasing consumer expectation of having no “nano” ingredients in the products.

The formulation challenge of μm -sized silica particles in fluid/semi-solid dermal formulations is the occurring sedimentation during storage. Increasing just the viscosity does not solve and delay the problem only. The **second aim** was therefore to develop physically stable, non-sedimenting formulations (**chapter 3**). The problem was solved by generating viscoelastic formulations – transferring viscoelastic stabilization from food to pharma industry (e.g. salad dressing with herbs). ι -carrageenan and polyacrylates were used as polymers – and as reference the polymer mixture from Kühne salad dressing. Gel properties were investigated by rotation rheology, amplitude sweep and a frequency sweep analysis. In addition, stability investigations with the LUMiSizer® were performed. From the overall data 3 years stability can be predicted.

Third aim was to identify silica particles being optimal for loading with dermal actives (**chapter 4 and 5**). A variety of silica particles was investigated differing in particle size, pore size and pore volume.

In **chapter 4** avobenzone was used as model active, as it shows high crystallization tendency. Thus, it was a challenging molecule to prove the capability of smartPearls to preserve the amorphous state. Five different silica were used ranging in pore size from 3 to 25 nm, pore volume from 0.4 to 1.8 mL/kg and BET surface from 740 to 320 m²/g. Optimal were silica particles with 6 nm and 10 nm pore size. Long-term stability of 1 year could be shown. A mechanism of the pore loading process was suggested, pore filling takes place primarily from bottom to top (localization on pore walls contributes little to the loading).

In **chapter 5** rutin was used as model active, having high relevance for cosmetic products but also in dermatopharmacy (anti-pollution strategy) at the same time. Rutin is poorly soluble and

shows little skin penetration. Optimal silica for loading with rutin were particles ranging in pore size from 6 nm to – in this case – 25 nm. The 6 nm pore particles have the advantage of a higher loading (25%, w/w), the 25 nm particles have a lower loading (18%, w/w) but a better processability.

Within the **fourth aim** a loading process was optimized, which is scale-able to industrial scale. The immersion-evaporation method was applied and DMSO, the solvent used in previous studies was replaced by more skin-friendly ethanol. A mechanistic model was developed for the evaporation process, based on the Ostwald-Miers region. During the evaporation process, the concentration of dissolved active needs to remain within the Ostwald-Miers region. This can be controlled via evaporation temperature and vacuum applied to the rotary evaporator. For up-scaling the evaporation velocity needs to be adjusted to be in the same range as in the used smaller rotary evaporator. This process optimized should allow medium sized cosmetic companies to produce products based on smartPearls.

Within the **final aim**, the acquired knowledge was used to ensure more efficient formulations with the challenging cosmetic active glabridin – highly effective whitening agent (**chapter 6**). It is poorly soluble, even applying it in a high concentration on the skin (suspension formulation) will not significantly improve its penetration. smartPearls are therefore an enabling technology for improving penetration into the skin by increasing the saturation solubility. Various pore-sized silica were investigated. Optimal were the silica particles with 6 nm pore size at 25% loading of the pore volume. Stability over 7 months was shown of the powdered silica. Glabridin has a high price (10,000 USD/kg), thus a formulation principle requiring very low concentrations of active is necessary and can be provided by smartPearls.

In overall the state of the art of smartPearls has been reviewed within this thesis. Physically stable dermal formulations were developed, based on viscoelasticity. Thus, one essential prerequisite for use as dermal product was fulfilled. Ideal silica particles for loading were identified, using model actives avobenzene and rutin. Large scale production – another prerequisite for use as dermal product – is now feasible based on the optimized immersion evaporation process. For better academic understanding mechanisms for the loading process (pore filling) and loading evaporation process (Ostwald-Miers based theory) were identified. Finally, the acquired knowledge was used for the formulation of a market relevant molecule in cosmetics and pharmacy – glabridin.

Zusammenfassung

Erstes Ziel dieser Arbeit war es, das vorhandene Wissen in einem Überblick zusammenzufassen, einem sogenannten "White Paper", das den wissenschaftlichen Hintergrund bildet (Kapitel 2). Betrachtet werden die historische Entwicklung, Aspekte des geistigen Eigentums (relevant für Industrieprodukte), mechanistische Überlegungen und Marketingaspekte. Die smartPearls-Technologie wurde mit dem bestehenden Goldstandard "Nanokristalle" verglichen. Dabei konnte gezeigt werden, dass smartPearls eine noch bessere oder zumindest ähnliche Penetrationsperformance zeigen. smartPearls haben den Vorteil, dass sie keine „nano“-Produkte sind und somit die steigende Kundenerwartung an Produkte ohne „nano“ Inhaltsstoffe erfüllen.

Die Herausforderung bei der Formulierung von μm -großen Silica Partikeln in flüssigen/semifesten dermalen Formulierungen ist die auftretende Sedimentation während der Lagerung. Eine alleinige Erhöhung der Viskosität löst das Problem nicht, sondern verzögert nur die Sedimentation. Das zweite Ziel war daher die Entwicklung physikalisch stabiler, nicht sedimentierender Formulierungen (Kapitel 3). Das Problem wurde durch die Entwicklung viskoelastischer Formulierungen gelöst. Die viskoelastischen Stabilisierung wurde von der Lebensmittelindustrie auf die Pharmaindustrie übertragen. Als Polymere wurden Carrageenan und Polyacrylate verwendet und als Referenz die Polymermischung aus dem Kühne Salatdressing. Die Gel-Eigenschaften wurden durch Rotationsrheologie, Amplituden-Sweep und eine Frequenz-Sweep-Analyse untersucht. Darüber hinaus wurden Stabilitätsuntersuchungen mit dem LUMiSizer® durchgeführt. Aus den Gesamtdaten können mindestens 3 Jahre Stabilität vorhergesagt werden.

Als drittes Ziel sollten Silica-Partikel identifiziert werden, die optimal für die Beladung mit dermalen Wirkstoffen sind (Kapitel 4 und 5). Eine Vielzahl von Silica-Partikeln die sich in Partikelgröße, Porengröße und Porenvolumen unterscheiden, wurde untersucht.

In Kapitel 4 wurde Avobenzon, ein UV Blocker mit hoher Kristallisationstendenz, als Modellwirkstoff verwendet. Fünf verschiedene Silica mit Porengrößen von 3 bis 25 nm, Porenvolumen von 0,4 bis 1,8 mL/kg und BET-Oberfläche von 740 bis 320 m^2/g wurden eingesetzt. Optimal waren Silica-Partikel mit 6 nm und 10 nm Porengröße. Es konnte eine Langzeitstabilität von einem Jahr nachgewiesen werden. Es wurde ein Mechanismus zum

Ablauf des Beladungsprozesses vorgeschlagen, die Porenfüllung erfolgt demnach primär von unten nach oben. Wirkstoff-Lokalisierung an den Porenwänden trägt wenig zur prozentualen Belastung bei.

In Kapitel 5 wurde Rutin als Modellwirkstoff eingesetzt, das gleichzeitig eine hohe Relevanz für Kosmetikprodukte, aber auch für die Dermopharmazie (Antipollutionsstrategie) hat. Rutin ist schwer löslich und weist eine geringe Hautpenetration auf. Optimale Silica für die Beladung waren Partikel im Bereich von 6 nm bis – in diesem Fall – 25 nm Porengröße. Die 6 nm Porenpartikel haben den Vorteil einer höheren Belastung (25%, w/w), die 25 nm Partikel haben eine geringere Beladung (18%, w/w), dafür aber eine bessere Prozessierbarkeit.

Im Rahmen des vierten Ziels wurde ein Beladungsprozess optimiert, der im industriellen Maßstab skalierbar ist. Es wurde die Immersions-Evaporations-Methode angewendet, das bisher verwendete Lösungsmittel DMSO wurde durch Ethanol ersetzt. Für den Verdampfungsprozess wurde ein mechanistisches Modell auf Basis des Ostwald-Miers Bereiches entwickelt. Während des Verdampfungsprozesses muss die Konzentration der gelösten Wirkstoffe innerhalb des Ostwald-Miers Bereiches bleiben. Dies kann über die Verdampfungstemperatur und das am Rotationsverdampfer anliegende Vakuum gesteuert werden. Für die Hochskalierung muss die Verdampfungsgeschwindigkeit angepasst werden, um im gleichen Bereich zu liegen wie bei dem verwendeten, kleineren Rotationsverdampfer. Dieser optimierte Prozess ermöglicht es, mittelständischen Kosmetikunternehmen Produkte auf Basis von smartPearls herzustellen.

Das erworbene Wissen wurde für die Formulierung des anspruchsvollen kosmetisch Wirkstoff Glabridin, ein hochwirksamer Melanininhibitor zur Hautaufhellung, angewendet (Kapitel 6). Es ist schwer löslich, auch in hoher Konzentration auf die Haut aufgetragen (Suspensionsformulierung), wird seine Penetration nicht wesentlich verbessert. smartPearls sind durch Erhöhung der Sättigungslöslichkeit ein möglicher Ansatz zur Verbesserung der Penetration von Glabridin in die Haut. Es wurden verschiedenporige Silica untersucht. Optimal waren die Silica-Partikel mit 6 nm Porengröße bei 25%iger Beladung des Porenvolumens. Die Stabilität der pulverförmigen Silica wurde über 7 Monate nachgewiesen. Der hohe Preis von Glabridin (10.000 USD/kg), fordert eine effiziente Formulierung, wie sie smartPearls ermöglichen.

ZUSAMMENFASSUNG

Innerhalb dieser Arbeit, wurde der Stand der Technik von smartPearls zusammengefasst. Physikalisch stabile dermale Formulierungen, die auf Viskoelastizität basieren, wurden entwickelt. Damit wurde eine wesentliche Voraussetzung für die Verwendung in dermalen Produkten erfüllt. Unter Verwendung der Modellwirkstoffe Avobenzon und Rutin wurden optimale Silica-Partikel für die Beladung identifiziert. Durch den optimierten Immersions-Evaporations-Prozess ist die Skalierung möglich. Zum besseren akademischen Verständnis wurden Mechanismen für den Ladeprozess (Porenfüllung) und den Verdampfungsprozess (Theorie basierend auf dem Ostwald-Miers Bereich) identifiziert. Das erworbene Wissen wurde für die Formulierung eines marktrelevanten Moleküls in Kosmetik und Pharmazie genutzt – Glabridin.

Publications

Peer reviewed articles

1. Pyo, S.M.; **Hespeler, D.**; Keck, C.M.; Müller, R.H.; 2017. Dermal miconazole nitrate nanocrystals – formulation development, increased antifungal efficacy & skin penetration. *International Journal of Pharmaceutics* 531(1), 350-359.
<https://doi.org/10.1016/j.ijpharm.2017.08.108>
2. Müller, R.H.; **Hespeler, D.**; Jin, N.; Pyo, S.M.; 2019. smartPearls – Novel physically stable amorphous delivery system for poorly soluble dermal actives. *International Journal of Pharmaceutics* 555, 314-321.
<https://doi.org/10.1016/j.ijpharm.2018.11.018>
3. **Hespeler, D.**; Kaltenbach, J.; Pyo, S.M.; 2019. Glabridin smartPearls – Silica selection, production, amorphous stability and enhanced solubility. *International Journal of Pharmaceutics* 561, 228-235. <https://doi.org/10.1016/j.ijpharm.2019.02.028>
4. **Hespeler, D.**; Knoth, D.; Keck, C.M.; Müller, R.H.; Pyo, S.M.; 2019. smartPearls® for dermal bioavailability enhancement – Long-term stabilization of suspensions by viscoelasticity. *International Journal of Pharmaceutics* 562, 293-302.
<https://doi.org/10.1016/j.ijpharm.2019.03.016>
5. **Hespeler, D.**; Kaltenbach, J.; Müller, R.H.; 2019. Nanoporous dermal smartPearls – development of industrial production process as pre-requisite for marketed products. *Beilstein Journal of Nanotechnology*, *submitted [Manuscript ID: 16769373]*.
6. **Hespeler, D.**; Pyo, S.M.; Müller, R.H.; 2019. Dermal smartPearls – Optimized silica particles for commercial products & mechanistic considerations. *International Journal of Pharmaceutics*, *submitted [Manuscript ID: IJP-S-19-01888]*.

Non peer-reviewed articles

1. Müller, R.H.; **Hespeler, D.**; Keck, C.M.; 2018. More beautiful than Cleopatra SmartCrystals® – the smart principle to deliver the beauty secrets of Cleopatra more efficiently into the skin. *Eurocosmetics* 26(11/12), 20-23.

Abstracts

1. **Hespeler, D.**; Pyo, S.M.; Kumpugdee Vollrath, M.; Keck, C.K.; 2016. Miconazole nitrate nanocrystals in hydrogel – optimized formulation and production parameters, CRS Local Chapter Germany – 20th Annual Meeting, Saarbrücken, March 7.
2. **Hespeler, D.**; Keck, C.K.; Kumpugdee Vollrath, M.; Müller, R.H.; 2016. Skin-friendly nanocrystals of miconazole nitrate – synergistic combination with chlorhexidine digluconate, poster 3, p. 5-6, Gesellschaft für Dermopharmazie – Annual Meeting, Berlin, March 14-16.
3. **Hespeler, D.**; Pyo, S.M.; Keck, C.M.; Vollrath, M.K.; Müller, R.H.; 2016. Synergistic miconazole nitrate nanocrystal formulation with chlorhexidine digluconate, p. 64, International Conference on Dermal Drug Delivery by Nanocarriers, SFB 1112, Berlin, March 14-16.
4. Keck, C.M.; Nguyen, M.; Pyo, S.M.; **Hespeler, D.**; Weis, M.; Arntjen, A.; Müller, R.H.; Lankers, M.; Sasse, M.; 2016. How many nanoparticles enter a patient during infusion therapy?, 4th World Congress of Vascular Access, Lisbon, June 22-24.
5. Pyo, S.M.; **Hespeler, D.**; Keck, C.M.; Müller, R.H.; 2016. Miconazole Nitrate Nanocrystals Combined with Chlorhexidine Digluconate for Improved Treatment of Fungal Skin Diseases, poster 34 0930, AAPS – Annual Meeting and Exposition, Denver, November 13-17.
6. **Hespeler, D.**; Pyo, S.M.; Müller, R.H.; 2017. smartPearls® – stabilization by viscoelastic formulations, p. 48, CRS Local Chapter Germany – 21th Annual Meeting, Marburg, March 2-3.
7. **Hespeler, D.**; Pyo, S.M.; Müller, R.H.; 2017. smartPearls® – dermal formulation by viscoelastic gels, poster P24, p. 143, Polish German Symposium, Krakow, May 26-28.
8. Pyo, S.M.; **Hespeler, D.**; Keck, C.K.; Müller, R.H.; 2017. smartPearls® – novel concept in dermal delivery, p. 65-66, Polish German Symposium, Krakow, May 26-28.
9. **Hespeler, D.**; Pyo, S.M.; Müller, R.H.; 2017. Dermal smartPearls® – formulation & stabilization by viscoelastic gels, poster P-354, CRS Annual Meeting, Boston, July 16-19.

10. **Hespeler, D.**; Knoth, D.; Pyo, S.M.; Keck, C.M.; Müller, R.H.; 2017. smartPearls® – Viscoelastic Gels for Dermal Delivery, poster T 8071, AAPS – Annual Meeting, San Diego, November 12-15.
11. **Hespeler, D.**; Arndt, C.; Müller, R.H.; Pyo, S.M.; 2018. Glabridin smartPearls – selection of appropriate mesoporous particles & optimization of production conditions, poster 8, Gesellschaft für Dermopharmazie – Annual Meeting, Berlin, March 12-13.
12. **Hespeler, D.**; Knoth, D.; Pyo, S.M.; Müller, R.H.; Keck, C.M.; 2018. smartPearls® – physical penetration enhancer for poorly soluble actives, poster P66, 76, APV Skin Forum – Annual Meeting, Tallinn, June 20-21.
13. **Hespeler, D.**; Pyo, S.M.; Müller, R.H.; 2018. smartPearls® – stable amorphous glabridin for improved dermal application, poster P21, DPhG Landesgruppe Berlin-Brandenburg – Tag der Pharmazie, Berlin, July 6.
14. **Hespeler, D.**; Kaltenbach, J.; Müller, R.H.; Pyo, S.M.; 2018. smartPearls® – stable amorphous glabridin for dermal application, poster T1330-09-068, AAPS – Annual Meeting: PharmSci 360, Washington DC, November 4-7.
15. **Hespeler, D.**; Müller, H.R.; Pyo, S.M.; 2019. Glabridin smartPearls® – increased saturation solubility by amorphization, poster P35, 62, CRS Local Chapter Germany – 23th Annual Meeting, Leipzig, March 7.
16. El Nomeiri, S.; **Hespeler, D.**; Müller, H.R.; Pyo, S.M.; 2019. Rutin smartPearls® – Optimized loading process for generation of stable amorphous state, poster P56, p. 62, CRS Local Chapter Germany – 23th Annual Meeting, Leipzig, March 7.
17. **Hespeler, D.**; El Nomeiri, S.; Müller, R.H.; Pyo, S.M.; 2019. Novel delivery system smartPearls – efficient delivery system for antioxidants in anti-pollution, Gesellschaft für Dermopharmazie – Annual Meeting, Düsseldorf, March 25-27.
18. **Hespeler, D.**; Pyo, S.M.; Müller, R.H.; 2019. Antioxidative rutin smartCrystals – commercial concentrates with skin friendly stabilization, Annual Meeting of DPhG, Heidelberg, September 1-4, *submitted [submission ID 113]*.
19. **Hespeler, D.**; Pyo, S.M.; Müller, R.H.; 2019. Dermal rutin smartCrystals – skin friendly commercial concentrates for anti-pollution products, AAPS – Annual Meeting: PharmSci 360, San Antonio, November 3-6, *accepted [abstract ID 686862]*.

Oral presentations

1. **Hespeler, D.**; Pyo, S.M.; Müller, R.H.; 2017. smartPearls® - dermal formulation by viscoelastic gels, poster P24, p. 143, Polish German Symposium, Krakow, May 26-28.
2. **Hespeler, D.**; El Nomeiri, S.; Müller, H.R.; Pyo, S.M.; 2019. Novel delivery system smartPearls – efficient delivery system for antioxidants in anti-pollution, Gesellschaft für Dermopharmazie – Annual Meeting, Düsseldorf, March 25-27.

Statement of Contributions

Chapter 2

The author of this thesis has designed and performed the sedimentation stability investigations and rheology measurements. Figure 1 to 4 were reproduced from the thesis of Nan Jin. The manuscript was conceptualized and elaborated in cooperation with Prof. Dr. Rainer H. Müller and Dr. Sung Min Pyo.

Chapter 3

The author has designed the experiments and performed the majority of them. The experiments with the analytical centrifuge were performed equally by the author and Daniel Knoth supervised by Prof. Cornelia M. Keck. The manuscript was conceptualized and elaborated under the supervision of Dr. Sung Min Pyo and Prof. Dr. Rainer H. Müller in cooperation with Daniel Knoth supervised by Prof. Cornelia M. Keck.

Chapter 4

The author of this thesis has designed the experiments and performed the majority of them. The XRD measurements were performed by Jonas Kaltenbach. The manuscript was conceptualized and elaborated under the supervision of Dr. Sung Min Pyo and Prof. Dr. Rainer H. Müller

Chapter 5

The author of this thesis has designed the experiments, performed the stability investigations and the saturation solubility measurements. The other experiments were performed by Sanaa El Nomeiri under the co-supervision of the first author. The XRD measurements were performed by Jonas Kaltenbach. The manuscript was conceptualized and elaborated under the supervision of Dr. Sung Min Pyo and Prof. Dr. Rainer H. Müller

Chapter 6

The author of this thesis has designed the experiments and performed the majority of them. The XRD measurements were performed by Jonas Kaltenbach. The manuscript was conceptualized and elaborated under the supervision Dr. Sung Min Pyo.

Acknowledgements

First of all, I would like to express my gratitude to Prof. Dr. Rainer H. Müller, who believed in my potential, gave me the opportunity to work on this interesting topic and for being my mentor for the last 3 years.

Special thanks go to Prof. Dr. Cornelia M. Keck for the successful collaboration, fruitful discussions, the co-evaluation of my thesis, and the possibility to perform experiments at the Department of Pharmaceutical Technology and Biopharmacy at the Phillips-Universität Marburg.

I am grateful to Dr. Sung Min Pyo for her thoughtful supervision, inspiring talks, making this thesis possible and of course the friendship.

Further I would like to thank Corinna Schmidt, Inge Volz and Gabriela Karsubke for the technical and administrative assistance.

Thank you to my colleagues for the collaboration, brainstorming, mutual support and of course for the friendship.

My warmest thank I would like to express to my family, friends, and Anna – the love of my life – for their never-ending support.

Curriculum Vitae

The curriculum vitae is not included in the online version for data protection reasons.

